Chapter 4
From Minerals to Nanoparticles

4.1 Introduction

In a typical technological process, the minerals are transformed by liquid and/or gas phase reactions at high temperatures and pressures. The final products are then separated from the by-products, from the remaining starting materials and/or from the solvent. Very often, the final product is solid again [Boldyrev 1998; Boldyrev and Tkáčová 2000].

Mechanochemical processing may offer the possibility to simplify the entire technological flowchart by avoiding operations in the gaseous and liquid states and to design the process according to the scheme [Boldyrev 1996a, b]:

$$\text{Mineral} \rightarrow \text{Solid state reaction} \rightarrow \text{Desired product.}$$

4.2 Solid–Gas Reactions Stimulated by Mechanical Activation

Reactivity of solids in heterogeneous reactions can be affected by different preparative treatments prior to the reactions. The possibilities for forming different solid state defects by various pretreatment techniques are presented in Table 4.1. Mechanical activation belongs among the effective processes enabling to control and regulate the course of solid-gas reactions via formation of different defects.

It has been shown the mechanical treatment influences the sorption processes by solid-gas reactions as well as the following reactions of adsorbed gases with solids. In several cases the strengthening of sorption processes by mechanical activation depends on the penetration depth of gas into disordered solids [Thiessen et al. 1970]. Butyagin illustrated the process by studying the oxidation of carbon monoxide and hydrogen on mechanically activated quartz mineral SiO_2 [Butyagin 1971, 1984].

As for gas phase selection in solid-gas reactions, methane, carbon monoxide and lately hydrogen have been used. Hydrogen has special position among gas reactants. In contrast to oxidizing processing where SO_2 is envolved and has to be utilized in the form of problematically soleble H_2SO_4, the utilization of H_2S as gaseous reduction product of hydrogen application is more hopeful. H_2S can be further utilized in

P. Baláž, *Mechanochemistry in Nanoscience and Minerals Engineering*,

Table 4.1 Relationship between different types of defects and preparative treatment of the solid phase [Boldyrev 1979]

Preparative treatment	Crystal defects				Lattice defects	
	Surface	Habit	Heterophase inclusions	Dislocations	Doping ions	Point defects
Control of crystal growth	+	+		+	+	+
Doping					+	+
Physical aging				+		
Chemical aging			+		+	
Chemical pretreatment			+			
Radiative pretreatment			+	+	+	+
Mechanical pretreatment	+		+	+		+

the form of elemental sulphur and hydrogen which is more prospective and ecologically less objectionable route. The arisen hydrogen can be recycled into the primary process [Prasad and Mankhand 1983].

However, hydrogen alone is mostly useless as a reducing agent from thermodynamical point of view (Table 4.2) but some reactions were studied and mechanical activation has been applied as an intensification step [Baláž 2000].

For the reaction

$$MeS + H_2 \leftrightarrow Me + H_2S \tag{4.1}$$

the equilibrium constant $K = P_{H_2S} / P_{H_2}$ at 1073 K is typically 2.10^{-1} to 6.10^{-3} for Cu, Ni, Co and Fe sulphides. Dynamic regime is important where hydrogen is

Table 4.2 Heats of reaction, ΔH° for the direct and lime-enhanced reduction by H_2, CO of selected MeS at 1200 K [Prasad and Mankhand 1983]

$MeS + H_2 \rightarrow Me + H_2S$ (A)
$MeS + H_2 + CaO \rightarrow Me + CaS + H_2O$ (B)
$MeS + CO \rightarrow Me + COS$ (C)
$MeS + CO + CaO \rightarrow Me + CaS + CO_2$ (D)

MeS	ΔH°, kJ per g-atom of sulfur			
	(A)	(B)	(C)	(D)
Sb_2S_3	−5.9	70.7	70.7	−105.9
Ag_2S	−15.9	−81.6	−81.6	−114.6
Bi_2S_3	26.8	−37.7	−37.7	−72.8
Cu_2S	39.9	−31.8	−31.8	−64.9
Ni_3S_2	51.0	−13.8	−13.8	−49.0
PbS	70.7	4.6	4.6	−28.5
Co_9S_8	77.4	12.6	12.6	−22.2
MoS_2	105.4	39.3	39.3	6.3
CdS	215.9	150.2	150.2	117.2
ZnS	297.1	231.4	231.4	198.3

continously added and H_2S is continously removed from the reaction system as soon as it is formed.

The enhancement of solid-gas reactions by mechanical activation has been studied for reduction of antimony, mercury, lead and zinc sulphides [Baláž and Godočíková 2001; Baláž and Briančin 2001].

4.2.1 Stibnite Sb_2S_3

The direct reduction of Sb_2S_3 by hydrogen is represented by the equation

$$Sb_2S_3 + 3H_2 \rightarrow 2Sb + 3H_2S \tag{4.2}$$

The reaction (4.2) has been investigated at atmospheric pressure and at temperatures of 473–873 K [Torma and Inal 1979]. The activation energy of this process has been found to be 72 kJ mol^{-1}. The H_2S liberated can be converted into elemental sulphur or H_2S. Consequently this method will not pollute the environment since all by-products are recovered and are saleable. On the basis of the experimental data a flow-sheet has been developed for the production of metallic antimony from high grade sulphide-bearing concentrates. However, only 60% of Sb_2S_3 was converted to metallic antimony.

The results of mechanically activated Sb_2S_3 reduction by hydrogen under dynamic conditions where hydrogen sulfide is carried out from the product are illustrated by the kinetic relationships in Fig. 4.1.

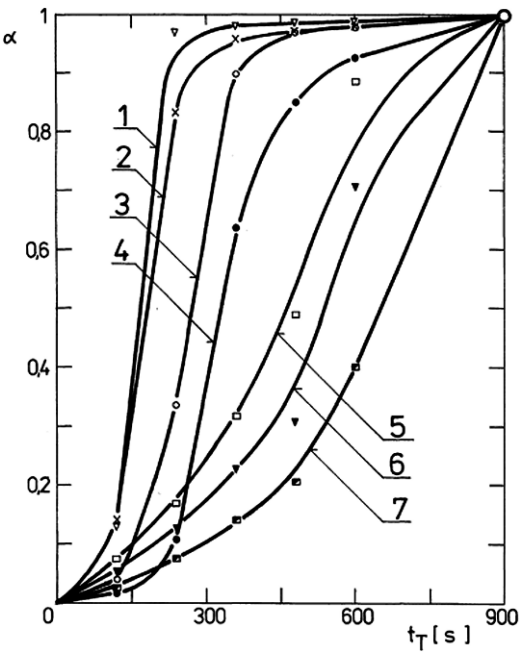

Fig. 4.1 The influence of the reaction time, t_T on the conversion degree, α of mechanically activated Sb_2S_3 for 15 min. Reaction temperatures: 1–954 K, 2–929 K, 3–903 K, 4–877 K, 5–851 K, 6–825 K, 7–800 K [Baláž and Godočíková 2001]

These plots show that the conversion reaches the value 100% and the temporal course of kinetic curves is dependent on temperature. X-ray phase analysis indicated the presence of metallic antimony (JCPDS 05-0562) together with small amount of monoclinic sulphur (JCPDS 13-0141). Mechanical activation brought about a decrease in activation energy from 130 kJ mol^{-1} for non-activated sample to 58 kJ mol^{-1} for a sample activated for 15 min. Both values indicate that the surface chemical reaction of the Sb_2S_3 particles is the rate determining step of reduction. The value 121 kJ mol^{-1} was found for both reactions performed under dynamic conditions [Chunpeng et al. 1988].

4.2.2 Cinnabar HgS

At temperatures exceeding 613 K the reaction between HgS and hydrogen takes place according to the equation [Mills 1974]

$$HgS + H_2 \rightarrow Hg + H_2S \tag{4.3}$$

The dependence of the degree of conversion α on the time of thermal decomposition t_T for mechanically activated HgS is given in Fig. 4.2.

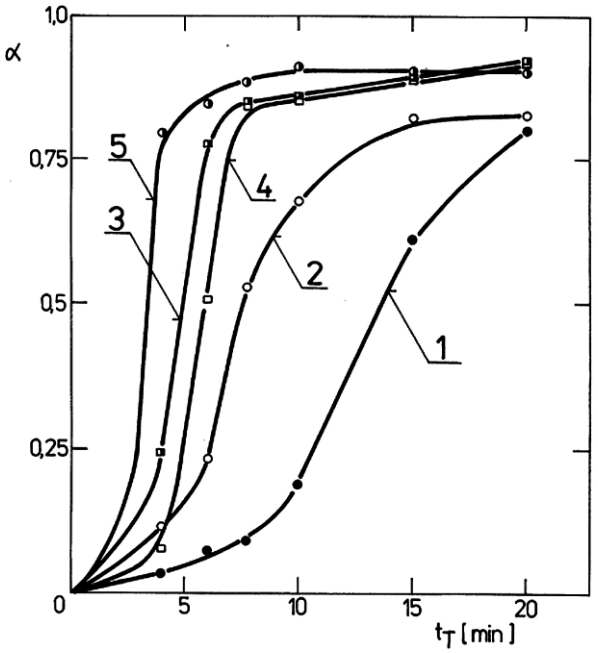

Fig. 4.2 The influence of reaction time, t_T on the conversion degree, α of mechanically activated HgS for 15 min. Reaction temperatures: 1–636 K, 2–679 K, 3–743 K, 4–722 K, 5–835 K [Baláž and Godočíková 2001]

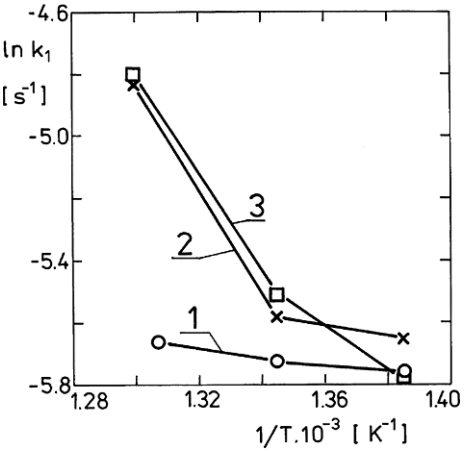

Fig. 4.3 The influence of mechanical activation of HgS on Arrhenius plot, T = 722–765 K. Time of mechanical activation: 1–0 min, 2–5 min, 3–15 min [Baláž and Godočíková 2001]

The Arrhenius plots in Fig. 4.3 give evidence of a change in reaction mechanism at T = 744 K ($1/T = 1.35.10^{-3}$ K) which is manifested by the change slope for the non-activated samples and mechanically activated samples for 5 and 15 minutes.

The change in mechanism can be related with the process of dissociative sublimation which begin just at this temperature [Baláž et al. 1992]. At temperatures above 744 K, a process involving simultaneous dissociative sublimation and reductive decomposition of cinnabar proceeds. The elemental sulphur formed in the first process immediately reacts with hydrogen under dynamic conditions to give H_2S, owing to which the reaction surface is set free and the overall process is accelerated. For the activated samples the values of apparent activation energy in the temperature region 744–751 K are equal to 155–162 kJ mol^{-1}, which points out that the chemical reaction is the rate determining step of the whole process.

4.2.3 Galena PbS

In the eighties several papers dealing with the kinetics of reduction of galena with hydrogen appeared [Onajev and Spitčenko 1988; Zviadadze et al. 1985, 1986; Jovanovic et al. 1986a, b]. It was found by thermogravimetric investigations that mass loss from galena heated in flowing hydrogen occurs at temperatures over 771 K. At temperature over 1023 K the reduced lead vaporizes. The stoichiometry of the process can be expressed by the equation

$$PbS + H_2 \rightarrow Pb + H_2S \tag{4.4}$$

The Arrhenius plots for the reduction of mechanically activated as well as for non-activated PbS by hydrogen are represented in Fig. 4.4.

Their character indicates that no change in mechanism due to temperature or structure disordering of mechanically activated sample takes place in the investigated

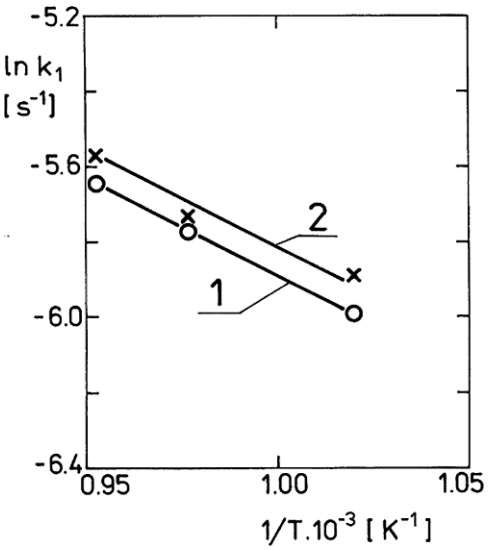

Fig. 4.4 The influence of mechanical activation of PbS on Arrhenius plot, T = 980–1048 K. Time of mechanical activation: 1–0 min, 2–5 min, 3–15 min [Baláž and Briančin 2001]

Table 4.3 Arrhenius data for PbS reduction by hydrogen [Baláž and Briančin 2001]

Mechanical activation (min)	Activation energy (kJ mol^{-1})
–	42 (r = 0.999)
15	38 (r = 0.979)

temperature interval. The values of activation energy for both samples (Table 4.3) indicate that chemical reaction is the rate determining step of PbS reduction.

4.2.4 Sphalerite ZnS

In comparison with galena the reducibility of ZnS is worse [Onajev and Spitčenko 1988]. The degree of reduction reaches only 35% for the temperature of 1070 K [Jovanovic et al. 1986]. This process is complicated by the fact that zinc is evaporated in the hydrogen flow at high temperatures. At the same time H_2S, originating in the reaction of hydrogen with the sulphur atoms of sphalerite leaves the surface. At the temperatures between 1173 and 1223 K hydrogen sulfide can react with Zn vapour to form secondary ZnS [Onajev and Spitčenko 1988; Čižikov 1976]. In temperature range 673–1023 K the reduction can be described by the equation

$$ZnS + H_2 \rightarrow Zn + H_2S \tag{4.5}$$

Elemental zinc (JCPDS 04-0831) and sulphur (JCPDS 08-0247) were detected by X-ray phase analysis of the sample mechanically activated for 15 min and

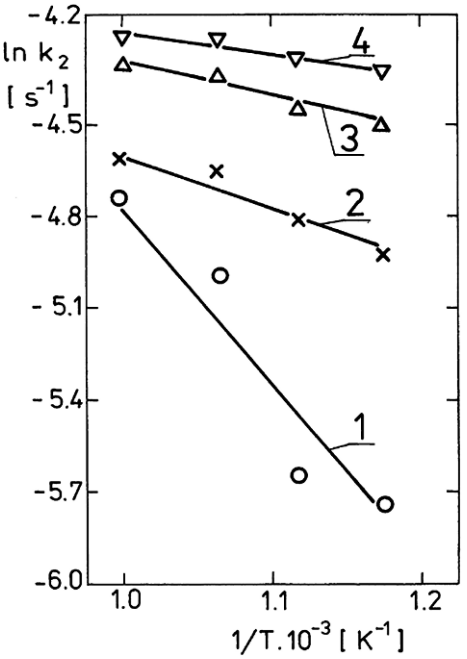

Fig. 4.5 The influence of mechanical activation of ZnS on Arrhenius plot, T = 851–1023 K. Time of mechanical activation: 1–0 min, 2–5 min, 3–10 min, 4–30 min [Baláž and Briančin 2001]

subsequently reduced by hydrogen for 20 min at 937 and 1023 K. The presence of elemental sulphur in reaction products may be a result of H_2S decomposition.

The values of activation energy calculated from plots in Fig. 4.5 are 49, 12, 7 and 4 kJ mol^{-1} for non-activated sample and samples mechanically activated for 5, 10 and 30 min, respectively. The disordering of sphalerite by milling brings about a reduction in the values of activation energy. These values show that the diffusion regime, probably involving the secondary ZnS originating from the above-mentioned recombination of Zn and H_2S determines the rate of reaction (4.5).

Generally, the direct reduction of metal sulphides by gaseous hydrogen is thermodynamically unfavorable (with exception of Sb_2S_3 and Ag_2S, see Table 4.2) and a shift of reaction regime into dynamic one and/or disordering of solids by mechanical activation is needed to improve the kinetics of the process [Baláž and Godočíková 2001]. A good way of driving such reactions forward is to decrease the in-situ partial pressure of gas products (H_2S in case of hydrogen reactant) and this may readily achieved by the incorporation of a powerful sulphur receptor [Prasad and Mankhand 1983].

Calcium oxide CaO is known to be one of the most potent absorbents for sulfur bearing gases and the reduction of metal sulphides by H_2 or CO in its presence may be represented by the overall reactions

$$MeS + H_2 + CaO \rightarrow Me + CaS + H_2O \quad (4.6)$$

$$MeS + CO + CaO \rightarrow Me + CaS + CO_2 \quad (4.7)$$

Except of MoS_2, CdS and ZnS, all other reduction reactions in CaO presence are highly feasible thermodynamically as it is evident from Table 4.2.

A major objective of the lime-enhanced reduction of metal sulphides is to exploit the sulphur fixation ability of lime (as solid CaS) to reduce atmospheric pollution. From a kinetic point of view, lime can be used effectively as a scavenger for sulphur bearing gases like H_2S only above 773 K [Prasad and Mankhand 1983]. In 1969, the lime-enhanced reduction of metal sulphides as means of preparing filamentary products of Cu, Ni and Co under suitable conditions was studied [Cech and Tiemann 1969].

The outstanding capacity of lime to enhance the reduction rates of copper sulphide Cu_2S by hydrogen is clearly demonstrated in Fig. 4.6 and in Table 4.4.

It is clear that the addition of even theoretical amount of lime enhances the reduction rate of the sulphide by a factor 24, which can be increased still further to 49 by employing 200% excess CaO in the reduction charge [Mankhand et al. 1978].

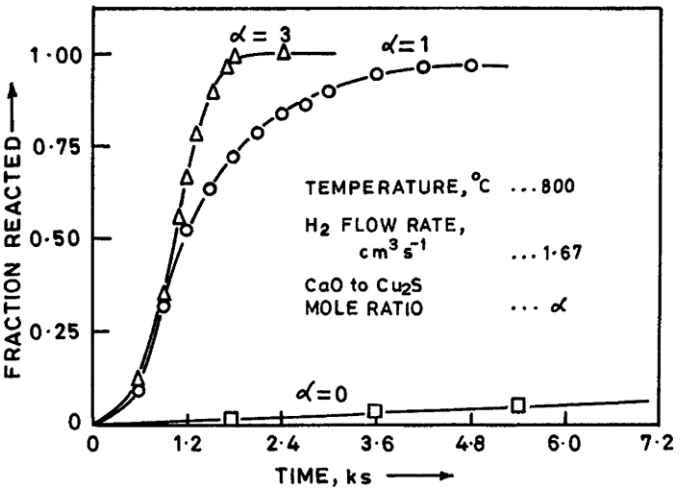

Fig. 4.6 Effect of CaO addition on the reduction of Cu_2S by hydrogen [Mankhand et al. 1978]

Table 4.4 Effect of CaO on the reduction of Cu_2S [Prasad and Mankhand 1983]

Reducing agent	CaO/Cu_2S (mole ratio)	Temperature (°C)	Fraction Cu_2S reacted
H_2	0	800	0.38
H_2	1	800	0.73
H_2	3	800	0.93
C	0	900	*
C	0.5	900	0.58
C	1	900	0.73
C	2	900	0.88

*not significant

An interesting observation from Table 4.4 is that whereas no significant reduction of Cu_2S was observed by carbon alone, the presence of CaO was found to drastically enhance the percent Cu_2S reduced.

It has been reported by different investigators that the time for lime-enhanced reduction may be shortened by the use of fine sized reactant sulphides. This can be a new challenge for application of mechanical activation. This beneficial effect, however, had to be viewed from the point of achieving separation of the reduced metal from the only dry slag (CaS+unused CaO).

Chalcopyrite $CuFeS_2$ reduction in the presence of CaO for sulphur elimination increases with the increasing temperatures and increasing amounts of CaO and is practically complete at 900°C at high CaO addition [Habashi 1986]. Depending on the amount of CaO added, the reduction follows equations

$$2CuFeS_2 + H_2 + CaO \rightarrow Cu_2S + 2FeS + CaS + H_2O \tag{4.8}$$

$$2CuFeS_2 + 3H_2 + 3CaO \rightarrow Cu_2S + 2Fe + 3CaS + 3H_2O \tag{4.9}$$

$$2CuFeS_2 + 4H_2 + 4CaO \rightarrow Cu_2S + 2Fe + 4CaS + 4H_2O \tag{4.10}$$

Due to the presence of metallic Fe the product after reduction is magnetic and can be separated by a magnet. Iron can be leached away by HCl leaving behind Cu powder, a typical analysis of which is shown in Table 4.5. In this process, ZnS initially present in the ore is also reduced and is alloyed with copper.

CaS can be best disposed of by heating in air at 500°C so that it is oxidized to $CaSO_4$

$$CaS + 2O_2 \rightarrow CaSO_4 \tag{4.11}$$

while $FeCl_2$ solution obtained by leaching the metallic iron can be decomposed according to the reaction

$$2FeCl_2 + 2H_2O + \frac{1}{2}O_2 \rightarrow Fe_2O_3 + 4HCl \tag{4.12}$$

Hydrogen chloride generated is recycled for leaching [Habashi 1986].

Table 4.5 Analysis of two chalcopyrite concentrates and copper prepared therefrom by reduction followed by leaching [Habashi 1986]

	Noranda concentrate (%)	Crude Cu (%)	Gaspe concentrate (%)	Crude Cu (%)
Cu	25.4	78.6	25.0	81.7
Fe	24.2	2.1	31.3	0.9
Zn	6.6	12.3	0.7	1.0
S	29.9	6.1	27.2	2.8
Gangue (by difference)	13.9	0.9	15.8	13.6

4.3 Mechanochemical Reduction via Solid–Solid Reactions

During the early history of the chemistry of solid state reactions, the question whether solid substances could react with each other without the aid of liquids or gases was strongly debated. The original view was that reactions could not occur directly between solids. The works of Tamman and Hedvall established in the 1930s that such reactions do occur in the solid state. By the end of the 1960s, it was generally accepted that the rate of a reaction between two solids could be substantial if the compounds were intimately mixed and heated. The reaction is initiated as lattice vibrations with increasing amplitude result in more frequent exchange of atomic positions in the crystal lattice, leading to faster macroscopic diffusion. The exchange of atomic positions is especially easy in disordered structures [Habashi 1969].

When intimate mixing of the solid reactants was carried out by using high-energy milling, the potential for initiating mechanochemical reactions was established. Until very recently, it was universally assumed that chemical reactions took place during the mechanical treatment of solids due to the evolution of heat. The increase of the reactivity was attributed to the increase of the specific surface of the solid upon treatment [Boldyrev 1993]. The importance of structural disorder, already well established in solid state chemistry [Hedvall 1938; Tamman 1932], was recognized by mechanochemists as the reason for enhanced reactivity. In early suggestions, it was accepted that the reactivity of solids is determined by the total content of defects. Later it was concluded that only those defects should be taken into account which directly or indirectly take part in the chemical reaction [Schrader and Hoffman 1973].

The preparation of metals and alloys by reduction of their salts with metals has been described in pyrometallurgy [Habashi 1969]. The method is characterized by the fact that the reducing metal is converted by high temperature to a solid or a liquid product and not to a gas in other reducing processes, e.g. by carbon and hydrogen where CO+CO_2 and H_2O are formed, respectively. In general, such processes are called *metallothermic*. In special case, when Al is used as a reducing agent the process is called *aluminothermic* reduction, when Ca is used it is called *calciothermic* reduction [Habashi 1969]. General scheme of metallothermic processes is given in Fig. 4.7.

As described by Habashi the different substances like *fluxes, thermal boosters* and *alloying metals* are added to improve the process of metallothermic reduction.

Fluxes form a fluid slag so that separation from the metal can be easily achieved. For example, in the production of metal Mg by ferosilicon process CaO·MgO is preferred to MgO as a raw material because CaO reacts with SiO_2 liberated to form a low-melting slag

$$2\mathrm{MgO.CaO} + \mathrm{FeSi} \rightarrow 2\mathrm{Mg} + \mathrm{Ca_2SiO_4} + \mathrm{Fe} \tag{4.13}$$

Thermal boosters are used to improve the thermal balance of reduction. These react with an excess reducing agent liberating appreciable amount of heat. For example, sulphur is added during the reduction of V_2O_5 by Ca; the formation of CaS is highly exothermic and raises the temperature of reduction.

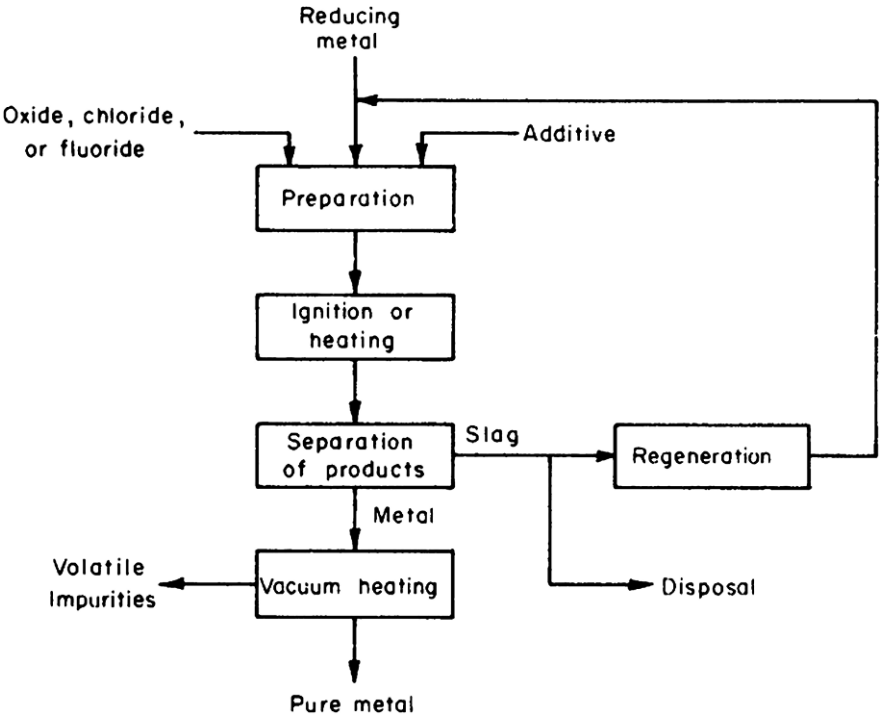

Fig. 4.7 General scheme of metallothermic reduction [Habashi 1969]

Alloying metals lower the melting point of the metal to be recovered. These metals can be removed from the alloy by vacuum distillation, e.g. Zn.

Solid-state reactions usually start at the contact points of reacting particles [Budnikov and Ginstling 1971]. It follows the number of contact points and their area has influence on solid-solid reactions. By applying mechanical activation these parameters can be increased. It has been shown that the coefficient of diffusivity of solids can be also enhanced: in case of Cr, diffusion into Fe is $10^{-12}\,cm^2\,s^{-1}$, at 1400–1600 K is equal to $2.10^{-8}\,cm^2\,s^{-1}$ but by mechanical activation of the system, the values 10^{-5}–$10^{-7}\,cm^2\,s^{-1}$ have been obtained [Butyagin and Yuščenko 1987].

4.3.1 Redox Reactions

These reactions can be expressed in general by equation

$$Me_1X + Me_2 \rightarrow Me_1 + Me_2X \tag{4.14}$$

where Me_1-reduced metal, Me_2-reducing metal, X-oxide, chloride, fluoride, sulphide, etc. Redox reactions involve simultaneous oxidation and reduction processes.

According to present views a redox reaction is a reaction in which there is a transfer of electrons from reducing metal to reduced metal. Sometimes they are called *exchange* or *metathesis reactions* [Treece et al. 1995; Gillan and Kaner 1996].

Many well-known industrial solid-state reactions are driven by these reactions. The most commonly used reducing metals are Al, Ca, Mg, Na and Si (as FeSi). The other metals such as Cu, Mn and Fe are also applied. The selected examples of application are given in Table 4.6.

Table 4.6 Commonly used reducing metals and their application [Habashi 1986]

Reducing metal	Metal produced	
	Large scale	Small scale
Al	V, Nb, Ca	Sr, Ba, Ta
Ca	V, U	rare earths, Ti, Cr
Mg	Be, Ti, Zn	Sc, Y, V, Nb, Ta
Na	Ta, Ti	Zr, Hf, V, Nb, Th
FeSi	Mg	

In choosing a metal for reduction, the following points should be observed [Habashi 1986]:

- the metal should have a strong affinity, based on thermodynamic consideration
- to ensure complete reduction, the reducing metal is usually added in slight excess
- the metal can be easily obtained in high purity and at low-cost
- the metal does not form intermetallic compounds and
- the metal should be easily handled, i.e. does not need inert atmosphere in a post-reduction operation.

Separation of reaction products play the important role in the process of reduction. The method of separation varies from one reduction process to the other. Sometimes small amounts of salts adhering to the metal have to be removed. The method of heating of the product under high vacuum is applied in this case. In mechanically activated solid–solid state reactions the problem of the reaction products separation is more underlined. Mechanical activation increases significantly kinetics in such reactions by the dynamic maintenance of high reaction volumes and rapid diffusion rates related to short diffusion paths, enhanced defect density and high reaction interface areas. In such cases where various nanostructures are formed the formation of nanocomposites is very probable.

4.3.2 Nanocomposites

In nanocomposites constituents are mixed on a nanometer-length scale. They have been generally classified based on the matrix (such as metal-matrix composites

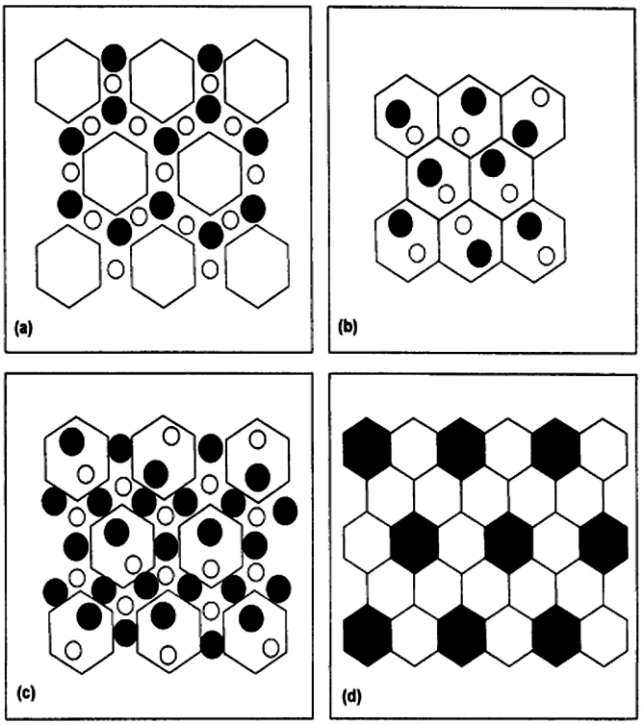

Fig. 4.8 Classification of nanocomposites: (**a**) intergranular, (**b**) intragranular, (**c**) hybrid, (**d**) nano/nano [Niihara 1991]

(MMC), ceramic-matrix composites (CMC) or polymer-matrix composites (PMC). Nanocomposites can be divided into four categories: intragranular, intergranular, hybrid and nano/nano composites (Fig. 4.8).

In the first three types, the reinforcement phase is in the nanometer level whereas the matrix is not. In the last cathegory, however, both the matrix and reinforcement are of nanometer division and these two components are randomly distributed. They often have properties that are superior to conventional microscale composites and can be synthesized using surprisingly simple and inexpensive techniques such as a mechanochemical method described above. Nanocomposites as systems with high density of interface boundaries provide the large surface of initial components. Moreover, concentration of atoms near boundaries reaches 15–30% of their total number. The mixing of components is performed at the nanometer level when the contact between the components is performed by atomically pure planes and the effect of the surrounding atmosphere is reduced to a minimum [Niihara 1991].

Nanocomposites are either prepared in a host matrix of inorganic materials or by using conventional polymer as one component of the nanocomposites. The second type of nanocomposites which are a special class of hybrid materials are termed *polymeric nanocomposites*. These materials are intimate combination (up to almost the molecular level) of one or more inorganic material (nanoparticles, e.g.) with a

polymer so that unique properties of the former can be mixed with the existing qualities of the polymer to result in a totally new material suitable for novel applications [Dutta and Hofman). Resulting nanocomposites have found successful applications in various fields of material application such as baterry cathodes [Nazar et al. 1992], microelectronics [Vassilion et al. 1990], nonlinear optics [Beecroft and Ober 1997], sensors [Cao et al. 1992], etc.

Ceramic nanocomposites bring new light into properties of brittle ceramics which play crucial role in technology. Brittle ceramic can be strengthened and toughened by the incorporation of various reinforcements. Ductile metallic reinforcement appear to be one of the most promising toughening mechanism. It has already been investigated and the enhancement is mainly contributed by plastic inclusions which bridge the advancing crack. They are stretched as the cracks opens until they fracture or separate from the matrix [Gaffet and Bernard 2002].

High-energy milling is a very effective process for synthesizing *metal-ceramic nanocomposites* as it allows incorporation of the metal and the ceramic phases into each powder particle, as shown schematically in Fig. 4.9.

In the initial stage, the microstructure of the composite powder particles is at the micrometer level. With further milling, the metal phase is deformed and fractured, while the ceramic phase is mainly fractured. If it is a metal matrix composite, the ceramic particles are continually fractured into small particles, so the ceramic particle size will keep decreasing until such a point that the fracture strength of the small particles will be equal to or grater than the stress caused by collision. Often this balance point corresponds to a ceramic particle size in the range of a few nanometers to 100 nm [Zhang 2004].

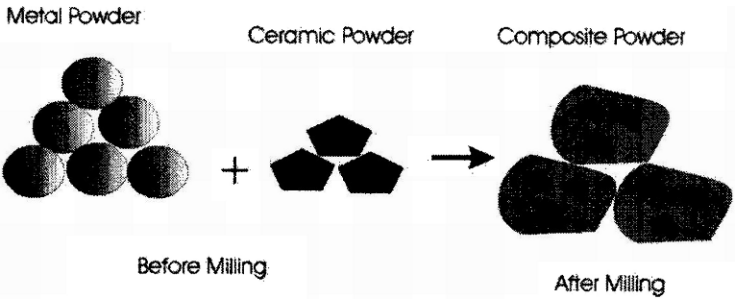

Fig. 4.9 Schematic diagram showing the formation of composite powder after high-energy milling [Zhang 2004]

4.3.3 Oxides

Mechanochemical solid-state reduction of oxides can be schematically expressed by general equation

$$Me_1O + Me_2 \rightarrow Me_1 + Me_2O \tag{4.15}$$

where Me_1-reduced metal, Me_2-reducing metal. A large variety of Me_1 and Me_2 combinations has been used, e.g. Me_1 = Fe, V, Cr, Mn, Co, Ni, Ti, Sn, Pb, Cu, Zn, Nb, Mo, W, Si and Me_2 = Al,C, Ti, B, Cr, Si, Mg, Zr, Ca, Zn, Ni and Mn (see Table 4.7).

One of the primary driving forces behind the design of successful solid-state reactions is a careful consideration of thermodynamics. The contribution of product formation on the overal heat of reaction (ΔH) varies greatly depending on such factors as product structure, type of bonding and lattice energy [Gillan and Kaner 1996]. Several mechanically induced systems will be studied in this Chapter where ΔH values summarized from literature are given in Table 4.7.

Mechanochemical reduction of oxides is an extention of the mechanical alloying process developed by Benjamin [Benjamin 1970]. At the laboratories of INCO Alloys International he applied this process as a means to overcome traditional problems associated with producing an oxide dispersion and γ'-strengthened nickel base superalloy. The scope and application of mechanical alloying have been considerably widened since the process was first announced. As with rapid solidification, with which it is often compared, mechanical alloying finds application in those high-value added materials which cannot be produced by alternative means [Schaffer and McCormick 1992a].

Mechanical alloying is a high-energy ball milling process where powder particles undergo repeated fracturing and cold welding during ball-powder-ball and ball-powder container collisions. Both processes can occur during a simple collision. When particles being impacted overlap, atomically clean interfaces are brought into contact. Cold weld form and layered composite powder particles are built up. Concurrently, work-hardened particles fracture, decreasing the particle size and creating new surfaces. This interplay between welding and fracture effectively kneads the internal structure so that the powders are continually refined [Schaffer and McCormick 1989a].

In these highly exothermic reactions, it has been shown that mechanical alloying can cause an unstable reaction which proceeds by the propagation of a combustion wave through the partly reacted powders. The combustion conditions is reached after a critical ignition time, t_{ig}, which has been shown to be the milling time required for the ignition temperature of the powder mixture, T_{ig}, to be reduced to a level equal to that achieved locally during collision event [Schaffer and McCormick 1989b, 1991].

The examination of powders immediately after combustion has revealed a rich variety of structures which reflect the high temperatures reached during the combustion event [McCormick 1995]. In general the as-combustioned mixtures of various size from nodules as large as 1–5 mm down to particles 10 nm in diameter are formed. A sudden conversion of reagents into products is observed in such processes, which is characteristic of systems displaying a high and negative reaction enthalpy.

The process also called *mechanically induced self-sustaining reactions* (MSR) was broadly studied [Tschakarov et al. 1982; Schaffer and McCormick 1992b; Yang and McCormick 1993, 1994; Takacs 1993, 1996a, b, c; Ye et al. 1995;

Table 4.7 Mechanically induced redox reactions of oxides

Reaction	ΔH° ($kJ\,mol^{-1}$)	ΔG° ($kJ\,mol^{-1}$)	Reference
$2CuO + Ti \rightarrow 2Cu + TiO_2$	−620		Mulas et al. 2001
$2CuO + Zr \rightarrow 2Cu + ZrO_2$	−736		Mulas et al. 2001
$2CuO + Hf \rightarrow 2Cu + HfO_2$	−796		Mulas et al. 2001
$3CuO + 2Al \rightarrow 3Cu + Al_2O_3$	−273		Schaffer 1990; Matteazzi and LeCaër 1992a
$CuO + Ca \rightarrow Cu + CaO$	−475		Schaffer 1989b; McCormick 1995
$2CuO + C \rightarrow 2Cu + CO_2$	−138		Tschakarov 1982
$4CuO + 3Fe \rightarrow 4Cu + Fe_3O_4$	−488		McCormick 1995; Schaffer 1990
$CuO + Mg \rightarrow Cu + MgO$	−445		McCormick 1995; Schaffer 1990
$CuO + Mn \rightarrow Cu + MnO$	−231		McCormick 1995; Schaffer 1990
$CuO + Ni \rightarrow Cu + NiO$	−382		Schaffer 1990
$2CuO + Si \rightarrow 2Cu + SiO_2$	−596		Xi 1996
$2Cu_2O + Ti \rightarrow 4Cu + TiO_2$	−598		Mulas et al. 2001
$2Cu_2O + Zr \rightarrow 4Cu + ZrO_2$	−754		Mulas et al. 2001
$2Cu_2O + Hf \rightarrow 4Cu + HfO_2$	−771		Mulas et al. 2001
$Cu_2O + Mg \rightarrow 2Cu + MgO$	−434		Banza and Gock 2003
$Cu_2O + Zn \rightarrow 2CuO + ZnO$	−183		Banza and Gock 2003
$3Ag_2O + 2Al \rightarrow 6Ag + Al_2O_3$	−532		Takacs 1993
$CdO + Ca \rightarrow Cd + CaO$	−377		McCormick 1995
$Cr_2O_3 + 2Al \rightarrow 2Cr + Al_2O_3$	−273		Matteazzi and LeCaër 1992a; Takacs 1993
$Cr_2O_3 + 3Zn \rightarrow 2Cr + 3ZnO$	+49		Takacs 1993
$3V_2O_5 + 10Al \rightarrow 6V + 5Al_2O_3$	−3727		Yang 1994
$V_2O_5 + 5Mg \rightarrow 2V + 5MgO$	−1457		Matteazzi and LeCaër 1992a; Yang 1994
$2V_2O_5 + 5Ti \rightarrow 4V + 5TiO_2$	−1623		Yang 1994
$WO_3 + 3Mg \rightarrow W + 3MgO$			Mukopadhyay et al. 1996
$WO_3 + 2Al \rightarrow W + Al_2O_3$	−833		Torosyan and Takacs 2004
$ZnO + Ca \rightarrow Zn + CaO$	−285		Schaffer 1989a; McCormick 1995
$ZnO + Mg \rightarrow Zn + MgO$	−253		Suryanarayana 2001
$2ZnO + Ti \rightarrow 2Zn + TiO_2$	−249		McCormick 1995
$2ZnO + 2Al \rightarrow 3Zn + Al_2O_3$			Matteazzi and LeCaër 1992a
$3CoO + 2Al \rightarrow 3Co + Al_2O_3$			Matteazzi and LeCaër 1992a
$3MnO_2 + 2Al \rightarrow 3Mn + 2Al_2O_3$			Matteazzi and LeCaër 1992a
$MoO_3 + 2Al \rightarrow Mo + Al_2O_3$			Matteazzi and LeCaër 1992a
$6Nb_2O_5 + 10Al \rightarrow 12Nb + 5Al_2O_3$			Matteazzi and LeCaër 1992a
$3NiO + 2Al \rightarrow 3Ni + Al_2O_3$			Matteazzi and LeCaër 1992a
$2NiO + Si \rightarrow 2Ni + SiO_2$			Suryanarayana 2001

Table 4.7 (continued)

Reaction	ΔH° (kJ mol^{-1})	ΔG° (kJ mol^{-1})	Reference
$3SiO_2 + 2Al \rightarrow 3Si + 2Al_2O_3$			Matteazzi and LeCaër 1992a
$WO_3 + 2Al \rightarrow W + Al_2O_3$			Matteazzi and LeCaër 1992a
$2WO_3 + 3Ti \rightarrow 2W + 3TiO_2$			Matteazzi and LeCaër 1992a
$3SnO_2 + 2W \rightarrow 3Sn + 2WO_3$		+25	Boldyrev and Avvakumov 1971; Avvakumov et al. 1974; Varnek et al. 1974; Avvakumov and Strugova 1974; Butyagin et al. 1974
$SnO_2 + Si \rightarrow Sn + SiO_2$		−276	Boldyrev and Avvakumov 1971; Avvakumov et al. 1974; Varnek et al. 1974; Avvakumov and Strugova 1974; Butyagin et al. 1974
$3SnO_2 + 4Al \rightarrow 3Sn + 2Al_2O_3$		−535	Boldyrev and Avvakumov 1971; Avvakumov et al. 1974; Varnek et al. 1974; Avvakumov and Strugova 1974; Butyagin et al. 1974
$2SnO + Si \rightarrow 2Sn + SiO_2$		−954	Patel et al. 2004
$2Sb_2O_3 + 3Si \rightarrow 4Sb + 3SiO_2$		−2823	Patel et al. 2004
$4CdO + 4S + 3Fe \rightarrow Fe_3O_4 + 4CdS$		−673	Zhang et al. 2001; Saito et al. 2004
$4PbO + 4S + 3Fe \rightarrow Fe_3O_4 + 4PbS$		−649	Zhang et al. 2001; Saito et al. 2004
$4ZnO + 4S + 3Fe \rightarrow Fe_3O_4 + 4ZnS$		−535	Zhang et al. 2001; Saito et al. 2004
$2Fe_2O_3 + Al \rightarrow 2Fe + Al_2O_3$			Nasu et al. 1999; Basset et al. 1994; Matteazzi and LeCaër 1992a; Matteazzi and LeCaër 1991
$Fe_2O_3 + 2B \rightarrow 2Fe + B_2O_3$			Matteazzi and LeCaër 1991
$Fe_2O_3 + 2Cr \rightarrow 2Fe + Cr_2O_3$			Matteazzi and LeCaër 1991
$2Fe_2O_3 + 3Si \rightarrow 4Fe + 3SiO_2$			Matteazzi and LeCaër 1991
$Fe_2O_3 + Ca \rightarrow 2Fe + 3CaO$	−1080		McCormick 1995
$Fe_2O_3 + 3Mg \rightarrow 2Fe + 3MgO$			El-Eskandarany et al. 2001
$Fe_2O_3 + 2Al + Cr_2O_3 \rightarrow FeCr + 2Al_2O_3$			Matteazzi and LeCaër 1992a
$Fe_2O_3 + 3Al + Cr_2O_3 + 3NiO \rightarrow FeCrNi + 3Al_2O_3$			Matteazzi and LeCaër 1992a
$3Fe_3O_4 + 8Al \rightarrow 9Fe + 4Al_2O_3$	−1716		Pardavi-Horvath and Takacs 1992; Takacs and Pardavi-Horvath 1994
$Fe_3O_4 + 2Ti \rightarrow 3Fe + 2TiO_2$	−395		Takacs 1993
$Fe_3O_4 + 2Zr \rightarrow 3Fe + 2ZrO_2$			Takacs 2002
$Fe_3O_4 + 4Zn \rightarrow 3Fe + 4ZnO$	−143		McCormick 1995; Takacs 1993; Takacs and Pardavi-Horvath 1994

Ma et al. 1993; Mulas et al. 2001]. MSR process has been recently reviewed [Takacs 2002]. High-energy milling induces self-sustaining reactions in many sufficiently exothermic powder mixtures. The process begins with an activation period, during which size reduction, mixing and defect formation take place. The MSR is ignited when the powder reaches a well defined critical state. Once started, the reaction propagates through the powder charge as a combustion process.

The first self-propagating solid state reaction was the so-called *thermite reaction*, in which a metal oxide is reduced with aluminium (this process is also called aluminothermic reduction, see Sect. 4.3). The process takes place in a mixture of the powders, initiated by either a high-temperature reaction or an electrically heated wire. A combustion front develops and propagates across the sample.

The first systematic investigations on ball milling induced self-propagating reactions-explosive mechanochemical reactions, according to the terminology of the authors-were performed in Bulgaria [Tschakarov et al. 1982]. The authors studied the formation of metal chalcogenides from mixtures of the elemental powders. The ignition of a self-sustaining reaction was detected by measuring an abrupt temperature increase inside the mill.

4.3.3.1 Copper Oxides

To test whether the mechanical alloying technique can be used as a vehicle for the chemical reduction of oxides, the powders of copper oxide and calcium metal were milled [Schaffer and McCormick 1989a, b, 1991]. The historically first mechanochemical reduction of oxides was reaction

$$\mathrm{CuO} + \mathrm{Ca} \rightarrow \mathrm{Cu} + \mathrm{CaO}. \tag{4.16}$$

The reaction (4.16) is associated with the high negative enthalpy ($\Delta H = -475\,\mathrm{kJ}$). Figure 4.10 shows X-ray diffraction patterns of samples milled for various times. Reducing metal such as Ca results in the reduction of the cupric oxide to form Cu metal.

The presented process effectively combines conventional mechanical alloying with the reduction-diffusion process [Schaffer and McCormick 1990].

The thermal reduction of copper oxide with the other solid reducing agent carbon

$$2\mathrm{CuO} + \mathrm{C} \rightarrow 2\mathrm{Cu} + \mathrm{CO_2} \tag{4.17}$$

is a widely used process for the production of copper. This reaction is thermodynamically favoured at room temperature ($\Delta H = -138\,\mathrm{kJ}$), but will not occur for kinetic reasons. However, it has been shown that CuO can be mechanochemically reduced with graphite [Cech 1974]. The reduction was found to occur via a two-stage, $\mathrm{CuO} \rightarrow \mathrm{Cu_2O} \rightarrow \mathrm{Cu}$, process. The efect of milling on the phase present as determined from quantitative analysis of X-ray diffraction patterns is shown in Fig. 4.11.

Examination of the powder using TEM method showed the as-milled particles contained copper crystallites of 15–30 nm in size.

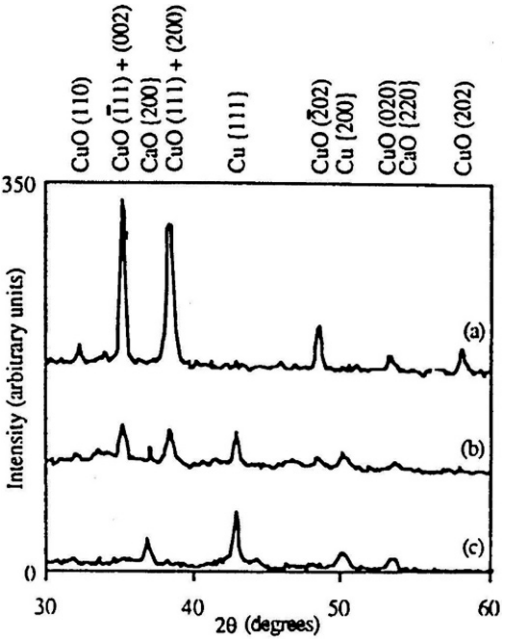

Fig. 4.10 X-ray diffraction patterns of the mixture of CuO+Ca as a function of milling time, (**a**) 7.5 min, (**b**) 60 min, (**c**) 1440 min [Schaffer and McCormick 1989a]

Italian researchers dealt with redox reactions in the Cu_2O+Me, and CuO+Me systems under self propagating regimes [Mulas et al. 2001]. Possible reaction schemes for the oxygen displacement in the studied systems are reported by equations

$$2Cu_2O + Me \rightarrow 4Cu + MeO_2 \tag{4.18}$$

$$2CuO + Me \rightarrow 2Cu + MeO_2 \tag{4.19}$$

where Me = Ti, Zr, Hf.

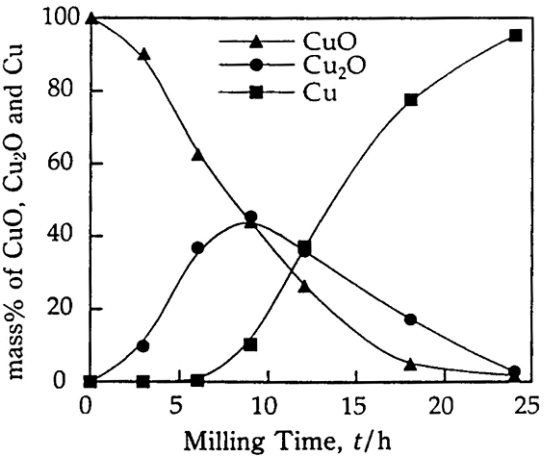

Fig. 4.11 Efect of milling time on the two stage reduction of CuO by carbon [Schaffer and McCormick 1989b]

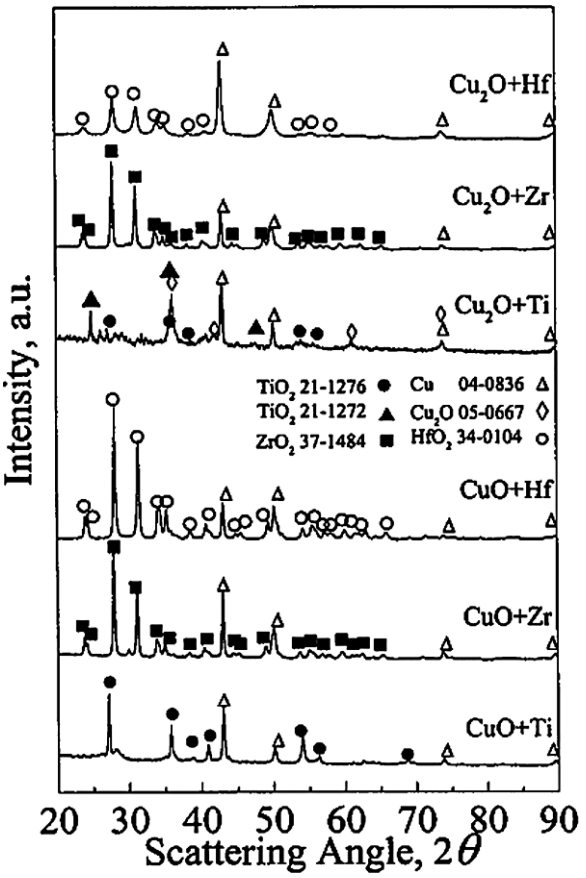

Fig. 4.12 X-ray diffraction patterns of copper oxides reacted systems [Mulas et al. 2001]

All these reactions are strongly exothermic and the values of reaction enthalpy ΔH are given in Table 4.7.

The almost complete transformation into products was definitely confirmed by XRD analysis of the combusted powders presented in Fig. 4.12. Almost in all cases, pure Cu and relative oxides are formed, while neither signals due to reaction precursors, nor intermediate phases are present.

In Fig. 4.13 ignition time, t_{ig} is plotted versus A_s. Value A_s is the work necessary to open a new surface area unit [Streleckij et al. 1996]. This correlation suggests that an active role is played by the metal partner in reaching a critical state of reactants dispersion before the ignition. Furthermore, a greater extention of fresh interface area is required to ignite the reaction in passing from Zr to Ti and to Hf, and therefore a proper amount of mechanical work, typical of the mechanical and elastic characteristic of each metal, must be done on the system to this end. Only when these conditions are met, the reaction spreads spontaneously, and the propagation can involve all the powder dispersed in the vial [Mulas et al. 2001].

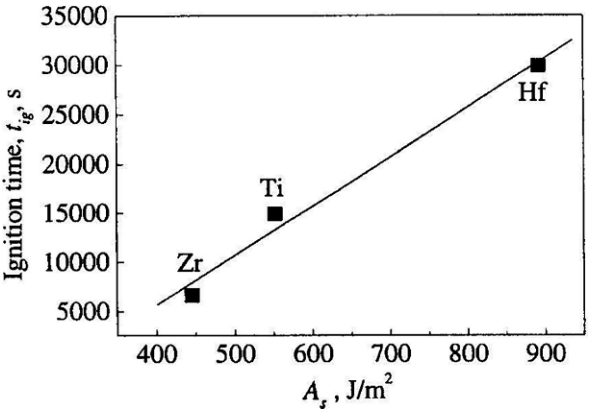

Fig. 4.13 Ignition time, t_{ig} as a function of the energy required to open a fresh interfacial surface, A_s [Mulas et al. 2001]

4.3.3.2 Iron Oxides

The reduction of hematite α-Fe_2O_3 by Al and Mg powder has been studied [Nasu et al. 1999]

$$Fe_2O_3 + 2Al \rightarrow 2Fe + Al_2O_3 \tag{4.20}$$

$$Fe_2O_3 + 3Mg \rightarrow 2Fe + 3MgO \tag{4.21}$$

The XRD patterns of hematite and Al powder are shown in Fig. 4.14 as a function of milling time.

The peak of α-Fe appeared suddenly at 1.8 ks of milling and, simultaneously, the peaks of starting materials disappeared. The same picture can be seen at Fig. 4.15

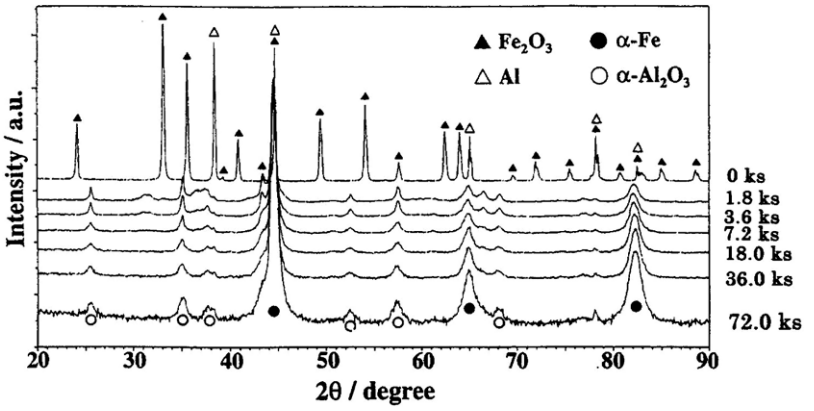

Fig. 4.14 X-ray diffraction patterns of the mixture Fe_2O_3+Al as a function of milling time in k_s [Nasu et al. 1999]

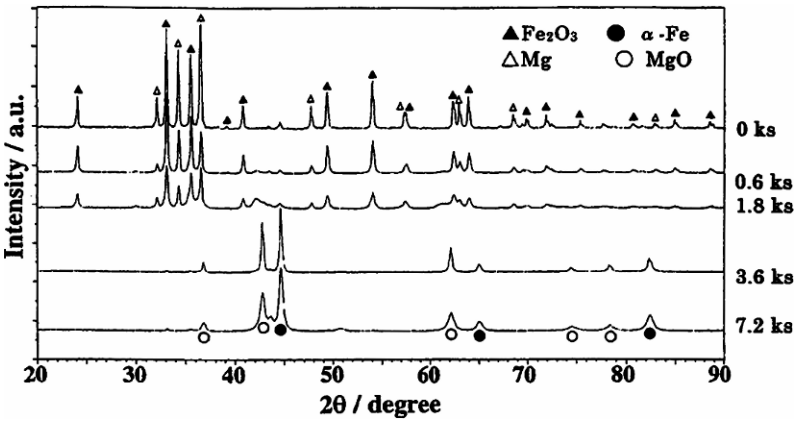

Fig. 4.15 X-ray diffraction patterns of the mixture Fe_2O_3+Mg as a function of milling time in k_s [Nasu et al. 1999]

where, together with the appearing of α-Fe the peaks for MgO can be seen. By the Mössbauer spectroscopy wustite-like phase, $Fe_{1-x}Mg_xO$ was also proved among the reaction products.

On the contrary in other paper more products in reaction (4.20) have been identified [Basset et al. 1994]. After the authors, the reduction of Fe_2O_3 with Al proceeds gradually with milling time and the reduction of hematite is accompanied by the formation of magnetite Fe_3O_4. The formation of Fe_3O_4 accompanies the reduction of hematite. The milling products are hercynite, $FeAl_2O_4$, an Fe-Al alloy (2–3% Al), α-Al_2O_3 and small iron clusters in alumina. The crystalline sizes of α-Al_2O_3 and of the Fe-Al alloy are below 15 nm after 6 h milling.

The mechanism and kinetics of reaction (4.21) has been studied [El-Eskandarany et al. 2001]. During the early stage of milling the Fe_2O_3 particles are embedded into soft matrix of Mg (reducing agent) particles to form coarse composite powders of the reactant materials. Increasing the milling time leads to the formation of fresh active surfaces of Mg which have high reducing potential and reacts with Fe_2O_3. After 120 hours the Mg powders are completely oxidized to MgO, whereas the $Fe_2O_3$is reduced successfully to metallic Fe.

The XRD patterns of the ball-milled hematite and magnesium powders are displayed in Figs. 4.16 and 4.17.

The kinetics of reaction (4.21) have been studied assuming the nucleation and crystal growth according to the Avrami equation

$$\sqrt[n]{-\ln(1-x)} = kt \tag{4.22}$$

where n is the order of the reaction and k is the reaction rate constant. From the calculated value of n and the behaviour of the experimental data is clear that reaction (4.21) is a first-order reaction. The reaction proceeds with one-dimensional growth and is diffusion controlled.

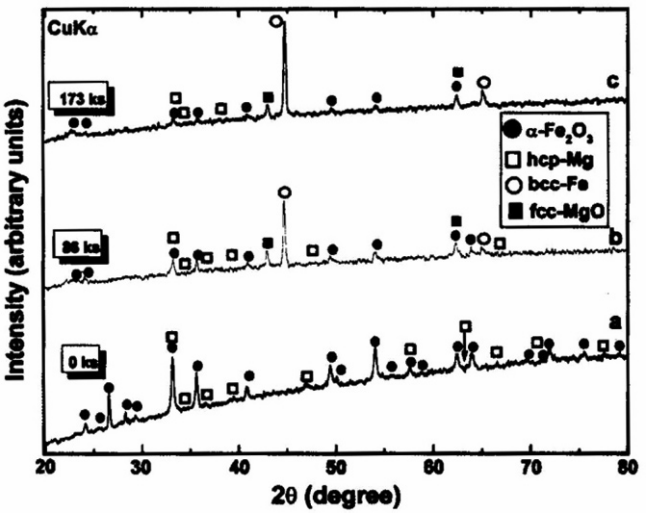

Fig. 4.16 X-ray diffraction patterns of the mixture Fe_2O_3+Mg as a function of milling time in k_s [El-Eskandarany et al. 2001]

The interest for new methods of preparation and properties of iron oxides stems from the fact that high-energy milling can lead to the preparation of new materials in magnetic materials technology.

A schematic representation of the iron oxides transformation is presented in Fig. 4.18 [Burkin 1966; Campbell et al. 1995]. Of concern here are the phases

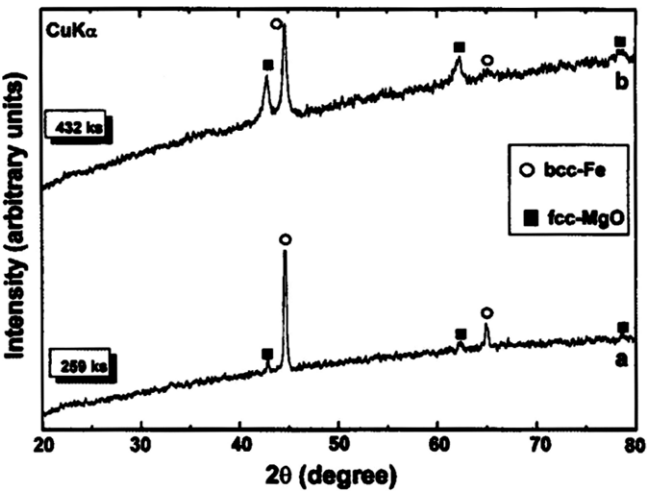

Fig. 4.17 X-ray diffraction patterns of the mixture Fe_2O_3+Mg as a function of milling time in k_s [El-Eskandarany et al. 2001]

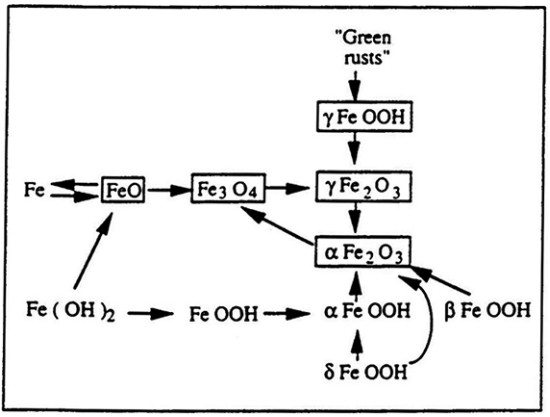

Fig. 4.18 A schematic diagram of the iron oxides transformations

magnetite Fe_3O_4, maghemite γ-Fe_2O_3 and hematite α-Fe_2O_3 that are "central" in this diagram. Phase transformations and reactions of Fe_2O_3 during milling were extensively studied [Lin et al. 1975; Senna and Kuno 1973; Nakatani et al. 1983; Kosmac and Courtney 1992; Matteazzi et al. 1993].

In the comprehensive investigation of the effects of a variety of dry and wet environments was concluded that the total phase transformation of α-Fe_2O_3 to Fe_3O_4 was best obtained by wet milling α-Fe_2O_3 in vacuum [Kaczmarek and Ninham 1994]. The mechanochemical reduction can be described by the equation

$$6Fe_2O_3 \rightarrow 4Fe_3O_4 + O_2 \tag{4.23}$$

Wet milling in low vacuum ($\sim 10^{-3}$ Pa) and by room temperature can be characterized as the fastest and total transformation hematite into magnetite. No other phases or contamination can be detected. It was suggested that oxygen bonds on the cleaved α-Fe_2O_3 oxide surface were broken during the milling and oxygen is released to the dispersing water and/or to the vial. It was also found that the oxygen pressure during the process as well the polar dispersing liquid or milling energy have a major influence on successful and fast phase transformation. All preparations performed in air, dry conditions or with hydrocarbons (benzene, anthracene) show the process of hematite reduction is non existent, or at last very slow. Normal air pressure and/or use of hydrocarbons suppress the oxygen release.

Mössbauer effect measurements have confirmed the transformation of α-Fe_2O_3 to Fe_3O_4on milling with no interdissolution of the phases. The milled products, of crystal block size $\sim$30 nm, exhibit hyperfine interaction parameters characteristic of the tetrahedral and octahedral sites of bulk Fe_3O_4.

The process of hematite-magnetite transformation has been verified with mechanically activated steelmaking dust where hematite was the main component (Fig. 4.19) [Baláž et al. 2001c].

Magnetite Fe_3O_4 shows mechanically induced self-sustaining reactions (MSR) [Takacs 2002]. The reaction of $Fe_3O_4$with zirconium

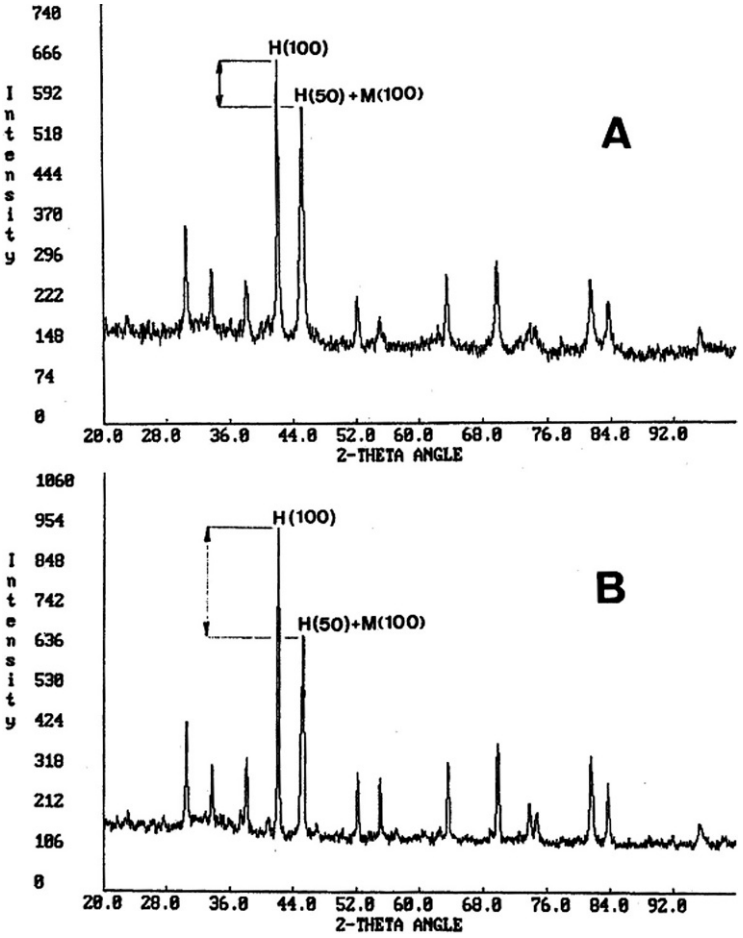

Fig. 4.19 The increase of magnetite Fe_3O_4 (M) in comparison with hematite α-Fe_2O_3 (H) in X-ray diffraction patterns for mechanically activated steelmaking dust, (**A**) sample milled in a planetary mill, (**B**) as received sample [Baláž et al. 2001c]

$$Fe_3O_4 + 2Zr \rightarrow 3Fe + 2ZrO_2 \tag{4.24}$$

has a typical temperature jump (Fig. 4.20) with three reaction steps

- the first 110 sec in the activation period, during which size reduction and mixing take place, chemically active sites are created, but very little product is formed. By the end of the activation period, the powder reaches a critical state
- ingnition occurs between two colliding balls or a ball and the wall of the vial and a combustion front propagates through the powder charge. Compared to the rest of the process, this step is almost instantaneous. The release of the reaction heat results in an abrupt increase of the temperature and

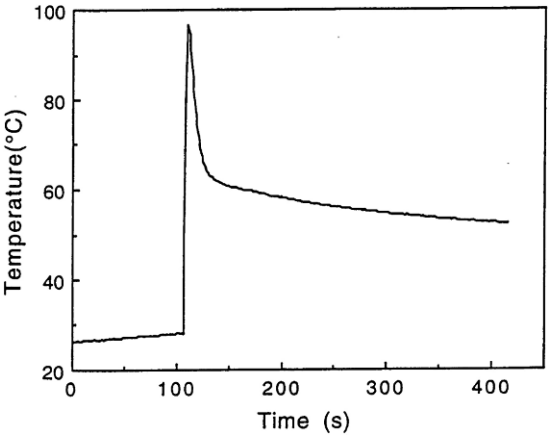

Fig. 4.20 Temperature of the milling vial during the mechanochemical reduction of Fe_3O_4 with Zr [Takacs 2002]

- the reaction is often incomplete immediately after the self-sustaining process. Continued milling is needed to obtain fully reacted product with uniform structure and properties [Takacs 2002].

4.3.3.3 Non-Ferrous Oxides

There is considerable interest in the synthesis of composites of non-ferrous metals for various applications such as conductive coatings, catalysis and energy sources (batteries).

One of the major components in alkaline batteries is γ-MnO_2. This phase is also present in Li-batteries as the intercalation host. The major commercial route to γ-MnO_2 is by electro-oxidation of purified $MnSO_4$ solution on Ti anodes. The crude solution is commercially prepared from natural Mn ores via thermal reduction to soluble MnO using carbon as reductant. In general, carbon reduction has been examined at $>1100°C$ with resultant formation of carbide phases. Lower temperatures have been examined, but these have used hydrogen, carbon monoxide or methane as reductant [Welham 2002].

It has been shown previously [Welham 1996, 1997, 1998a, 2000] that the rate of carbothermic reduction reactions can be greatly increased by premilling the mineral and carbon together when compared with powders milled separately and then mixed. This rate increase leads to a larger amount of material reduced per unit time and therefore increases the throughput of the thermal reduction stage by the simple addition of a mill prior to the kiln.

Premilling of manganese ore, comprised of cryptomelane KMn_8O_{16}, braunite Mn_7SiO_{12} and an unidentified Mn-phase with graphite led to enhanced reduction at decreased temperatures. The longer premilled powder showed complete reduction to MnO within 30 min at 600°C, the unmilled powder showed Mn_3O_4 as the major phase after 30 min at 800°C [Welham 2002].

Tin and antimony compounds are attractive candidates for advanced materials because of their unique electrical and electrochemical properties. For example, antimony compounds have been investigated as possible superconducting materials due to their semiconductor nature. Likewise, in an experiment on tin oxide anodes, it was discovered that, during lithium alloying, the oxide is chemically reduced resulting in the formation of Li_2O clusters surrounding nanosized clusters of tin [Courtney and Dahn 1997; Parson et al. 2000; Patel et al. 2004].

The mechanochemical reduction of tin and antimony oxides by silicon proceeds according to equations

$$2SnO_2 + Si \rightarrow 2Sn + SiO_2 \tag{4.25}$$

$$2Sb_2O_3 + 3Si \rightarrow 4Sb + 3SiO_2 \tag{4.26}$$

After 170 min of milling tin oxide, and 230 min of milling antimony oxide, the above reactions progressed to completion. The non-ferrous metal/insulator composites were analyzed by X-ray diffraction (Fig. 4.21).

The X-ray patterns of the fully reduced metal oxides indicate only peaks corresponding to tin or antimony metals. The results indicate the metal oxides are chemically reduced. However, the formation of silica (SiO_2) is not obvious from XRD results, although it is possible that the silica is amorphous. FTIR analysis clearly indicates that the silicon fully consumes the oxygen with typical asymmetric stretching of the silicon-oxygen bond occuring at 1060–1080 cm^{-1}. The particle size 156 nm and 173 nm have been estimated using Scherrer equation for tin and antimony metal, respectively. Based on SEM analysis it was shown that the homogeneous metal/insulator composite was formed and the composite particles were less than a micron [Patel et al. 2004].

The mechanochemical reduction of tin oxide has also been studied [Boldyrev and Avvakumov 1971; Avvakumov et al. 1974; Avvakumov and Strugova 1974; Varnek et al. 1974; Butyagin et al. 1974; Avvakumov et al. 1975]. Tungsten, silicium and aluminium have been applied as reducing metals

$$2SnO_2 + 2W \rightarrow 3Sn + 2WO_3 \tag{4.27}$$

$$SnO_2 + Si \rightarrow Sn + SiO_2 \tag{4.28}$$

$$3SnO_2 + 4Al \rightarrow 3Sn + 2Al_2O_3 \tag{4.29}$$

Tin in form of β-Sn has been registered as reduced metal in products of reactions (4.27–4.29). The kinetics of reactions is shown in Fig. 4.22.

A new geometry was proposed and explored for the investigation of mechanochemical reduction of lead, copper and tungsten oxides with Al as the reducing metal [Torosyan and Takacs 2004]. Instead of starting with a mixture of two powder reactants, aluminium is introduced in the form of plate attached to the inside wall of the milling vial and only the oxide is milled in a powder form.

The suggested "powder-plate" geometry was applied to oxi-reduction reactions between a 1-mm thick aluminium plate and the oxide powders PbO, CuO and WO_3. The reactions are

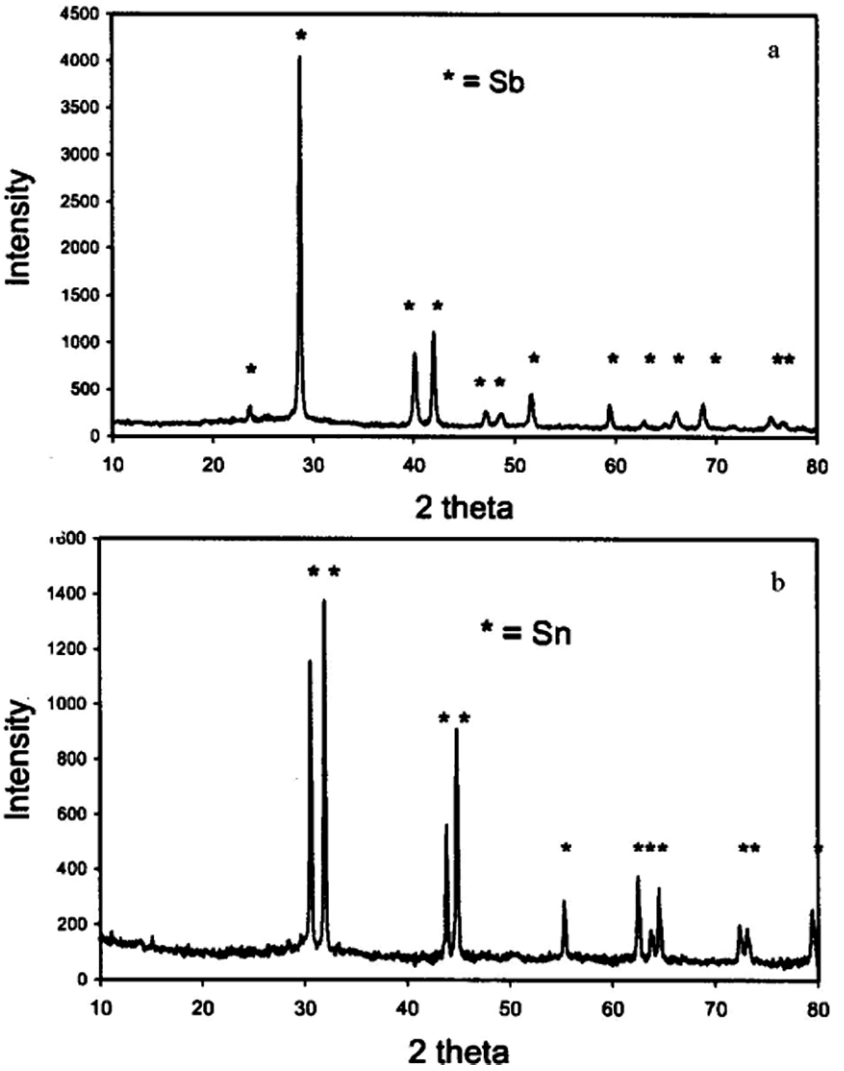

Fig. 4.21 X-ray diffraction patterns of: (**a**) the as-milled powder obtained after milling Sb_2O_3 and Si for 230 min and (**b**) the as-milled powder obtained after milling SnO and Si for 170 min [Patel et al. 2004]

$$3PbO + 2Al \rightarrow 3Pb + Al_2O_3 \tag{4.30}$$

$$3CuO + 2Al \rightarrow 3Cu + Al_2O_3 \tag{4.31}$$

$$WO_3 + 2Al \rightarrow W + Al_2O_3 \tag{4.32}$$

XRD patterns reflect the deposition of the oxide powder onto the Al plate as well as its chemical interaction with the plate. The products of reactions (4.30–4.32) are clearly visible [Torosyan and Takacs 2004].

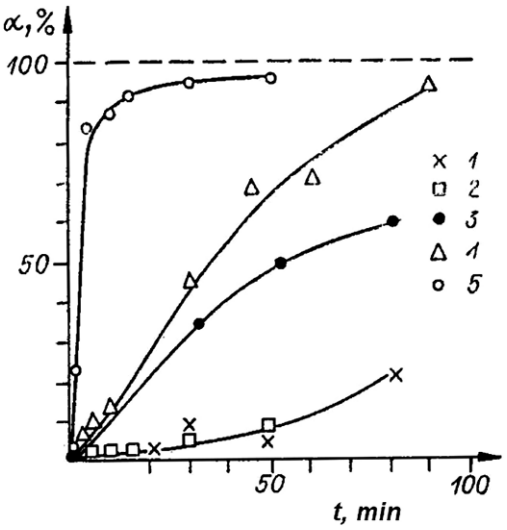

Fig. 4.22 Kinetics of mechanochemical reduction of SnO_2 by various reducing elements: 1 – without reducing element, 2 – carbon, 3 – W, 4 – Si, 5 – Al [Avvakumov et al. 1975]

The above method can be extended from the investigation of metal oxide mechanochemical redox reactions to other systems such as the formation of a carbide layer when milling graphite in the presence of a metal plate. This arrangement may also lead to useful technologies for the mechanochemical preparation of coatings [Takacs 1996a; Torosyan et al. 2002].

A different approach has been applied by Urakajev et al. who used for performing the mechanochemical reactions a reactive wear from milling balls instead of static reducing metal plate [Urakajev et al. 2001, 2003, 2004].

Precursors of redox reaction (4.33) have been mechanically activated and then the onset temperature has been studied

$$3TiO_2 + 13Al \rightarrow 3TiAl_3 + 2Al_2O_3 \tag{4.33}$$

This temperature was observed to decrease from 1050 to 660°C after 5 hours of milling. Increasing the milling time to 100 h decreased the onset to 560°C [Welham 1998b, c].

The XRD traces are shown in Fig. 4.23.

Clearly, after 100 hours of milling, there is no evidence of reaction with only peaks for Al and rutil TiO_2 present. The longer milling times caused a broadening of all the peaks indicating that a decrease in the crystallite size and an increase in the lattice strain was occuring. The crystallite size for Al decreased more rapidly than for rutile, as it has been stated in literature [Koch 1991; Gaffet and Harmelin 1990; Weeber and Bakker 1998] that in two phase milling systems the softer material amorphises more rapidly. Elemental mapping of the powders showed that milling for 5 hours caused significant intermixing between the original phases which was not evident at shorter milling times. The reaction became net exothermic after 5 hours

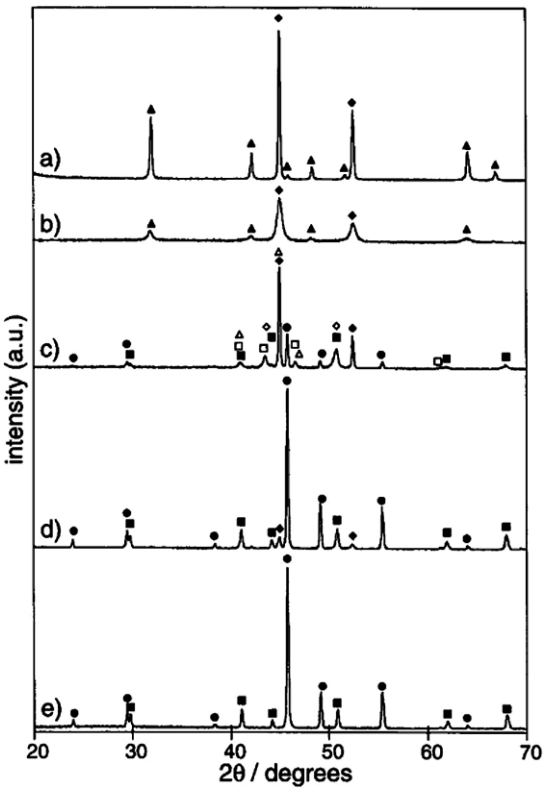

Fig. 4.23 X-ray diffraction patterns of 3:13 molar ratio TiO_2+Al, milling time 1 h (**a**) and 100 h (**b**) respectively; (**c**) and (**d**) 1 h milled powder heated to 900°C and 1200°C, respectively; (**e**) 100 h milled powder heated to 1200°C. ♦ Al, ■ Al_2O_3, • $TiAl_3$, □ Ti, ❖ TiO, Δ Ti_2O [Welham 1998a]

of milling turning from an endothermic process into a potentially self-propagating reaction once the initial thermal reaction has started.

Overview of mechanically induced redox reactions performed with oxides is given in Table 4.7.

The new method has been developed for preparation of nanocrystalline compounds by redox reaction of corresponding oxides with elements [Zhang et al. 2001; Saito et al. 2004]. The method is based on co-milling of corresponding oxide with sulphur and iron and stimulation of solid-state reaction to form nonferrous metal sulfides and iron oxides

$$4\mathrm{MeO} + 4\mathrm{S} + 3\mathrm{Fe} \rightarrow 4\mathrm{MeS} + \mathrm{Fe_3O_4} \tag{4.34}$$

where Me = Zn, Pb, Cd.

Comparison of ΔG^0 changes for reactions of type (4.34) and possible iron sulfide formation is summarized in Table 4.7. The thermodynamic data indicate not only the negative changes in ΔG^0 values but also higher thermodynamical probability for metal sulfidization in comparison with the iron sulfide formation.

4.3.3.4 Mechanism of Redox Reactions in Oxides

In most solid-state reactions, the reaction volume continually diminishes as the reactants become spatially separated by products. The chemical kinetics of these reactions are therefore determined by the diffusion rates of the reactants through the product phases, and the activation energy for the reaction is that for the diffusion of the reactant through the products [Carter 1991]. The reaction is therefore generally controlled by factors which influence diffusion rates. These include defect structures, defect densities and local temperatures.

Apart from diffusion, reaction rates are influenced by initial contact areas. However, for most solid-state process, the initial contact area is fixed and diffusion is the rate-limiting step. It is for this reason that solid-state reactions are so temperature dependent and that the reactions are thermally induced. The reaction interfacial area is not only dependent on initial contact areas but increases during milling [Schaffer and McCormick 1992b]. Furthermore, this increased reaction interface area is dynamically maintained during milling as the precursors are continuously broken up during fracture events. Moreover, diffusion rates are substantially increased in mechanically treated substances. This arises from the large number of crystal defects introduced through plastic deformation, which allows significant diffusion to occur at room temperature [Schaffer and McCormick 1991]. Diffusivities in nanocrystalline particles can be many orders of magnitude higher than both lattice and grain boundary diffusion in conventional polycrystalline materials [Karch et al. 1987).

The redox mechanochemical reactions are typical example of ductile (metal)/brittle (metal oxide) systems. In these systems the brittle constituent becomes evenly distributed through the ductile metal reductant powders at the beginning of redox reaction. However, the reaction will produce two new phases, one brittle and one ductile. Both reactants and products are evenly dispersed through the reaction volume at later stage of redox reaction. Particles are reduced to nanometer-sized crystallites and brought into intimate contact, thus greatly increasing reacting areas. The high defect densities induced in the powder further increase reaction rates by providing short circuit diffusion path [Schaffer and McCormick 1990].

In special cases, the combination of small particle size, high defect densities, and the effective of product from between the reactants caused the material to be brought to a critical precombustion condition when ignition can occur. This is the case of several redox reactions covered in this Chapter.

4.3.3.5 Ferrite-Type Complex Oxides

Spinel ferrites $MeFe_2O_4$ (Me is divalent cation) posess great potential for many applications. Owing to the flexibility of their spinel structure, these compounds provide a wide range of physical and chemical behaviour which can be tuned by mechanical activation [Pavlyuchin et al. 1981, 1982, 1983, 1984, 1988; Jermakov et al. 1982]. The spinel structure provides interstices of tetrahedral and octahedral coordination, part of which is occupied by Me^{2+} and Fe^{3+} cations. In general,

cations can reside on both types of sites, thus giving rise to a characteristic cation distribution [O'Neill and Navrotsky 1983, 1984]. The crystal structure of spinel ferrites can be formulated in greater detail as $(Me_{1-\lambda}Fe_{\lambda})\,[Me_{\lambda}Fe_{2-\lambda}]O_4$, where round and square bracket enclose ions on sites of tetrahedral and octahedral coordination, respectively, and where γ denotes the so-called degree of inversion. The most important changes occur during mechanical activation in the cation sublattice, which are manifested in the redistribution of bi- and trivalent cations over the tetrahedral and octahedral cavities. An annealing of spinel ferrites at 500–600°C results in the return of the cations to their typical positions so that the normal properties of these substances are restored [Boldyrev 2006].

The results on several mechanically treated spinel ferrites like $ZnFe_2O_4$, $MgFe_2O_4$, $CuFe_2O_4$, $MnFe_2O_4$, $NiFe_2O_4$ and $CoFe_2O_4$ have been recently summarized [Šepelák et al. 2005]. Several interesting properties were determined, e.g. superparamagnetism, an enhanced chemical reactivity, an irreversible magnetic behaviour and an altered saturation magnetization in comparison with the corresponding bulk materials. As for reactivity, the hot-gas desulphurization tests have revealed that mechanochemically synthesized $ZnFe_2O_4$ posesses the highest sulfur absorption capacity when compared with the reactivity of the unmilled ZnO/Fe_2O_3 mixture as well as with the reactivity of milled $ZnFe_2O_4$ that was prepared by the conventional thermal method [Šepelák et al. 1997].

The application of high-energy milling to the chemical reduction of spinel ferrites has been reported in several papers [Takacs 1993; Takacs and Pardavi-Horvath 1994; Sorescu 1988; Botta et al. 2000; Šepelák and Becker 2000; Menzel et al. 2001; Shi and Ding 2001; Goya et al. 1998].

The high-energy milling of $NiFe_2O_4$ in a steel vial using steel balls was found to induce a mechanochemical reduction process of the material leading in a redox process to the formation of a disordered solid solution of FeO and NiO with wüstite structure [Menzel et al. 2001; Shi and Ding 2001]. To determine the phase evolution of $NiFe_2O_4$ during high-energy milling the mechanochemical reduction was followed by X-ray powder diffraction. The XRD-pattern of the non-activated sample (Fig. 4.24) is characterized by the sharp crystalline peaks corresponding to $NiFe_2O_4$ (JCPDS 10-0325). During the early stage of milling, XRD reveals only a decrease of the intensity and an associated broadening of the Bragg peaks of the spinel. This reflects the formation of the disordered state with a small crystallite size and with internal strain introduced during the mechanical treatment. With increasing milling time, changes in diffraction intensities are observed. This can be attributed to the formation of a solid solution of $Ni_{1-x}Fe_xO$ and of crystalline iron (JCPDS 06-0696) which are formed in addition to the formation of nanoscale ferrite particles. The fraction of the reduced phases increases with increasing milling time.

Mechanochemical reduction of magnesium ferrite $MgFe_2O_4$ has been studied [Šepelák et al. 2002]. The XRD pattern of the non-activated sample is characterized by the sharp peaks corresponding to $MgFe_2O_4$ (Fig. 4.25).

During the early stage of milling, XRD merely reveals a decrease of intensity and an associated broadening of the Bragg peaks of the ferrite. This reflects the formation of the disordered state with a small crystallite size and with internal strain

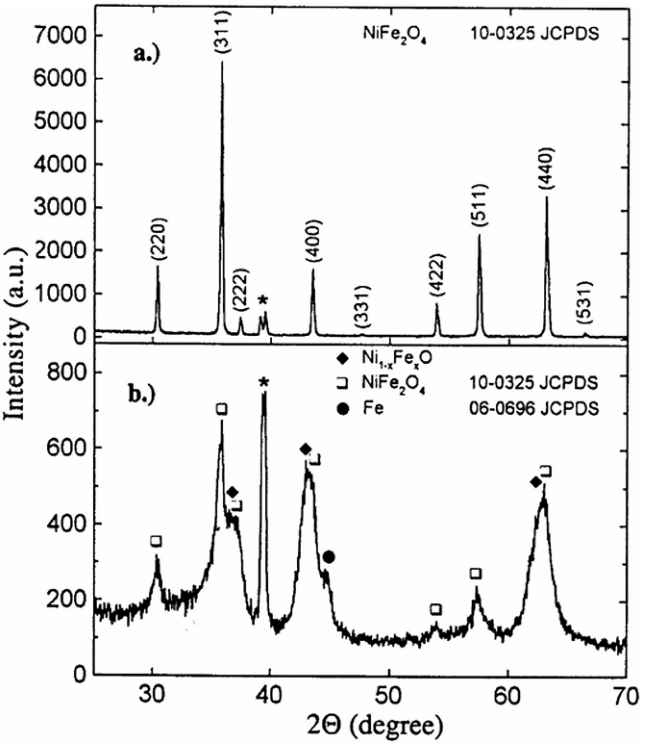

Fig. 4.24 X-ray diffraction patterns of (**a**) non-activated $NiFe_2O_4$ and of (**b**) $NiFe_2O_4$ activated for 20 min. Asterisk indicates a diffraction peak of the sample holder [Menzel et al. 2001]

introduced during the mechanical treatment. With increasing milling time, qualitative changes are observed in diffraction patterns of the samples. This can be attributed to the formation of a solid solution of $Mg_{1-x}Fe_xO$ which possesses the wüstite structure and of crystalline iron. It was concluded that both the solid solution of $Mg_{1-x}Fe_xO$ and the ferromagnetic Fe are predominantly obtained as the result of the mechanochemical reduction of $MgFe_2O_4$.

In the contact of a mechanistic analysis, it was concluded that the metallic nature of the vial and of the balls plays an essential role in the mechanochemical reduction process of $MgFe_2O_4$. It appears that also in case of ferrite-type complex oxides the event of mechanically induced redox reactions present novel opportunities for the nonthermal manipulation of such type of materials [Šepelák et al. 2002].

4.3.4 Wolframates

Tungsten carbide WC is probably the most common hard material in use today for cutting edges and other high strength applications [Welham 1999]. It is usually

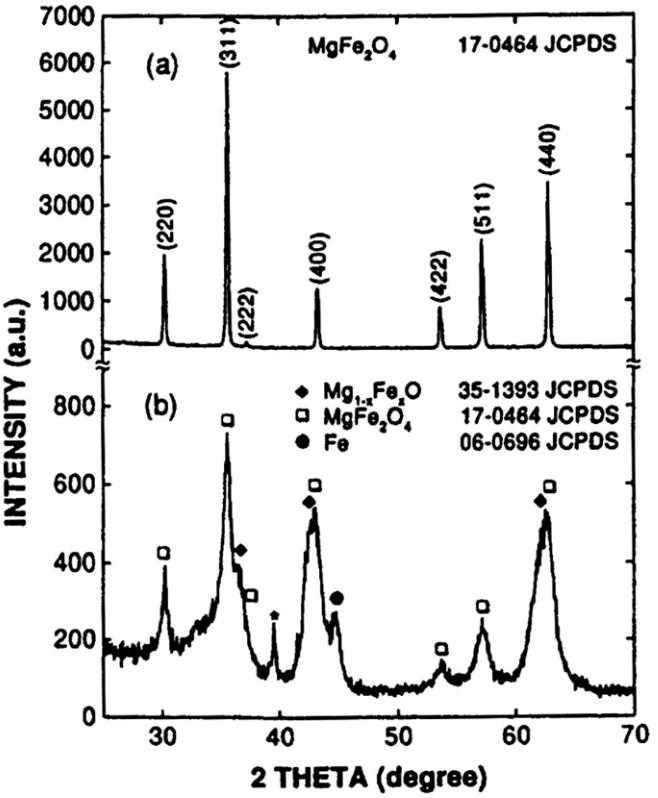

Fig. 4.25 X-ray diffraction patterns of non-activated $MgFe_2O_4$ (**a**) and of material mechanically treated for 20 min (**b**). [Šepelák et al. 2002]

made by a somewhat complicated route from either wolframite $FeWO_4$ or from scheelite $CaWO_4$ minerals. Previous attempts to produce WC directly have shown that the reduction is possible using excess carbon at temperatures $>1200°C$ [Terry et al. 1994].

Scheelite reduction has been tested by milling in a laboratory stainless steel ball mill. The XRD trace of the as-milled carbon bearing powder is presented in Fig. 4.26b.

Clearly, there has been a significant change from the original $CaWO_4$, shown in Fig. 4.26a. The peaks present seemed to be for MgO and W_2C. No calcium-bearing phase was apparently present, presumably due to a small crystallite size. After annealing for 1 h at 1000°C, trace (c) was obtained. There has been significant crystallite grows with narrower, more intense peaks now evident for both W_2C and MgO. After milling in nitrogen the XRD trace is much clearer. Figure 4.26d shows that the as-milled powder contains elemental W and MgO. The crystallite size of the tungsten was estimated to be 9.5 nm. Only the two main MgO peaks are evident.

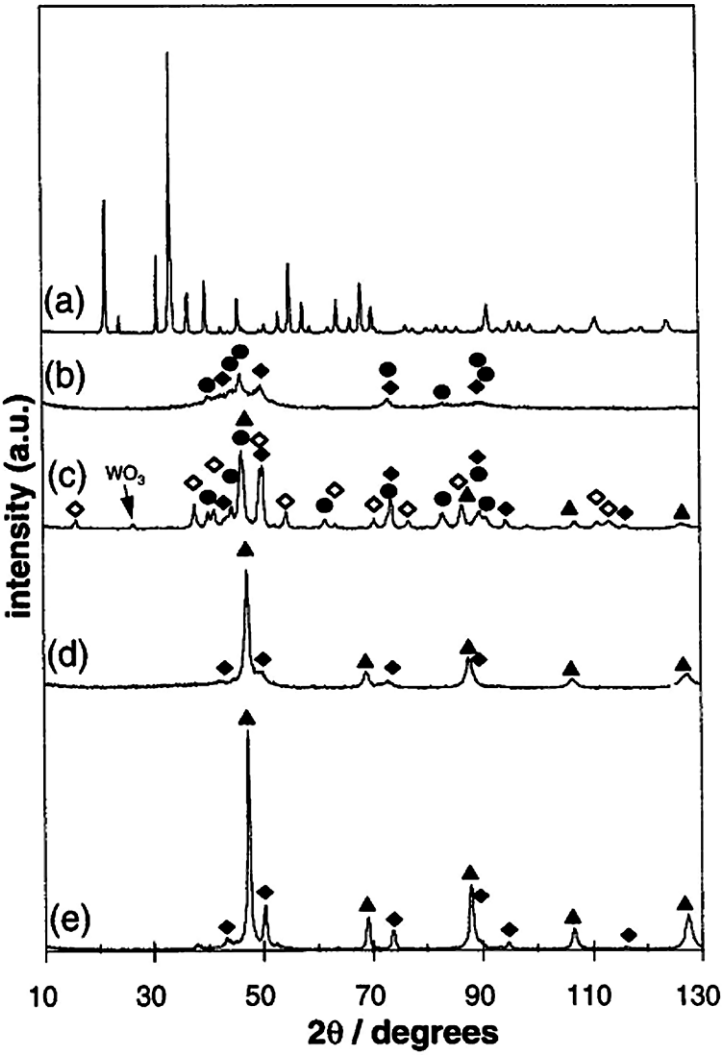

Fig. 4.26 X-ray diffraction patterns of $CaWO_4$ treatment: (**a**) milled for 1 h in vacuum, (**b**) milled for 100 h with carbon, (**c**) powder (**b**) heated for 1 h at 100°C in argon, (**d**) milled for 100 h under nitrogen and (**e**) powder (**d**) heated for 1 h at 1000°C in argon, ♦ W, ◆MgO, ◊ Fe_3W_3C, ■ WC, • W_2C, [Welham 1999]

These peaks are broad and comparatively weak, which is typical of phases that have a small crysatllite size. On heating this powder for 1 h at 1000°C in argon, the MgO peaks had narrowed considerably. The tungsten crystallite size increased to 21 nm. A simple acid leach of the powder removed all of the MgO, leaving behind either W_2C and Fe_3W_3C or W. The elemental tungsten formed was ∼99% W [Welham 1999].

4.3.5 Titanates

The mineral ilmenite $FeTiO_3$ is a huge resource of rutile TiO_2 for the production of titanium dioxide, which can be used directly as a pigment or in the manufacture of titanium. A number of methods have been proposed for extraction rutile from ilmenite [Chen et al. 1996]. However, most of them involve either a hot chemical process or a high temperature reduction process (Becher process). These processes are both expensive and complicated, and have many associated environmental implications. Therefore, the search for a simple and economic extraction method remains of high interest to industry [Henn and Barclay 1995].

Mechanochemical reduction of ilmenite $FeTiO_3$ by silicon Si has been described [Welham 1998d]. XRD traces for 2:1 $FeTiO_3$:Si powder milled under low and high intensity for up to 200 h are shown in Fig. 4.27.

After 100 h milling under low intensity trace (a) was obtained. The only peaks present are for $FeTiO_3$ and Si, although the peaks are somewhat wider and less intense than the feed powder due to crystallite size refinement. After a further 100 h of milling the trace (b) showed major changes, both $FeTiO_3$ and Si were absent with the only peak present due to elemental iron. The apparent absence of phases for both Ti and Si is probably due to an extremely small crystallite size and the presence of many phases each of low abundance.

Annealing of the 200 h milled powder for 1 h at 800°C under argon gave trace (c), clearly, peaks for TiO_2 have emerged along with a small peak for Si. There may be a small peak for SiO_2 at 305°C but it is overlapped by that of rutile and, in the absence of other SiO_2 peaks, no positive confirmation of quartz can be made. Thus, it would seem that the reaction had occurred after 200 h with the annealing stage causing recrystallization of nanocrystalline phases.

Under high intensity milling there was clearly Fe present after 50 h, trace (d), implying that the reduction of $FeTiO_3$ had started within 50 h. However, the presence of peaks for $FeTiO_3$ and Si show that the reaction was of relatively low extent. After 100 h of milling (e) shows that the reaction was apparently complete, neither $FeTiO_3$nor Si peaks were present, only those for Fe and TiO_2. Further milling to 200 h showed no significant changes in the XRD trace (f), other than a widening and weakening of the TiO_2 peaks as the crystallite size decreased [Welham 1998c].

The chemistry of the whole process of ilmenite reduction by silicon can be described [Chen et al. 1996].

$$2FeTiO_3 + Si \rightarrow 2Fe + 2TiO_2 + SiO_2 \tag{4.35}$$

$$Fe + xSi \rightarrow FeSi_x, x = 1 \text{ or } 2 \tag{4.36}$$

$$2nTiO_2 + Si \rightarrow 2Ti_nO_{2n-1} + SiO_2 \tag{4.37}$$

The final stage is the reduction of the remaining Ti-O compounds to a titanium silicide

$$Ti_nO_{2n-1} + (16n-5)Si \rightarrow 2nTi_5Si_3 + (10n-5)SiO_2 \tag{4.38}$$

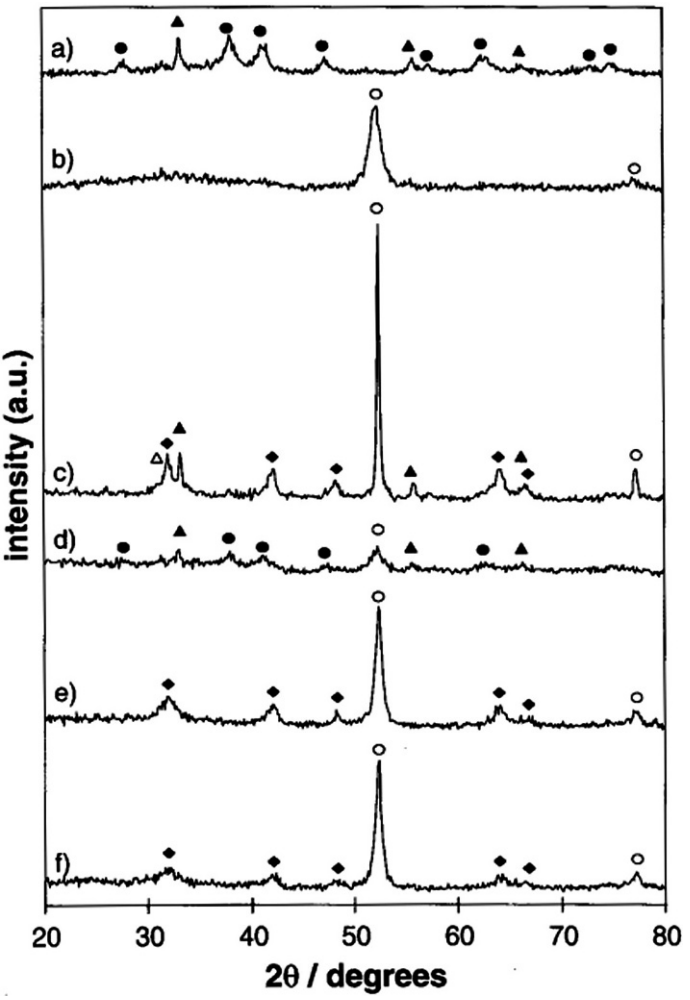

Fig. 4.27 X-ray diffraction patterns of 2:1 molar ratio $FeTiO_3$+Si milled for (**a**) 100 h, and (**b**) 200 h under low intensity, (**c**) sample b annealed for 1 h at 800°C under argon, (**d**) 50 h, (**e**) 100 h and (**f**) 200 h under high intensity; ♦ Si, ⧫ TiO_2, ● $FeTiO_3$, ○ Fe, Δ SiO_2 [Welham 1998c]

Mechanochemical reduction of ilmenite $FeTiO_3$ by sulphur has been studied by two groups in Australia [Henn and Barclay 1995; Welham 1998d]. The reaction has been suggested as a route to the formation of rutile and pyrrhotite in geological systems [Frost 1991]. Iron is known to have a very high affinity for sulphur, and a range of iron sulfides has been formed by milling elemental iron and sulphur together at room temperature [Baláž et al. 1995].

Thermodynamical calculation performed in work of Frost (1991) showed two ilmenite-to-sulphur molar ratios were worth investigating. A 3:2 ratio shows

$$3FeTiO_3 + 2S \rightarrow F_2O_3 + FeS_2 + 3TiO_2 \quad (\Delta G_{298} = -96.5\,kJ\,mol^{-1}) \tag{4.39}$$

The 4:7 ratio show

$$4FeTiO_3 + 7S \rightarrow FeSO_4 + 3FeS_2 + 4TiO_2 \quad (\Delta G_{298} = -231\,kJ\,mol^{-1}) \tag{4.40}$$

For 2:4 ratio the following reaction was suggested

$$2FeTiO_3 + 4S \rightarrow 2FeS_2 + O_2 + 2TiO_2 \tag{4.41}$$

The X-ray diffraction traces of the as-milled products (Fig. 4.28) show $FeTiO_3$ was still a major phase, present in all samples immediately after milling, although the peaks were somewhat less intense and broader then those of the original material. Elemental sulphur was present only in the products of the 4:7 ratio run and its absence in the other products may be due to either amorphization of reaction. TiO_2 was found to be present in all of the samples, but the level was similar to that previously observed as an impurity in the ilmenite starting powder and could not be confirmed as a reaction product [Welham 1998d].

The reaction between S and $FeTiO_3$ during ambient temperature milling was only evident in samples which were milled dry in an inert atmosphere, preferably under pressure. The reaction found to be incomplete, with the formation of FeS_2 and rutile TiO_2 and from industrial viewpoint is not viable. However, ilmenite milled

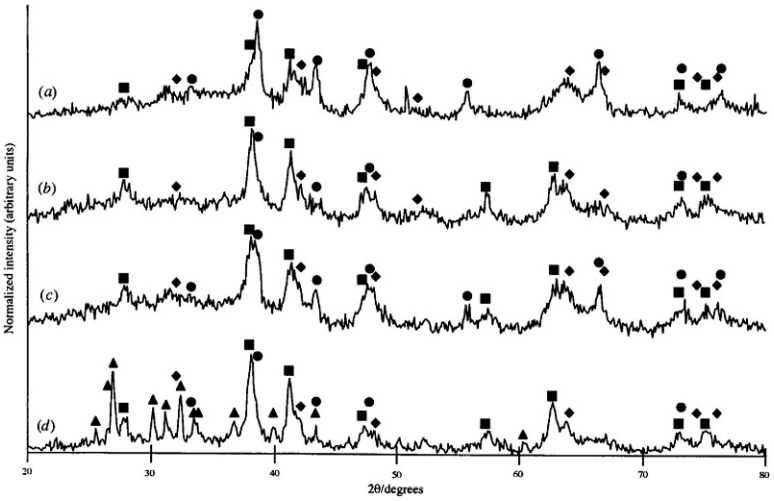

Fig. 4.28 X-ray diffraction patterns of as-milled powders, milling time 100 h. (**a**) 3:2 $FeTiO_3$+S ratio, 100 kPa He; (**b**) 3:2 $FeTiO_3$+S ratio, 5.0 ml H_2O, open to air; (**c**) 3:2 $FeTiO_3$+S ratio, dry vacuum; (**d**) 4:7 $FeTiO_3$+S ratio, dry, vacuum. ■ $FeTiO_3$, ♦ TiO_2, ♦ α-S, ● FeS_2 [Welham 1998d]

alone may prove to be a viable feedstock for a thermal reactor in which sulphur is maintained at a high partial pressure.

The observations show that the milling can be alternative to traditional processes. Obviously, further investigation is needed [Welham 1998d].

An ilmenite mineral and Al powder have been mechanically milled together for 100 h in a laboratory ball mill. The reaction

$$FeTiO_3 + 7Al \rightarrow FeAl_2 + TiAl_3 + Al_2O_3 \tag{4.42}$$

has been considered as a guide. The as-milled powder and an unmilled powder of identical composition were annealed at up to 1200°C and examined by X-ray diffraction and DTA methods. The unmilled sample showed Al melted prior to an exothermic reaction starting at ~ 850°C. In the milled powder the aluminium had been completely consumed below its melting point. The milled powder showed no thermal activity, other than a reversible phase transition at 1067 ± 4°C, indicating that reaction occured within the mill. The products of both powders were the same, $TiAl_3$, Fe_3Al_{13} and Al_2O_3, although in the milled powder these phases were nanocrystalline until annealing caused crystallite growth [Welham 1998e].

The mechanochemical reduction of $FeTiO_3$ and TiO_2 by Mg metal has been studied [Welham 1998f] for reactions

$$FeTiO_3 + Mg \rightarrow MgTiO_3 + Fe \tag{4.43}$$

$$MgTiO_3 + Mg \rightarrow 2MgO + TiO \tag{4.44}$$

$$TiO + Mg \rightarrow MgO + Ti \tag{4.45}$$

Rutil was predicted to be reduced to TiO, and then to titanium metal by reaction

$$TiO_2 + Mg \rightarrow TiO + MgO. \tag{4.46}$$

The phases present in the as-milled powder changed with the ratio $FeTiO_2$: Mg (Fig. 4.29a). The 1:1 ratio showed that the ilmenite and $MgTiO_3$ could both be present (the peak positions for these phases overlap considerably), the small peaks at $2\theta = 50$ and 52° indicate MgO and Fe respectively. As the ratio increased (Fig. 4.29b and 4.29c), $FeTiO_3$ peaks weakened and peaks for Fe and MgO become more intensive, this is due to the increasing reduction of $FeTiO_3$ to Fe and an unidentified titanium product. After milling, neither mixture of TiO_2 and Mg showed many XRD peaks (Fig. 4.29d and 4.29e). There was only the main TiO_2 peak and the two main peaks for MgO indicating that reduction had occured. The MgO peaks were much more intense than any other peak, implying the main phase present was MgO [Welham 1998f].

In a high temperature process ilmenite is purified by reduction to TiO_2 and elemental iron which is then leached to form an inpure TiO_2. The 88–92% TiO_2 is then chlorinated. To produce metallic titanium the chloride is reacted with molten Mg under an inert atmosphere. The further processes are needed to obtain metallic Ti [Welham 1998f].

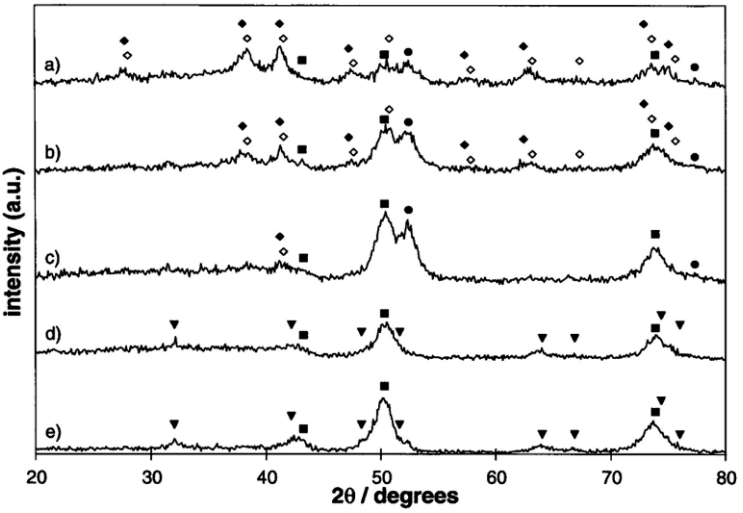

Fig. 4.29 X-ray diffraction patterns of as-milled powders, milling time 100 h. (a) 1:1, (b) 1:2, (c) 1:3 $FeTiO_3$+Mg ratio, (d) 1:1 and (e) 1:2 TiO_2+Mg ratio. ♦ $FeTiO_3$, ◊ $MgTiO_3$, • Fe, ■ MgO, ▼ TiO_2 [Welham 1998f]

4.3.6 Sulphides

Sulphides exhibit a great variety of chemical and physical properties. They display similar structural defects as oxides with cation vacancies, intersticial cations or anionic defects all possible. However, the concentration, structure and mobility of these defects are much more varied in the case of sulphides [Mrowec 1988].

The cationic vacancies change their properties according to conditions. For instance, their influence on electric properties and character of the chemical bond of sulphides is dependent on temperature [Vanjukov et al. 1978]. The formation of interesticial defects, in which metal ions are displaced from a normal lattice position to an intermediate position, depends on strength of the metal-sulphur bond. The Me-S and S-S bond in sulphides are similar to each other and the difference between them decreases with increasing temperature. However, if sulphur is released, the metal present in the normal crystallografic position remains without a partner and the defectiveness of sulphide increases. The influence of defects on solid state reactions is frequently more significant than the influence of the sulphide structure [Tkáčová 1989].

Sulphides play an important role in traditional technological applications as well as advanced materials (Table 4.8).

Solid state reactions of sulphides to prepare the elemental nanometals or their oxides proceed via two routes

$$Me_1S + Me_2 \rightarrow Me_1 + Me_2S \quad (4.47)$$

$$Me_1S + CaO \rightarrow Me_1O + CaS \quad (4.48)$$

Table 4.8 Sulphides in traditional technology and as advanced materials

Traditional applications		Advanced materials	
Chemical engineering		High-energy batteries	TiS_2
Hydrodenitrogenation	Co_9S_8	Solar cells	$CuInS_2$, FeS_2, CuS
Hydrodesulfurisation	MoS_2, WS_2	Diagnostic materials	Ag_2S
Dehydratation	MnS, CuS, ZnS	Luminiscence materials	ZnS, CdS: Mn, Cu
		Superconductors	La_2S_3, CuS
Mechanical engineering		Intercalates	TiS_2, TaS_2, NbS_2
Lubricants	MoS_2	Ion-selective sensors	PbS, CdS, CuS
		Optical coatings	ZnS
Extractive metallurgy		Photoconductors	ZnS, Ag_2S
Pyrometallurgy	Cu_3AsS_4, PbS	Lasers	CdS
Hydrometallurgy	$CuFeS_2$, ZnS, $Cu_{12}Sb_4S_{13}$	Photolithographic materials	As_2S_3
Biohydrometallurgy	FeAsS, FeS_2, ZnS	Holographic recordings	SnS
		Optical fibres	As_2S_3
Mineral processing		Infra-red detectors	PbS
Sulfidizers	Na_2S	High-temperature termistors	Cu_2S
		Quantum dots	$Cd_{1-y}Zn_yS$

In reaction (4.47) the reduction of the metal sulphide Me_1S is performed with a reducing element Me_2 (usually Fe, Mg, Al, Si) and is called redox reaction (see Chapter 4.3.1). The reaction (4.48) represents a displacement reaction. Sometimes combined effect of redox and displacement reaction is applied.

4.3.6.1 Thermal Treatment

It has to be mentioned that in modern technology reducing of sulphides by metals is practicized to a limited extent. The most frequently applied reducing agent is iron [Szczygiel et al. 1998]. The process is inefficient because the metal sulphide dissolves in the FeS formed. Nowadays it is used for the reduction of rich antimonite Sb_2S_3 ores or concentrates and to some extent for reduction galena PbS [Habashi 1986].

During the Industrial Revolution in Germany (1750–1850), antimony was sometimes obtained by heating the sulphide with scrap iron, which combined with sulphur and an alkali carbonate. The Sb was purified by fusion with a little antimony sulphide Sb_2S_3 and sodium carbonate Na_2CO_3 [Habashi 1993].

In principle non-metal reducing element can be applied. Reduction of PbS and $CuFeS_2$ by carbon in the presence of calcium oxide has been studied [Kharitidi et al. 1981, 1983].

Reduction of galena by solid carbon in the presence of CaO occured through stages of sulphide sublimation and reaction between the gaseous sulphide and CaO. Carbon did not participate in direct reduction but intensify PbS sublimation and reducing sulphur dioxide to S_2, CaS and CS_2

$$3PbS\,(g) + CaO \rightarrow 3Pb + 2CaS + SO_2 \tag{4.49}$$

Heating in helium to 1200°C at 10°/min were used for reaction (4.49).

Reduction of chalcopyrite $CuFeS_2$ with carbon in the presence of CaO was studied at 1100°C. The overall reaction is governed by the equation

$$CuFeS_2 + 2CaO + 2C \rightarrow Cu + Fe + 2CaS + 2CO \tag{4.50}$$

4.3.6.2 Mechanochemical Treatment

The concept of direct reduction of sulphides to metals by mechanochemical treatment was introduced by Soviet Scientists [Molčanov and Jusupov 1981]. The authors named the process *mechanometallurgy*. By dry milling of cinnabar HgS in a planetary mill equipped with copper vials and balls it was possible to obtain elementary mercury according to the following reaction

$$HgS + 2Cu \rightarrow Cu_2S + Hg \tag{4.51}$$

By the authors the reduction also proceeds in the course of milling of HgS in water using iron vials and balls

$$2HgS + 7H_2O \rightarrow 2Hg + H_2SO_3 + H_2SO_4 + 5H_2 \tag{4.52}$$

The transformations of selected sulphides by milling with the different metals have been studied. The solid state reduction of the sulphides have been performed by room temperature ball milling of powder mixtures [Matteazzi and LeCaër 1992b].

4.3.6.3 Reduction with Aluminium

The most results were obtained with aluminium as reducing element. The reaction of iron sulphide with Al

$$3FeS + 2Al \rightarrow 3Fe + Al_2S_3 \tag{4.53}$$

shows the predominant presence of patterns belonging to bcc α-Fe (Fig. 4.30) with some Al in it, since the lattice parameter $a = 0.2876$ nm is greater than that for pure

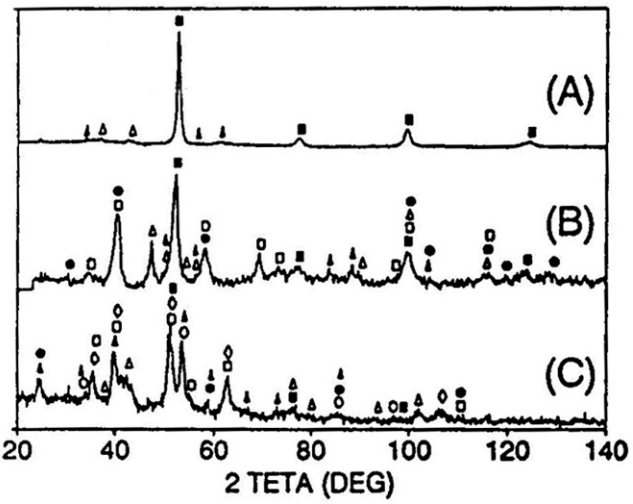

Fig. 4.30 X-ray diffraction patterns of as-milled powders, milling time 24 h. (**A**) 3:2 molar ratio FeS+Al; (**B**) 1:1 molar ratio FeS+Mn; (**C**) 2:1 molar ratio FeS+Si. Symbols: (**A**) ■α-Fe, Δ $FeAl_2O_4$, ▲ Al_2O_3; (**B**) ■α-Fe, Δβ-Mn, ▲γ-Mn,□ MnS, ● MnS_2; (**C**) ■α-Fe, ◊ FeS, □ $Fe_{1-x}S$, ▲ SiS_2, Δ WC, ○ FeSi, ● α-$FeSi_2$ [Matteazzi and LeCaër 1992b]

α-Fe (a = 0.2866 according to JCPDS 6-694) to an Fe-Al alloy with about 7 at % Al. Further weak components are present in the pattern, corresponding to tetragonal Al_2S_3 (JCPDS 24-14) and cubic hercynite $FeAl_2O_4$.

The reaction of copper sulphide

$$3Cu_2S + 2Al \rightarrow 6Cu + Al_2S_3 \tag{4.54}$$

shows clearly the presence of the following products: fcc Cu with a lattice parameter a = 0.3617 nm very close to that of pure Cu (a = 0.3615 nm according to JCPDS 34-348) and crystallite size d = 23 ± 3 nm, γ-Al_2S_3 (JCPDS 34-348).

The reactions of cobalt, lead and zinc sulfides

$$3CoS + 2Al \rightarrow 3Co + Al_2S_3 \tag{4.55}$$

$$3PbS + 2Al \rightarrow 3Pb + Al_2S_3 \tag{4.56}$$

$$3ZnS + 2Al \rightarrow 3Zn + Al_2S_3 \tag{4.57}$$

shows common X-ray diffraction patterns (Fig. 4.31). The patterns reveal, that cobalt sulphides and Al are no longer present and cobalt metasl is present in hexagonal as well as cubic form. Among products Al_2S_3 and cobalt aluminide Co_2Al_5 were identified. For reaction (4.56) Al lines are no longer present and cubic Pb, mixture of hexagonal Al_2S_3 and cubic Al_2S_3 have been formed. For reaction (4.57) the starting ZnS powder was constituted mainly by cubic β-ZnS (sphalerite) and a small amount of hexagonal ZnS (wurtzite). There remains some β-ZnS, while both

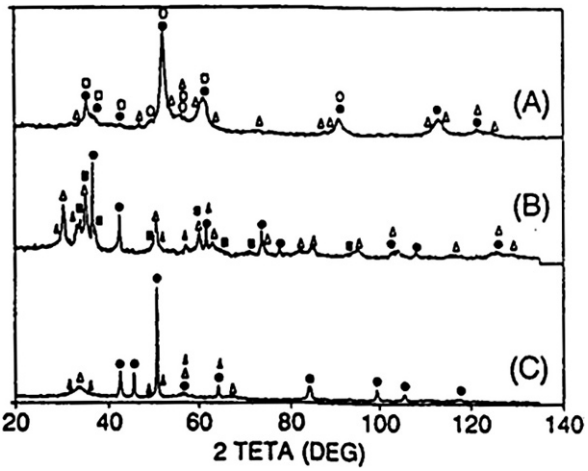

Fig. 4.31 X-ray diffraction patterns of as-milled powders, milling time 24 h. (**A**) 3:2 molar ratio CoS+Al; (**B**) 3:2 molar ratio PbS+Al; (**C**) 3:2 molar ratio ZnS+Al. Symbols: (**A**) • Co (cub); (**B**) • Pb; (**C**) – Zn; ○ Co (hex), ▲ Al_2S_3 (hex), □ Al_2S_3 (tetr), ■ Al_2S_3 (cub); (**A**) $-\Delta$ Co_2Al_5, (**B**) $-\Delta$ PbS, (**C**) $-\Delta\beta$-ZnS [Matteazzi and LeCaër 1992b]

the reaction products according to reaction (4.57) are present: hexagonal Zn (most intense pattern) of $d = 32 \pm 5$ nm crystallite size and hexagonal Al_2S_3. As for the two previous cases, a Zn-Al_2S_3 nanocomposite has been obtained.

It was concluded by the authors the reduction of metal sulphides by room temperature ball milling with a suitable reducing agent has been shown to be feasible. The feasibility of a particular reaction by mechanical activation appears not to be limited to negative free energy or enthalpy as shown for FeS reduction by silicium. Metal-(alloys)-(intermetallic compounds)-sulphide nanocomposites are obtained in this way with crystallite sizes in the range 10–30 nm. The ball milling-induced reduction of molybdenite MoS_2 by Al has been investigated in paper [Takacs et al. 2006]. The reduction takes place according to the equation

$$3MoS_2 + 4Al \rightarrow 3Mo + 2Al_2S_3 \tag{4.58}$$

The kinetics of reaction (4.58) is given in Fig. 4.32.

The graph clearly shows that most of the reaction takes place between 20 min and 60 min and it is practically complete after 120 min of milling. Although the reduction of MoS_2 with Al is a highly exothermic reaction that was expected to progress in the form of a self-sustaining process, ignition could not be achieved by ball milling. It is suggested that the reason is in the lubricant property of MoS_2. It prevents the formation of large composite agglomerates where the conditions for the initiation and propagation of the reaction would support MSR. The existing agglomerates are porous and they start breaking up before the reaction could accelerate.

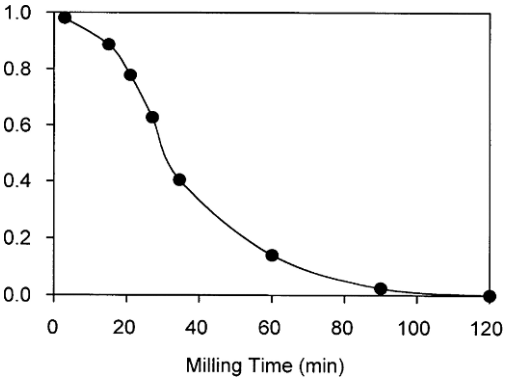

Fig. 4.32 The kinetics of MoS_2 consumption as a function of milling time [Takacs et al. 2006]

4.3.6.4 Reduction with Iron

Several papers have been published using iron metal as reducing element for mechanically induced solid state reduction by sulfides [Baláž et al. 2002a, b, 2004a, b, c, 2005a, 2007; Godočíková et al. 2004a, b].

The mechanochemical reduction of iron disulphide FeS_2 (pyrite) by elemental iron can be described by the simplified equation

$$FeS_2 + Fe \rightarrow 2FeS \tag{4.59}$$

The reaction is thermodynamically possible at ambient temperature, as the enthalpy change is negative. The value $\Delta H^{\circ}_{298} = -13.3\,\mathrm{kJ\,mol^{-1}}$ was calculated from the thermodynamic data.

Its progress with milling time is illustrated by selected XRD patterns in Fig. 4.33.

The process of product formation is clearly seen for samples milled for 25 and 45 min. Hexagonal troilite FeS (JCPDS 75-0602) has been indicated as the only reaction product. Figure 4.34 shows the room temperature magnetization data for investigated samples as a function of external magnetic field. It is evident that the resulting magnetization curves are well saturated after application of magnetic field higher than 2 T. The difference in the saturation magnetization of the samples milled for different times, as displayed in the inset of this Figure is mainly caused by a various amount of the ferromagnetic component in these samples. The inset shows that the amount of metallic iron decreases continuously for milling time up to 45 min. For longer milling time the saturation magnetization is negligible indicating that the constituent phases are almost entirely paramagnetic i.e. the reaction (4.59) tends to be finished.

The increasing paramagnetism can well be seen in Mössbauer spectra on Fig. 4.35a. Spectrum for sample milled for 5 min is a superposition of a doublet corresponding to FeS_2 and a sextet corresponding to Fe. The spectra during milling are changed and their analysis is given in Fig. 4.35b in the form of Mössbauer parameters dependence on the milling time. There are two characteristics sextets and

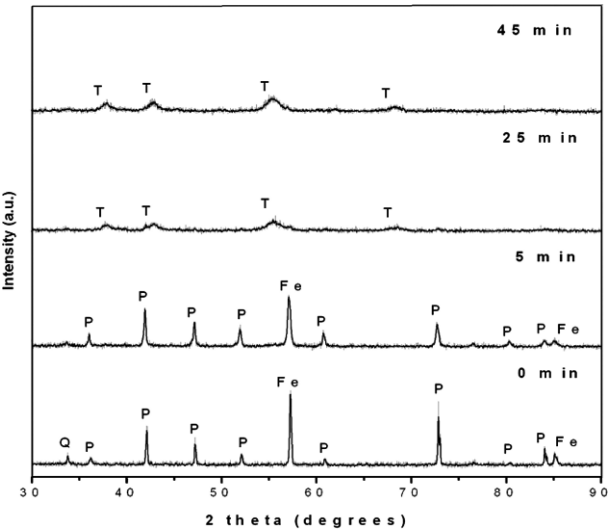

Fig. 4.33 X-ray diffraction patterns at different stages of reaction (4.59) as a function of milling time. T – troilite FeS, P – pyrite FeS_2, Q – quartz SiO_2 [Baláž et al. 2004a]

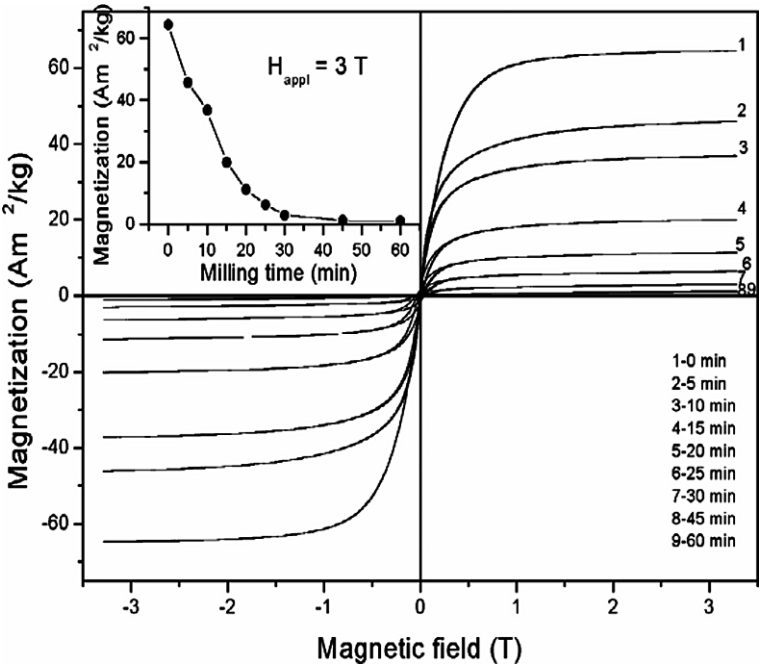

Fig. 4.34 Magnetization as a function of external magnetic field and/or of milling time for reaction (4.59) [Baláž et al. 2004a]

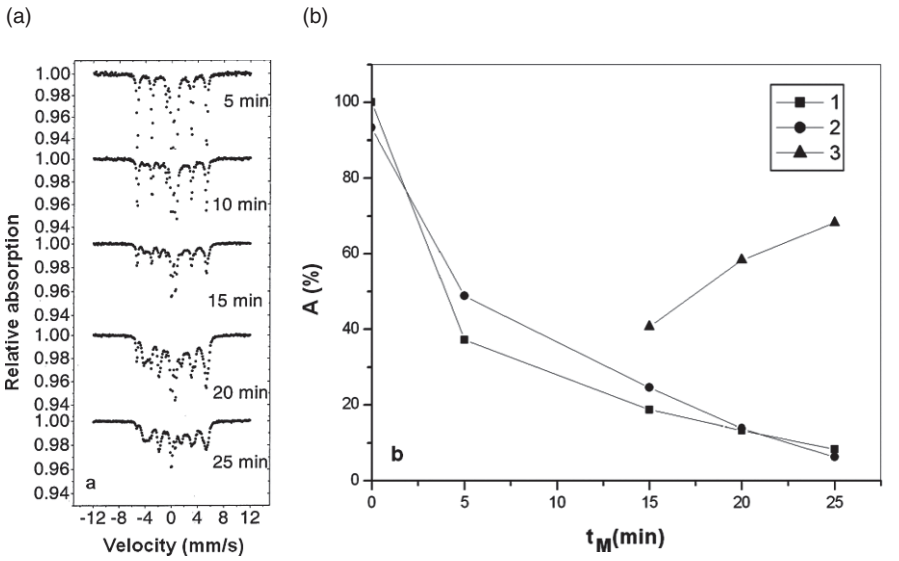

Fig. 4.35 (**a**) Mössbauer spectra for reaction (4.59); (**b**) Mössbauer parameters for reaction (4.59), A – total area of component, t_M – milling time; 1 – pyrite FeS_2 (doublet: IS = 0.31 mm s^{-1}, QS = 0.63 mm s^{-1}), 2 – Fe (sextet A: MF = 32.90 T), 3 – troilite FeS (sextet B: MF = 28.40 T), [Baláž et al. 2004a]

one doublet. The doublet with IS = 0.31 mm s^{-1} and QS = 0.63 mm s^{-1} corresponds to FeS_2 which is consumed during milling.

Elemental Fe which is also consumed, as can be seen from kinetics for sextet A with MF = 32.90 T. Beginning with t_M = 15 min, the new sextet B (MF = 28.40 T) has been identified with an increase in the total area component A. In accordance with XRD patterns in Fig. 4.33 and literature data [Matteazzi and LeCaër 1992b; Baláž et al. 2002b] this sextet can be described as troilite FeS. Stoichiometric FeS is antiferromagnetic with alternate layers of Fe atoms magnetized in opposite direction [Shuey 1975].

In the Mössbauer spectrum taken at 25 min, the traces of elemental Fe are still visible. However it is clear that antiferromagnetic troilite FeS is the dominant phase in the milled powders. From Fig. 4.34, it can be seen that this phase contributes only very little to the overall magnetization of our system.

The conventional high-energy temperature lead recovery process from lead sulphide PbS is based on reduction with iron scrap [Habashi 1986]. Recently, 92–94% lead recovery has been obtained by the direct reduction of lead sulphide with elemental iron in the temperature interval 1000–1150°C for 180 min [Szczygiel et al. 1998].

The mechanochemical reduction of lead sulphide with elemental iron under ambient temperature has been studied [Baláž et al. 2004b; Godočíková et al. 2004a,b].

The reaction can be described by the equation

$$PbS + Fe \rightarrow Pb + FeS \tag{4.60}$$

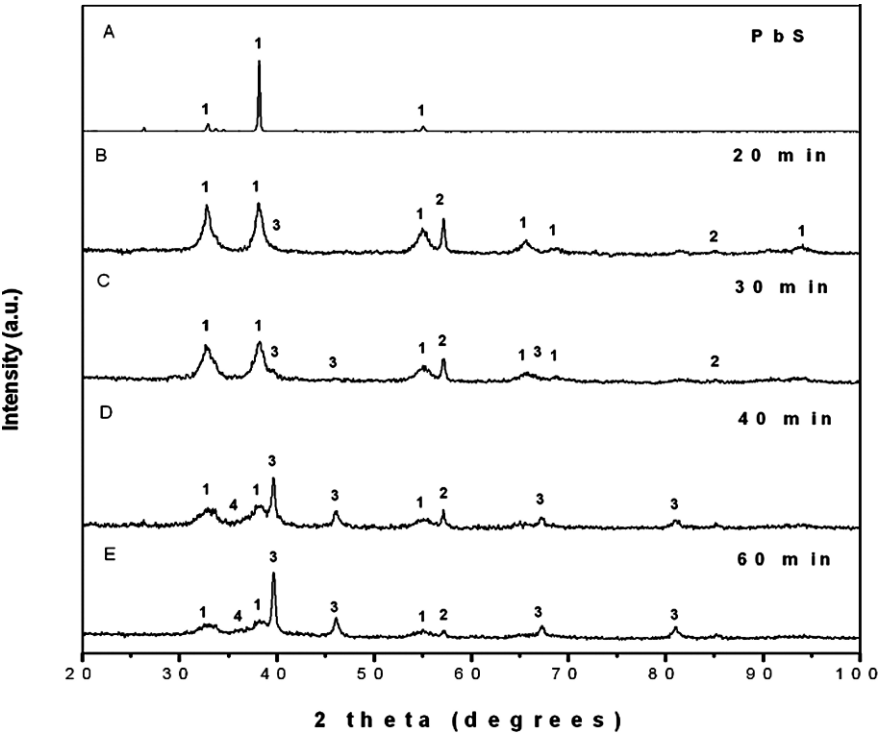

Fig. 4.36 X-ray diffraction patterns at different stages of reaction (4.60) as a function of milling time, A: PbS, B–E: PbS + Fe milled for 20–60 min (1 – lead sulfide, 2 – iron, 3 – lead, 4 – FeS (cubic)) [Godočíková et al. 2004b]

The reaction is thermodynamically possible at ambient temperature, as the enthalphy change is negative ($\Delta H^{\circ}_{298} = -1.3\,\mathrm{kJ\,mol^{-1}}$). The process is illustrated by the XRD patterns in Fig. 4.36.

The primary process – the reduction of lead sulfide by iron while lead metal and iron sulfide are formed – is clearly seen. After 20 min of milling, the relative amount of lead sulfide decreased and the lead is formed as indicated by the diffraction peak at 39.9° (JCPDS 04-0686). The process kinetics as described by the conversion degree, β is shown in Fig. 4.37.

Only 19% conversion to lead metal was achieved during the initial 20 min of milling. The intensity of the iron (JCPDS 06-0696) and lead sulphide (JCPDS 78-1897) reflections decreases upon continued milling, but these phases are detectable even after 60 min of milling. After 60 min, the reflections from lead metal and cubic FeS (JCPDS 23-1123) can be observed and 75% conversion to lead was achieved.

The reaction products are present in the form of nanocrystalline particles. Particle size of 13–21 nm for lead have been obtained. Figure 4.38 shows a typical TEM image of the polydisperse Pb/FeS nanoparticles formed by mechanochemical reduction of lead sulphide with iron during 60 min.

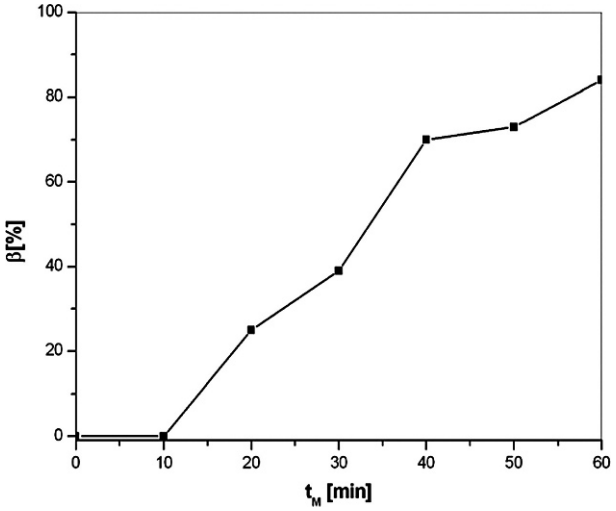

Fig. 4.37 Conversion degree, β for reaction (4.60) as a function of milling time, t_M [Godočíková et al. 2004b]

Examination of TEM shows that the as-milled powder is composed of spherical and rod-like particles. Dimensions of spherical particles are close to nanolead particle size determined by XRD.

It is evident from magnetic measurements (Fig. 4.39) that the magnetization curves are well saturated after the application of a magnetic field higher than 2 T.

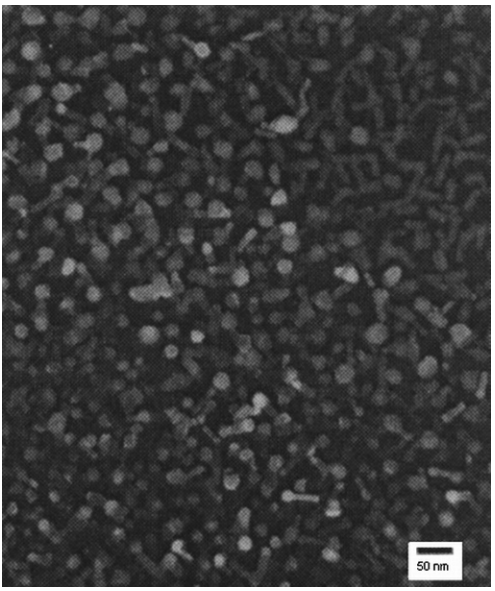

Fig. 4.38 TEM image of Pb/FeS nanoparticles formed by reaction (4.60) after 60 min milling [Godočíková et al. 2004b]

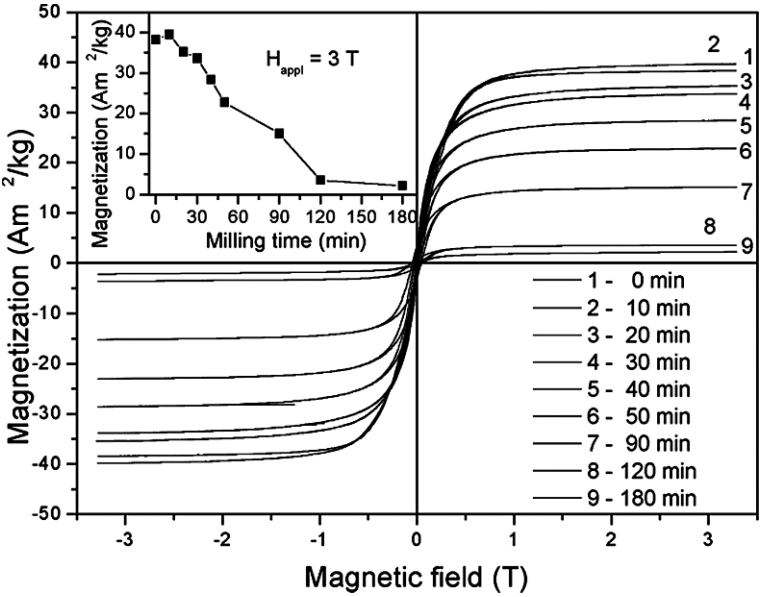

Fig. 4.39 Magnetization as a function of external magnetic field and/or of milling for reaction (4.60) [Godočíková et al. 2004b]

The difference in the saturation magnetization of the samples, as displayed in the inset of this Figure, is mainly caused by the different amount of the ferromagnetic component (bcc-Fe) in the milled samples. For longer milling times, the saturation magnetization is negligible indicating that the constituent phases are almost entirely paramagnetic and the mechanochemical reduction is completed.

The changes in the magnetic nature of the samples can be well seen in Mössbauer spectra in Fig. 4.40a. There is a small doublet in pattern of PbS which belongs to admixtured pyrite FeS_2. With the increasing milling time, the original sextet of iron hyperfine splitting is changing as well. The changes of Mössbauer parameters are given in Fig. 4.40b. Sextet A, with hyperfine magnetic field MF = 32.84 T originating from elemental Fe, is diminishing with milling time. For $t_M \leq 20$ min, iron is preferentially consumed by reaction with the present pyrite FeS_2 in sample and this reaction is thermodynamically more viable in comparison with the reaction (4.60).

Doublet with IS = 0.31 mm s^{-1} and quadrupole splitting QS = 0.59 mm s^{-1} correspond in accordance with literature, to FeS_2 [Marfunin and Mkrtčjan 1967]. At $t_M > 20$ min the formation of pyrrhotite $Fe_{1-x}S$ characterized by a sextet C (MF = 25.37 T) is evident and supported by the XRD patterns in Fig. 4.36. Pyrrhotite $Fe_{1-x}S$ sample rarely consist of only one structural type because at temperatures below 350°C the iron vacancies in the Fe-S system start to order producing a series of superstructures, which could exhibit antiferromagnetic, ferrimagnetic or paramagnetic behaviour. As an example, in our system at $t_M > 30$ min the formation of a further doublet have been observed. In accordance with literature this belongs to cubic

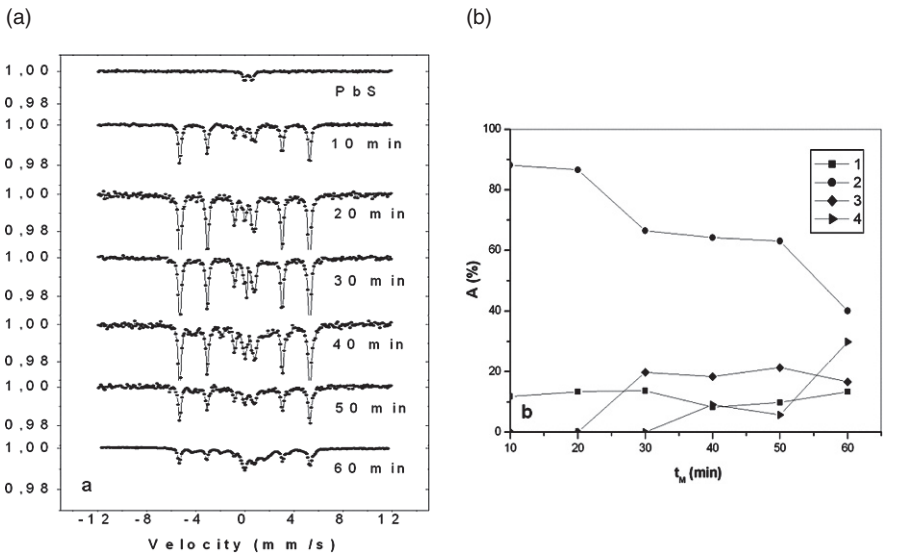

Fig. 4.40 a) Mössbauer spectra for reaction (4.60); b) Mössbauer parameters for reaction (4.60), A – total area of component, t_M – milling time; 1 – pyrite FeS_2 (doublet: IS = 0.31 mm s^{-1}, QS = 0.63 mm s^{-1}), 2 – Fe (sextet A: MF = 32.845 T), 3 – pyrrhotite $Fe_{1-x}S$ (sextet C: MF = 25.37 T), 4 – cubic $Fe_{1+x}S$ (doublet: IS = 0.85 mm s^{-1}, QS = 1.69 mm s^{-1}), [Baláž et al. 2004a]

$Fe_{1+x}S$ which is known only from synthetic studies. The magnetic characterization of the pyrrhotites thus presents a complex problem [Vaughan and Lennie 1991].

Conventionally, antimony sulphide Sb_2S_3 is reduced via high-energy temperature annealing in the presence of reducing agents such as hydrogen or iron. The reduction of antimony sulphide with hydrogen at atmospheric pressure and at temperature 473–873 K has been studied [Torma and Inal 1979]. Only 60% of Sb_2S_3 was converted to metallic antimony. The reduction with elemental iron is possible at temperatures 773–823 K but the process is inefficient because the metal sulphide dissolves in the already formed iron sulphide [Habashi 1986]. The yield of both processes is low, they need high temperatures and the products have large grain size.

The direct reduction of antimony sulphide has been studied [Baláž et al. 2007]. The reaction with elemental iron during milling proceeds at ambient temperature, according to the equation

$$Sb_2S_3 + 3Fe \rightarrow 2Sb + 3FeS \tag{4.61}$$

The reaction is thermodynamically feasible, as the enthalpy change for reaction under study is negative ($\Delta H^{\circ}_{298} = -116.7$ kJ mol^{-1}).

The progress of the mechanochemical reaction (4.61) is illustrated by the selected XRD patterns in Fig. 4.41. The process is rather straightforward with elemental antimony Sb (JCPDS 05-0562) and FeS (pyrrhotite-4H, JCPDS 22-1120) being the

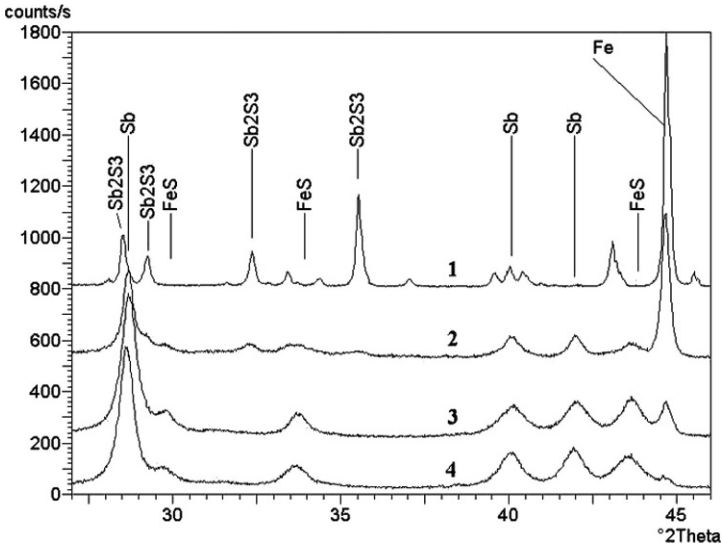

Fig. 4.41 X-ray diffraction patterns at different stage of reaction (4.61) as function of milling time. 1–0 min, 2–20 min, 3–60 min, 4–120 min [Baláž et al. 2007]

only solid state products. The intensity of the metal iron reflexion (110) decreases upon continued milling and only a very small amount of iron is detectable at 60 min (pattern 4). In the starting material (pattern 1) more small peaks are seen which belong to stibnite Sb_2S_3 (JCPDS 42-1393).

The conversion degree for precursors (Sb_2S_3, Fe) and product (Sb) of reaction (4.61) as obtained by normalization of the XRD intensities is shown in Fig. 4.42. It is clear that most of the reduction is complete after 60 min with the intensity of Sb_2S_3 decreasing faster than Fe. There is no reason to expect different phase ratios here as the content of Fe and Sb_2S_3 should change parallel according to Eq. (4.61). A possible explanation is the partial amorphization of stibnite which is indeed manifested in an increased background of the XRD patterns.

Figure 4.43 shows the room temperature magnetization data for investigated samples as a function of external magnetic field. It is evident that the resulting magnetization curves are well saturated after an application of magnetic field higher than 2 T. The variation of the saturation magnetization as a function of milling time, as displayed in the inset of Fig. 4.43, reflects the amount of metallic iron, the only ferromagnetic component in the samples. In good agreement with the XRD results shown in Fig. 4.42, the Fe fraction decreases continuously for milling times up to 180 min, with more than 80% being transformed during the first 60 min. After 180 min of milling the saturation magnetization is negligible indicating that the constituent phases are almost entirely paramagnetic and/or antiferromagnetic, i.e. reaction (4.61) is practically complete.

The XRD line width of the sample milled for 180 min have been analyzed in order to confirm the presence of nanosize particles. The grain size of Sb was found

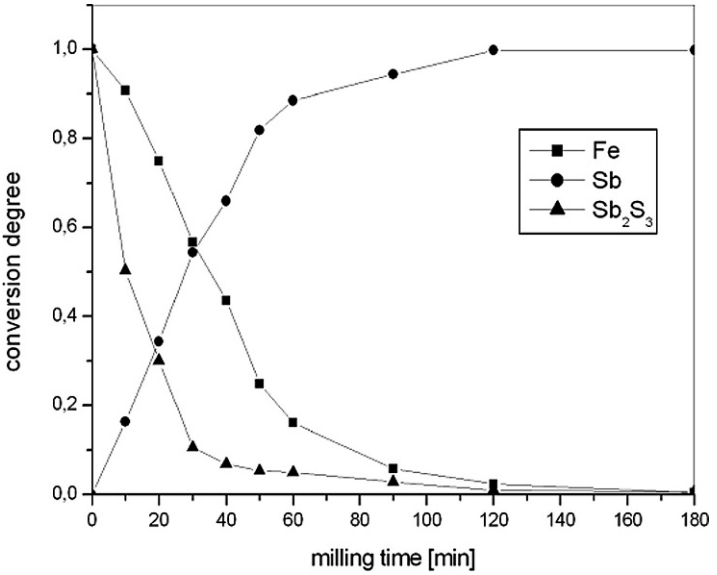

Fig. 4.42 Conversion degree for reaction (4.61) as a function of milling time [Baláž et al. 2007]

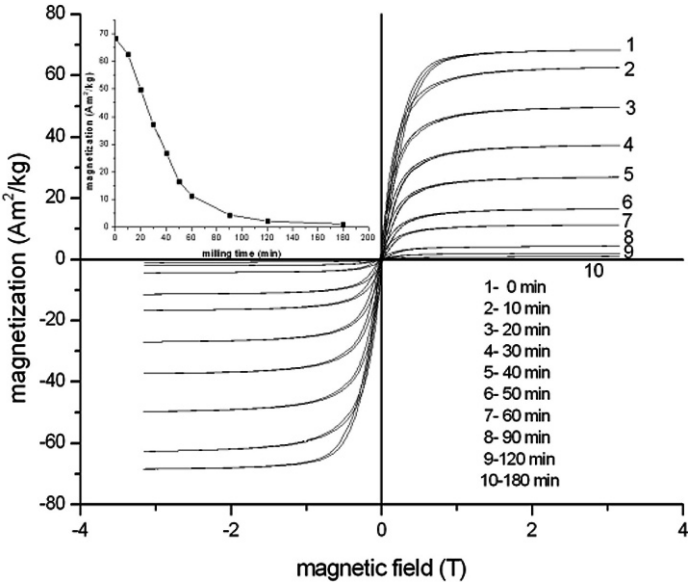

Fig. 4.43 Magnetization as a function of external magnetic field for several milling times. The inset shows the saturation magnetization as a function of milling time [Baláž et al. 2007]

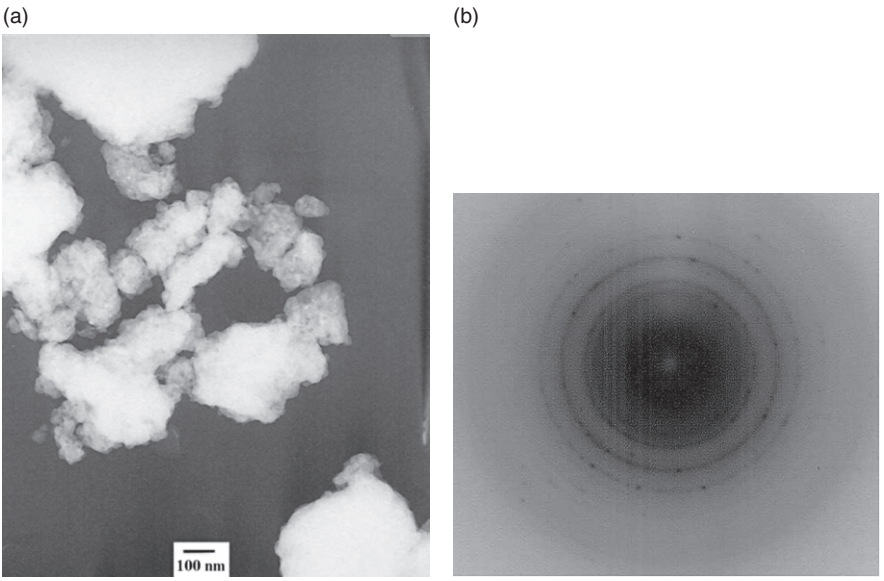

Fig. 4.44 (**A**) Dark field TEM image and (**B**) SAED pattern of nanoparticles formed by reaction (4.61), milling time 180 min [Baláž et al. 2007]

to be 19 nm with 0.35% residual strain and the particle size of FeS is about 10 nm. Figure 4.44A shows a typical dark field TEM image obtained using beams from the diffraction rings of the irregular shaped nanoparticles formed during 180 min of milling. Figure 4.44B shows the SAED pattern of an area containing some nanoparticles. The SAED pattern shows a set of rings instead of spots due to the random orientation of the nanoparticles. The TEM image is consistent with the XRD grain size but also shows the strongly agglomerated nature of the powder. The agglomeration of nanoparticles is a general phenomenon originating from the tendency to reduce the surface area.

The reaction (4.61) was also studied with mineral sample from Romania (deposit Baiut) [Baláž et al. 2005a]. XRD revealed that next to main phase stibnite Sb_2S_3 also quartz SiO_2 was present (Fig. 4.45A). The starting material was milled with elemental Fe in a ratio corresponding to Eq. (4.61) in a planetary mill and the XRD patterns were taken to identify the main components (Fig. 4.45B). Both product phases predicted by Eq. (4.61) were identified: elemental Sb (JCPDS 35-0732) and pyrrhotite–1T (JCPDS 29-0726). In addition, a substantial amount of non-reacted Fe is present. This is explained by the approximately 10% SiO_2 contained in the starting material.

The mechanochemical reaction between arsenic sulphide As_2S_3 and elemental iron can be described by the equation

$$As_2S_3 + 3Fe \rightarrow 2As + 3FeS \tag{4.62}$$

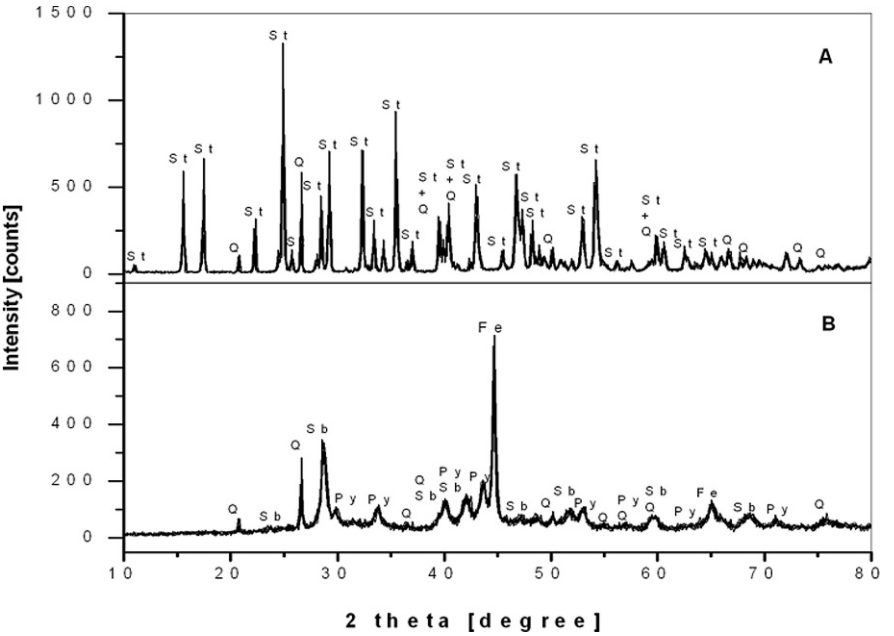

Fig. 4.45 X-ray diffraction patterns for reaction (4.61), **A**: starting stibnite Sb_2S_3 (Baiut, Romania), **B**: Sb_2S_3 with Fe milled for 10 min. St – stibnite, Sb_2S_3, Q – quartz, SiO_2, Sb – antimony, Py – pyrrhotite 1T, Fe – iron [Baláž et al. 2005a]

The reaction is thermodynamically feasible, as the enthalpy change is negative, $\Delta H^{\circ}_{298} = -160.7\,\mathrm{kJ\,mol^{-1}}$.

The starting material was mineral obtained from Manhattan, Nevada (USA). Its XRD analysis (Fig. 4.46) revealed that the main phase was auripigment As_2S_3 with a small amount of realgar As_4S_4. The mineral was milled with elemental Fe in stoichiometric molar ratio in a planetary mill and XRD patterns were measured to identify the main components of the reaction (4.62). Surprisingly, the only reaction product was iron sulphide, identified as pyrrhotite-4M Fe_7S_8 (JCPDS card 24-0079.) Only partial conversion to reaction products was achieved as can be seen from the presence of non-reacted Fe in this figure. Neither elemental arsenic nor any arsenic sulphide is detected among the products of mechanochemical reaction (4.62). This fact can be interpreted by the low thermal stability of arsenic sulphides [Vaughan and Craig 1978] and the possible volatization of the arsenic species during milling.

The mechanochemical reaction between copper sulphide and elemental iron has been studied very carefully [Matteazzi and LeCaër 1992b; Baláž et al. 2002b, 2004a, c, 2005a]. The reaction can be described by equation

$$Cu_2S + Fe \rightarrow 2Cu + FeS \tag{4.63}$$

The reaction (4.63) is thermodynamically possible, as the enthalpy change is negative, ($\Delta H^{\circ}_{298} = -21.0\,\mathrm{kJ\,mol^{-1}}$).

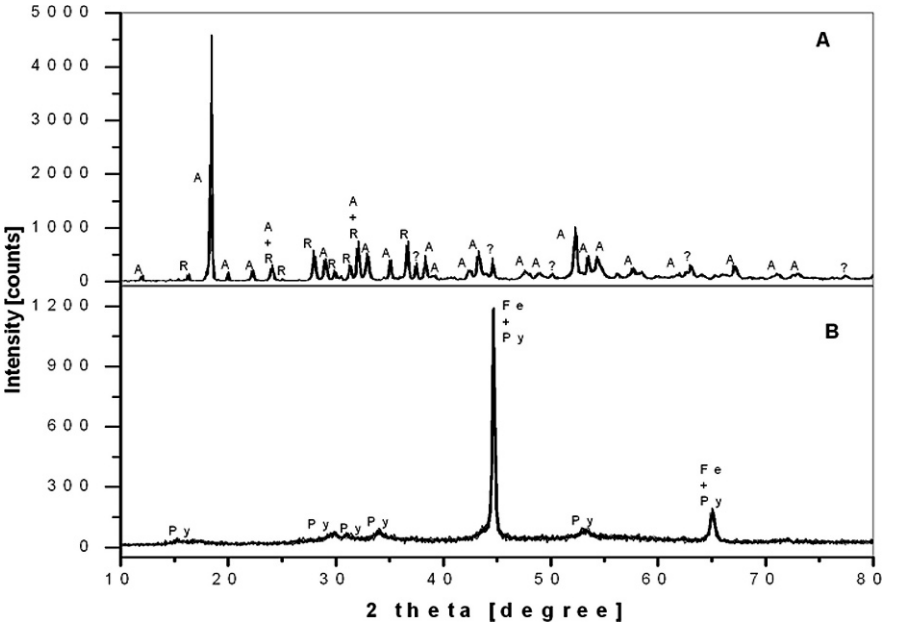

Fig. 4.46 X-ray diffraction patterns for reaction (4.62), **A**: starting mineral auripigment As_2S_3 (**A**) with small amount of realgar As_4S_4 (R), **B**: As_2S_3 with Fe milled for 10 min. Py – pyrrhotite 4M, Fe_7S_8, Fe – iron [Baláž et al. 2005a]

The progress of the mechanochemical reaction is illustrated by the selected XRD patterns in Fig. 4.47.

The primary process – the reduction of copper sulphide by iron while copper metal and iron sulphides are formed – is clearly seen, particularly by inspecting the relative intensities of the diffraction lines of Cu and Fe metal.

The conversion degree, β, can be defined as $\beta = I_{Cu}/(I_{Cu} + I_{Fe})$, where I_{Cu} and I_{Fe} are the intensities of the Cu(111) and Fe(110) diffraction lines. The process kinetics as described by this parameter is shown in Fig. 4.48.

The process is significantly complicated by the existence of several copper sulphide and iron sulphide phases. Any external influence, such as high temperature treatment and ball milling [Baláž et al. 2003], can cause phase transformations in sulfides. Already 1 min of milling decreased the relative amount of djurleite $Cu_{1.94}S$ and increased the fraction of chalcocite Cu_2S. In addition, a new tetragonal phase $Cu_{1.81}S$ (JCPDS 41-0959) formed as indicated by the diffraction peaks at 32.5° and 39°. Another tetragonal phase Cu_2S (JCPDS 72-1071) may also be present.

Most of the copper sulfide is consumed during the first minutes of milling. After 10 min, only the reflections from Cu, cubic FeS (JCPDS 23-1123) and Fe can be observed. The presence of iron without residual copper sulphides requires either significant off-stoichiometry of the iron sulphide or the presence of free sulphur. Unfortunately, free sulphur may remain undetected by XRD due to the low scattering amplitude of sulphur and its tendency toward amorphization. The intensity of

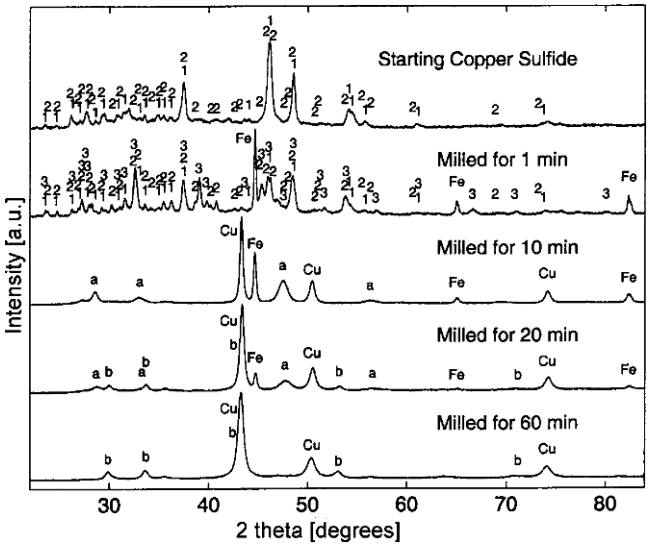

Fig. 4.47 X-ray diffraction patterns for reaction (4.63) as a function of milling time, 1 – djurleite $Cu_{1.94}S$, 2 – chalcocite Cu_2S, 3 – tetragonal $Cu_{1.81}S$, a – cubic FeS, b – hexagonal FeS [Baláž et al. 2002b]

the iron reflections decreases upon continued milling and no iron is detectable after 60 min. Simultaneously, FeS changes to its hexagonal modification troilite (JCPDS 75-0602). This phase is considered the stable modification of stoichiometric FeS [Shuey 1975].

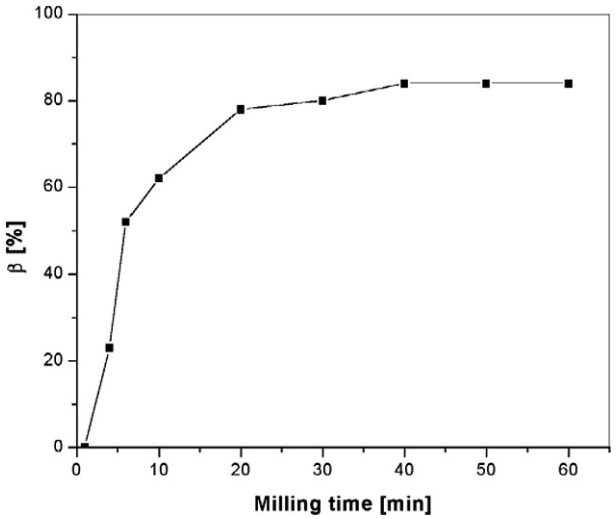

Fig. 4.48 Conversion degree for reaction (4.63) as a function of milling time [Baláž et al. 2002b]

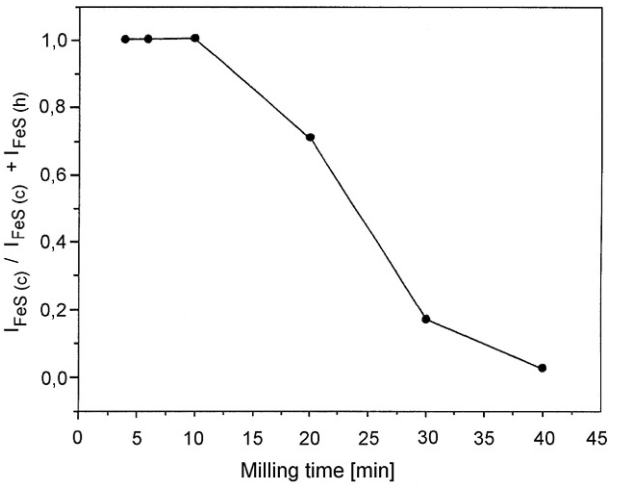

Fig. 4.49 Conversion of cubic FeS (c) to hexagonal FeS (h) as a function of milling time [Baláž et al. 2005a]

The kinetics of the cubic iron sulphide transformation to hexagonal iron sulphide is shown in Fig. 4.49 based on the intensity ration of XRD peaks. Iron sulphides (pyrrhotites) belong to a group of complicated compounds containing ordered iron vacancies. The distribution of vacancies distinguishes the individual pyrrhotite types. At temperatures below 350°C, the vacancies start to order producing a series of superstructures based on the Ni-As type structure [Shuey 1975; Vaughan and Craig 1978; Vaughan and Lennie 1991]. Cubic FeS is a metastable phase that can be synthesized in the laboratory, but it is not found naturally.

The Mössbauer spectra presented in Fig. 4.50 support the interpretation given for the XRD results above. The spectra are dominated by two overlapping sextets with a paramagnetic doublet appearing in the center, especially at milling times between 4 and 10 min. The relative intensities of both sextets as well as the observed doublet are given in Fig. 4.51 as a function of milling time.

The parameters of the high-field sextet (hyperfine field 32.9 ± 0.3 T, isomer shift 0.01 ± 0.01 mm/s and quadrupole shift 0.01 ± 0.01 mm/s) indicate that it originates from elemental Fe. Its relative fraction is diminishing with the milling time (Fig. 4.51) consistent with XRD results. The sextet, which dominates the patterns after longer milling times, is characterized by the hyperfine field between 30.0 T and 30.9 T, isomer shift of 0.75 ± 0.01 mm/s and quadrupole splitting of 0.07 ± 0.01 mm/s.

These parameters are typical of iron monosulphides. The small magnetization observed after prolonged milling is probably due to the ferrimagnetic contribution of Fe-deficient $Fe_{1-x}S$ [Vaughan and Lennie 1991; Jiang et al. 1998]. The isomer shift of the doublet varies from $0.44\,mm\,s^{-1}$ to $0.50\,mm\,s^{-1}$ and the quadrupole splitting increases from $0.96\,mm\,s^{-1}$ to $1.11\,mm\,s^{-1}$ with increasing milling time. This component probably originates from an increasingly disordered intermediate state. Avvakumov observed a transition from sextet to doublet as the consequence of

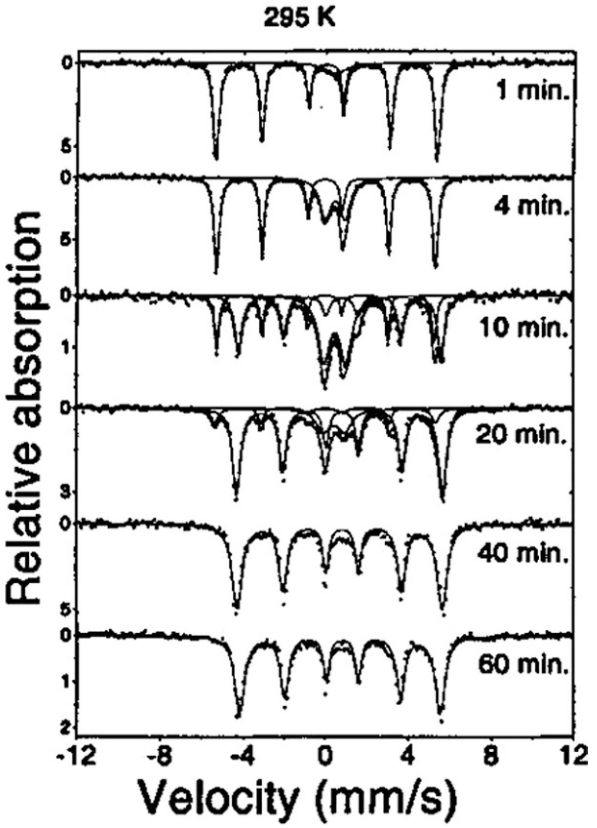

Fig. 4.50 Mössbauer spectra for reaction (4.63) mixtures as a function of milling time [Baláž et al. 2005b]

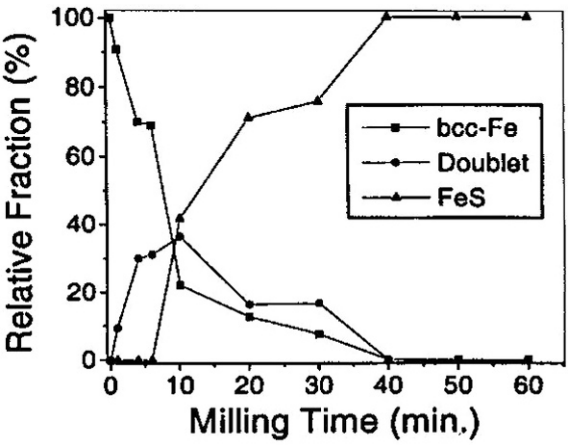

Fig. 4.51 The relative intensities of the Mössbauer sub-spectra as a function of milling time [Baláž et al. 2005b]

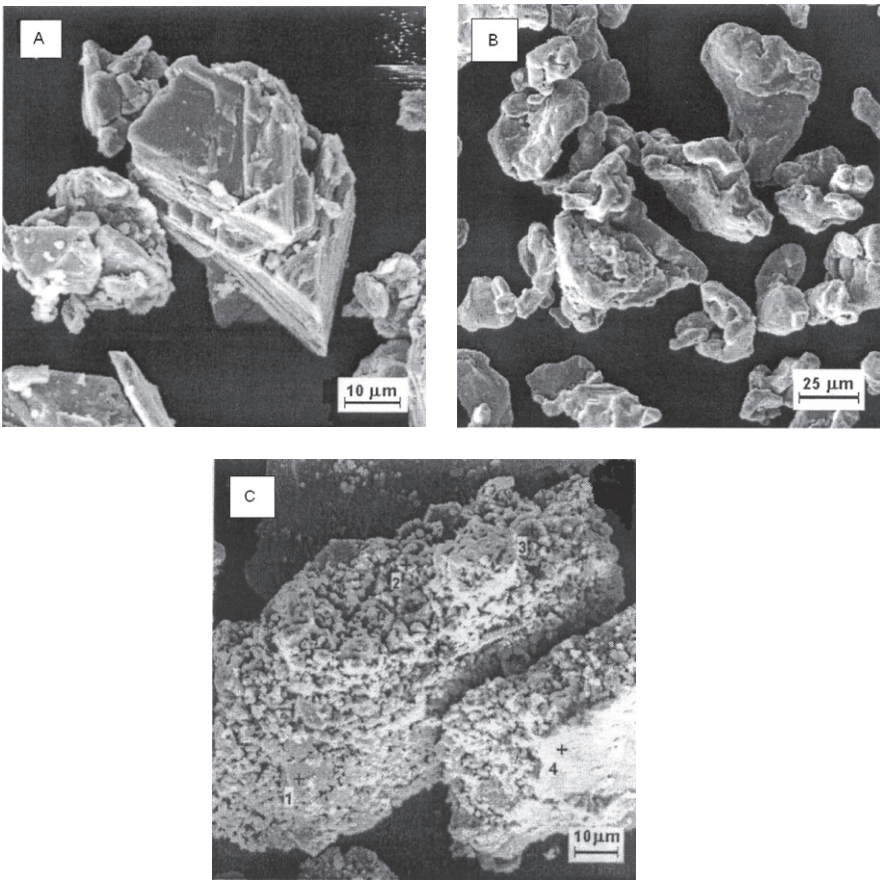

Fig. 4.52 SEM study of the mechanochemical reduction of copper sulphide by iron: (**A**) elemental Fe, (**B**) copper sulphide, (**C**) Cu/FeS nanocomposite [Baláž et al. 2004d]

mechanical disordering of the iron sublattice when milling a single-phase pyrrhotite sample [Avvakumov 1986].

Micrometer aggregates of nanoparticles are formed during milling of copper sulphide with iron (Fig. 4.52). Usually each micrometer-sized powder particle is comprised of a mixture of nanosized grains of the product phases as can be observed in our case [Gaffet et al. 1999; Koch 1991; McCormick et al. 2001]. The dimension of the grains is changing with milling time (Fig. 4.53).

The very similar results have been obtained with chalcocite Cu_2S mineral from deposit Khan (South-western Africa) [Baláž et al. 2004c].

4.3.6.5 Scaling-Up the Process

Several processes have been designed for production of pure metals from compounds including minerals with iron as reducing metal (Fig. 4.54) [Habashi 1986].

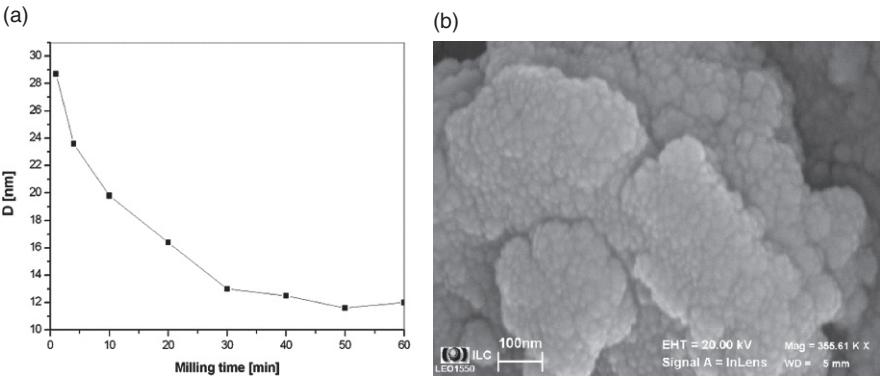

Fig. 4.53 Crystallite size, D, of product copper in reaction (4.63) as a function of milling time [Baláž et al. 2005a]

The selection of a solid–solid reduction process depends on numerous factors and usually a compromise is made between the advantages and the disadvantages. Suitable additives are used to improve the process [Habashi 1986]. However, the conventional metallothermic reduction is not capable of making nano-size metals and or Me/FeS nanocomposites due to the high temperature.

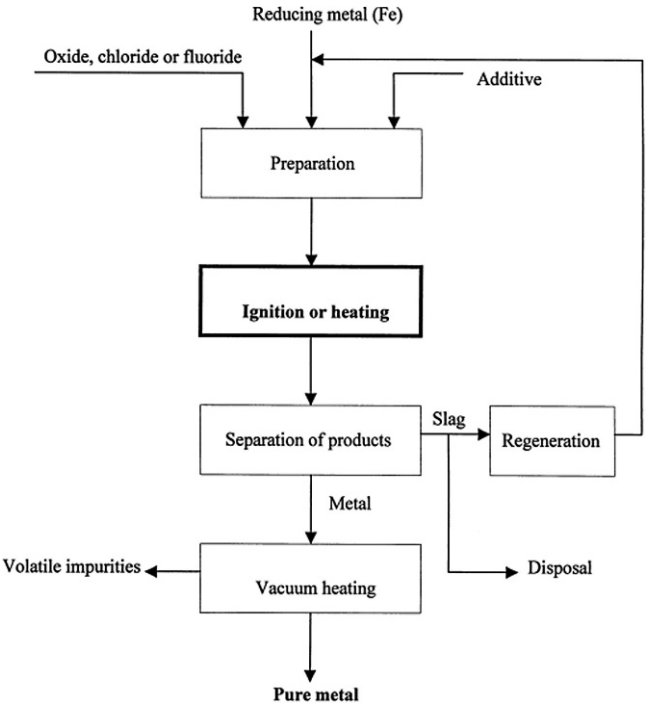

Fig. 4.54 General scheme of metallothermic reduction [Habashi 1986]

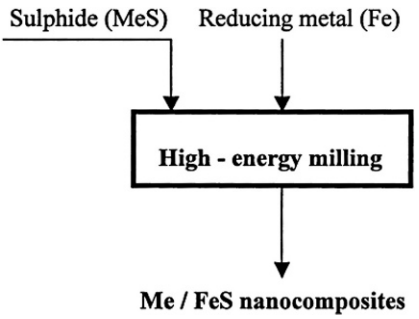

Fig. 4.55 General scheme of mechanochemical reduction [Baláž et al. 2005a]

Mechanochemical reduction as outlined in Fig. 4.55 is a very straightforward, one-step, ambient temperature process without many operations. The key step is the high-energy milling which requires a suitable industrial mill for scaling up the process. In mechanochemical processing of sulfides with elemental iron as reducing agent, the product is in the form of Me/FeS (Me = Pb, Sb, Cu) nanocomposite particles. They can be applied in technology as produced, e.g. as supported metal catalysts in chemical engineering [Weisser and Landa 1972] or have to be separated into components in order to prepare nanometals with unique properties [Baláž et al. 2004d]. The reduction of sulphides in a ball mill is an example of a so-called "dry" technology, as reactions in gas and liquid phases are excluded.

In case of copper sulphide mechanochemical reduction the simplified flowchart can be outlined as in Fig. 4.56. The very straightforward one-step solid state process is characterized by the formation of Cu/FeS nanocomposite. If we need nanocopper,

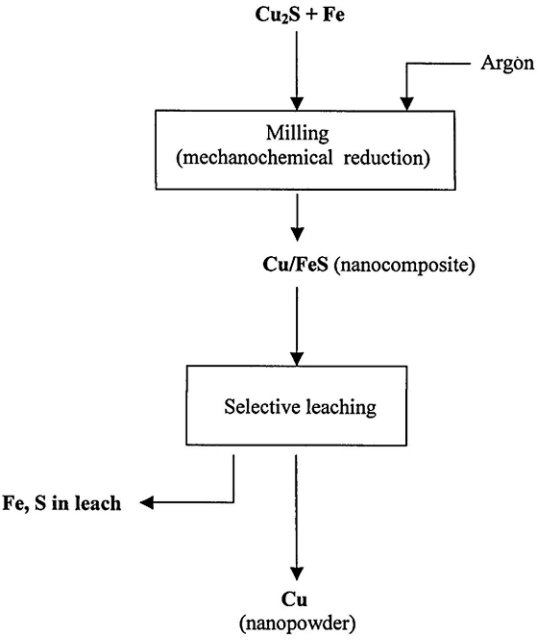

Fig. 4.56 Scheme of copper nanopowder production [Baláž et al. 2004c]

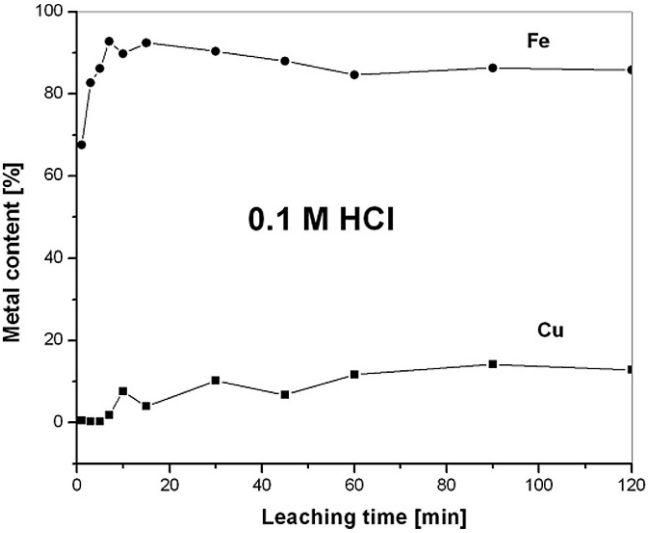

Fig. 4.57 Metal recovery vs. leaching time for Cu/FeS nanocomposite

the product of reaction (4.63) has to be separated into its components. Selective leaching of the iron sulphide can be an appropriate method of producing copper nanopowder. Several acids (H_2SO_4, HNO_3, HCl) have been tested for the selective leaching of iron sulphide from the nanocomposite with the aim to preserve nanocopper in solid form. The best results have been obtained with HCl: more than 86% Fe was dissolved together with the marginal amount of copper (0.2%), Fig. 4.57.

4.3.6.6 Reduction with Magnesium

Ultrafine Mo particles can be produced as a result of the slow burning transition into detonation in reaction of molybdenite MoS_2 with Mg reducing metal according to the reaction

$$MoS_2 + Mg \rightarrow Mo + 2MgS \tag{4.64}$$

The mechanical treatment of the reactant mixture results in a considerable decrease of the ignition temperature and in a strong increase of the burning speed [Gaffet and LeCaër 2004].

The same reducing element has been applied for decomposition of stibnite Sb_2S_3 [Godočiková et al. 2007] following the reaction

$$Sb_2S_3 + 3Mg \rightarrow 2Sb + 3MgS \tag{4.65}$$

The reaction is thermodynamically possible, as the enthalpy change for reaction (4.65) is negative, ($\Delta H^{\circ}_{298} = -872.4\,\mathrm{kJ\,mol^{-1}}$).

The progress of the mechanochemical reduction is illustrated by XRD patterns (Fig. 4.58) of the starting powder (A) and taken after 20 (B), 30 (C), and 120 (D)

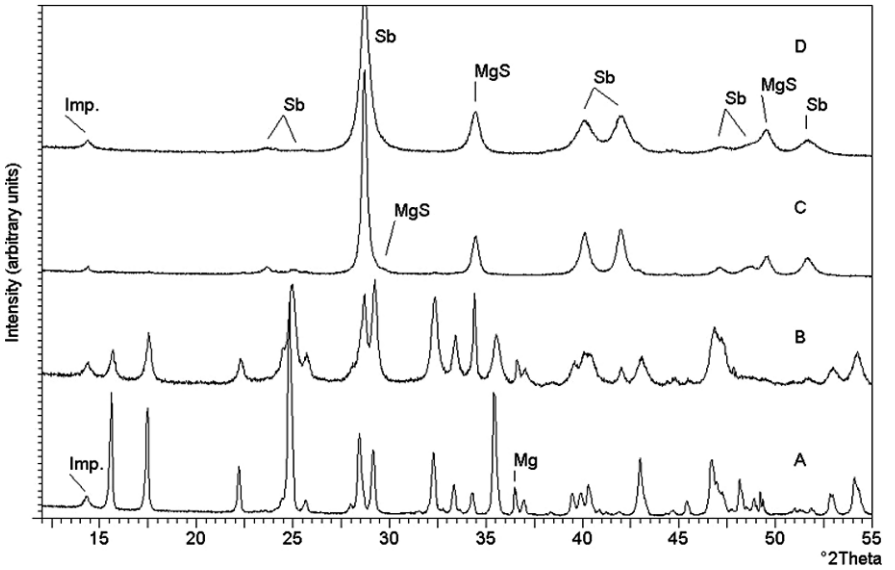

Fig. 4.58 X-ray diffraction patterns as a function of the milling time. A-stoichiometric mixture of Sb_2S_3 and Mg before milling. The milling times for patterns B-D are 20 min, 30 min and 120 min, respectively [Godočiková et al. 2008]

min of milling. Pattern A is dominated by stibnite, Sb_2S_3 (JCPDS 75-1310); all the unmarked lines correspond to this phase. The (101) peak of magnesium (JCPDS 35-0821) and an unidentified peak at about 14.3° are also visible. This latter line probably originates from an inert impurity that does not participate in the reaction. There is very little chemical change during the first 20 min of milling, although the presence of some rombohedral Sb metal (JCPDS 35-0732) is indicated by the (012) peak at 28.7° and the (110) peak at about 42°. The most obvious change is the broadening of the diffraction peaks.

There is a qualitative difference between patterns B and C, indicating a fast chemical change between 20 and 30 min. It seems that most of the reaction takes place as a self-sustaining reaction some time between 20 and 30 min; the transformation is practically complete at 30 min. This is not surprising. The ratio of the reaction heat to the room temperature heat capacity is about 4660 K and values above 2000 K indicate the possibility of a self-sustaining reaction [Takacs 2002]. Elemental antimony and niningerite MgS (JCPDS 35-0730) are the only solid state reaction products. The lines are relatively narrow after 30 min of millling, suggesting that a high temperature process resulted in larger particles. Only the line broadening changes between 30 min and 120 min.

The reaction proceeds according to Eq. (4.65) without intermediate phases and it is complete by 30 min. Just as there is little transformation before 20 min, little Sb_2S_3 remains after at least 30 min of milling. A small shoulder at 43.2° is the only sign that a minor amount of Sb_2S_3 is present after 30 min. The reason can be that a

small fraction of the Mg was oxidized and therefore not available as reducing agent. The X-ray patterns were measured to 120°, but we opted to show a narrower range of angles with better resolution.

The detailed analysis of XRD patterns has been performed in order to determine grain sizes and strains using the Williamson-Hall method [Williamson and Hall 1953]. During the first 20 min the particle size of stibnite decreases: it is 65 nm after 10 min and 35 nm after 20 min. The random strain is less than 0.1% as expected for a brittle substance. Right after the reaction at 30 min, the particle size is 130 nm with 0.3% strain. The strain remains the same until 90 min, the particle size drops to 25 nm and remains about the same from 40 min to 90 min. There is a little extra broadening after 120 min of milling, providing 18 nm particle size and 0.35% strain.

The dependence of the specific surface area on milling time is shown in Fig. 4.59. Two phases of the formation of new specific surface area can be identified. In the first period up to 30 min, the specific surface area increases; the effect of the reaction is not obvious. After 40 min the surface area is approximately constant, suggesting a dynamic equilibrium between particle fracturing and agglomeration [Baláž 2000]. In a polydisperse systems like the current one, the presence of very fine particles along with relatively coarse particles greatly promotes the formation of aggregates, due to the enhanced role of the van der Waals forces. Particles in the nanometer size range have a strong tendency to agglomerate due to their relatively large specific surface area.

The surface morphology of the mechanochemically synthesized Sb/MgS nanoparticles is depicted in Fig. 4.60 where the agglomeration of nanoparticles can be clearly seen. The agglomeration increases with the increasing milling time. The

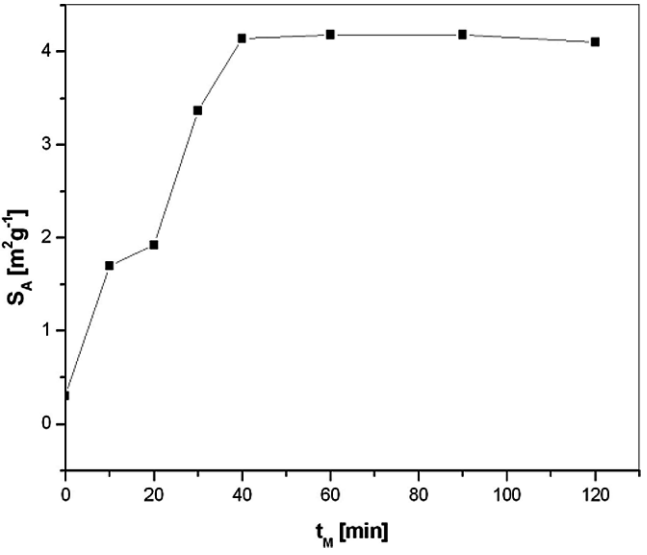

Fig. 4.59 Specific surface area as a function of the milling time [Godočiková et al. 2007]

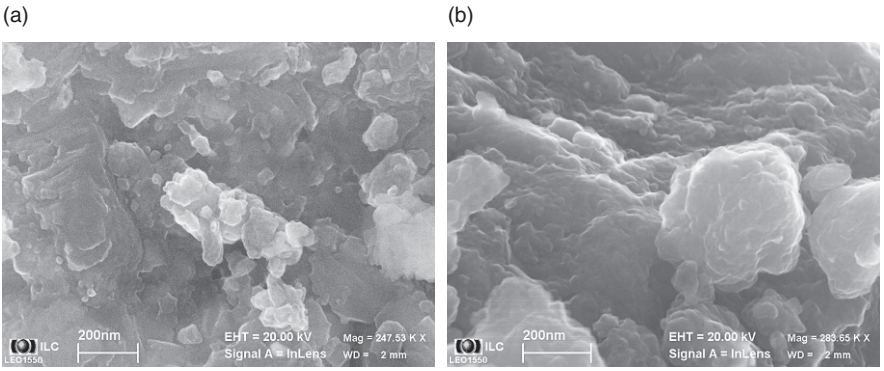

Fig. 4.60 SEM image of Sb/MgS nanocomposite; milling time 30 min (**A**) and 120 min (**B**) [Godočiková et al. 2008]

solid state combination of nanoparticles into agglomerates is a general phenomenon which is one of the ways a nanocrystal system is able to compensate for its unsaturated surface forces via surface reconstruction.

4.3.6.7 Reduction with Silicon

The mechanochemical reduction of copper sulphides with silicon as reducing element has been studied in [Baláž et al. 2005b]. XRD analysis of the starting materials (Fig. 4.61A) revealed that the main present phases were chalcocite Cu_2S, djurleite $Cu_{1.94}S$ and elemental silicon. The behaviour of sulphides and silicon at separate milling is different. There are no new phases at silicon milling on XRD pattern except of tungsten carbide (5) which is a consequence of wear from milling vial and balls. The shape of diffraction peaks and their positions illustrate the effect of particle size diminution as a consequence of milling. However, the phase transformations are unambiguously observed: anilite Cu_7S_4 and digenites $Cu_{9-x}S_5$ have been identified among the products of milling. It has been described recently [Baláž et al. 2003] that digenite, which is in fact a group of copper sulphides [Gaines et al. 1997] is one of the main phase during copper sulphide milling. Anilite has been observed as an intermediate product and this phase is transformed into low digenite modification due to milling [Morimoto et al. 1969]. The presence of anilite (Fig. 4.61B) can not be excluded also in our case.

The set of starting copper sulphide and silicon mixtures has been milled in different time and the products have been identified by X-ray diffractometry (Fig. 4.62). Djurleite $Cu_{1.94}S$ and chalcocite Cu_2S together with unreacted silicon have been identified in powders milled till 3 min (Fig. 4.62A and B). $Cu_{1.96}S$ phase formed at milling time 6 min (Fig. 4.62C) seemed to be the most stable phase even in case when ternary sulphide is formed during prolonged milling. In higher time of milling (Fig. 4.62D–F) elemental copper (1) and the ternary copper silicon sulphide Cu_8SiS_6 are the main reaction products together with the described $Cu_{1.96}S$ phase.

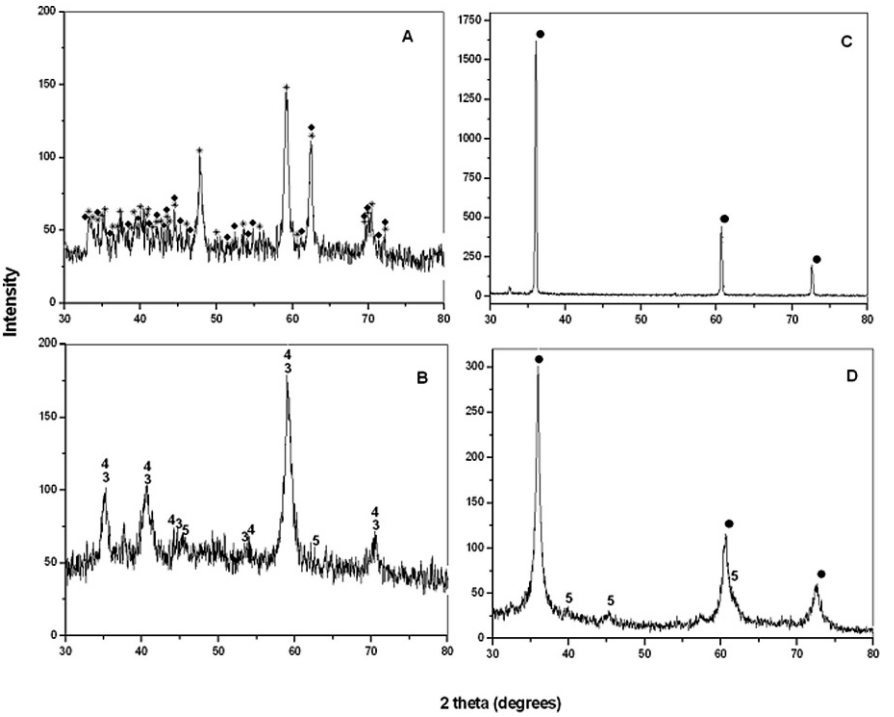

Fig. 4.61 XRD patterns of starting copper sulphides (**A**) and silicon (**C**) and products of their separate milling for 20 minutes (**B** and **D**): ♦ – Cu_2S (chalcocite) (JCPDS 23-962); ∗ – $Cu_{1.9375}S$ (djurleite) (JCPDS 23-0960); ● – Si (silicon, syn) (JCPDS 27-1402); 3 – $Cu_{9-x}S_5$; $Cu_{1.765}S$ (digenite) (JCPDS 47-1748); 4 – Cu_7S_4 (anilite) (JCPDS 34-0489); 5 – WC (tungsten carbide) (JCPDS 25-1047) [Baláž et al. 2005b]

The dependance of specific surface area on milling time for starting copper sulphides (A), starting silicon (B) and reaction mixture of copper sulphides with silicon (C) is given in Fig. 4.63. There are small changes in values of S_A for copper sulphide milling in contrast to silicon which seemed to be strong agglomerated after 10 min of milling. Anomalous behaviour of surface area increase for starting mixture milled for 6–20 min ($S_A = 0.4$–$4.9\ m^2g^{-1}$) can be related to the formation of ternary copper silicon sulphide Cu_8SiS_6 because the specific surface area of any milled copper sulphide is not higher than $0.2\ m^2\ g^{-1}$.

The overall process of mechanochemical transformations in copper sulphide-silicon system proceeds via complicated mechanism with several overlapping steps. Phase transformations in copper sulphide phases, the formation of elemetal nanocopper with X-ray determined particle size of 23 nm and creation of ternary sulphide Cu_8SiS_6 with anomalous surface area values are the main products of the hypothetical reaction

$$6Cu_2S + Si \rightarrow 4Cu + Cu_8SiS_6 \tag{4.66}$$

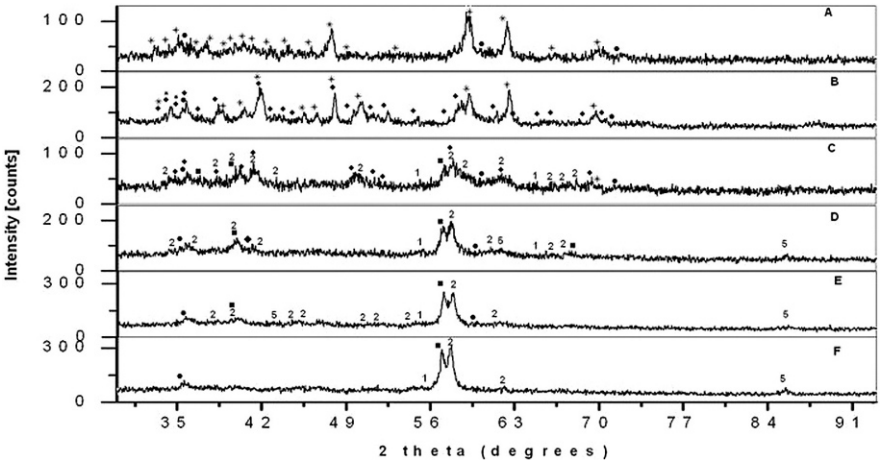

Fig. 4.62 XRD patterns of mixture of starting copper sulphides with silicon milled for different times: A – 1 min; B – 3 min; C – 6 min; D – 10 min; E – 15 min; F – 20 min (silicon has been pre-milled for 10 min for all samples): ♦ – Cu_2S (chalcocite) (JCPDS 46-1195, JCPDS 84-1770, JCPDS 72-1071); ∗ – $Cu_{1.9375}S$ (djurleite) (JCPDS 34-0660); ■ – $Cu_{1.96}S$ – (JCPDS 12-0174); ● – Si (silicon, syn) (JCPDS 27-1402); 1 – Cu (copper, syn) (JCPDS 04-0836); 2 – Cu_8SiS_6 (copper silicon sulphide) (JCPDS 21-0305); 5 – WC (tungsten carbide) (JCPDS 25-1047) [Baláž et al. 2005b]

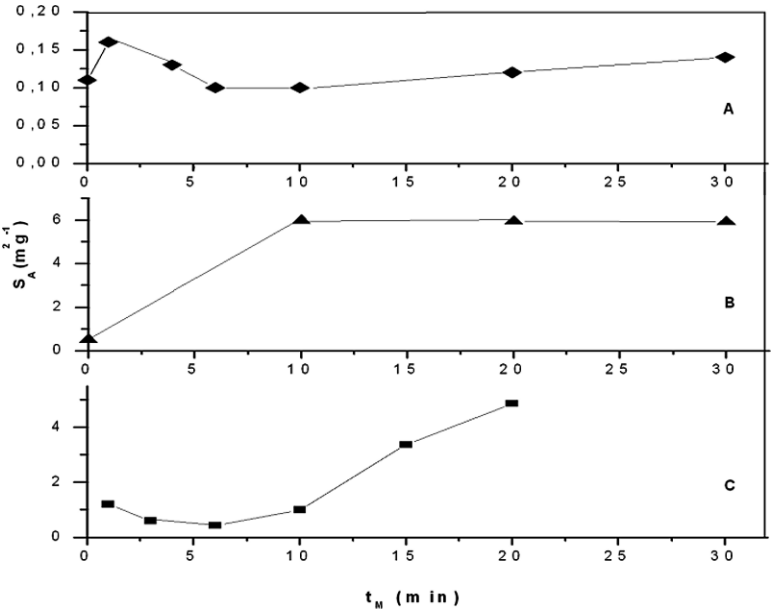

Fig. 4.63 Specific surface area, S_A vs. milling time, t_M: A – copper sulphides; B – silicon; C – mixture of copper sulphides with silicon [Baláž et al. 2005b]

4.3.6.8 Thermodynamics of Sulphide Reduction

The heats of formation of sulphides are much smaller than the corresponding values for oxides (Table 4.9). Consequently, the redox reactions between a sulphide and a more reactive metal is less exothermic than the analogous reaction between the corresponding oxide and the same metal. Nevertheless, in several cases the reaction heats are high enough to permit mechanically induced self-sustaining reactions [Takacs 2002].

Table 4.9 Mechanically induced redox reactions of sulphides

Reaction	ΔH° (kJ mol^{-1})	Reference
$3Cu_2S + 2Al \rightarrow 6Cu + Al_2S_3$	−485	Matteazzi and LeCaër (1992b)
$Cu_2S + Fe \rightarrow 2Cu + FeS$	−21	Matteazzi and LeCaër (1992b)
$3PbS + 2Al \rightarrow 3Pb + Al_2S_3$	−267	Matteazzi and LeCaër (1992b)
$PbS + Fe \rightarrow Pb + FeS$	−1	Baláž et al. (2004b); Godočíková et al. (2004a, b)
$Sb_2S_3 + 3Fe \rightarrow 2Sb + 3FeS$	−117	Baláž et al. (2007)
$Sb_2S_3 + 3Mg \rightarrow 2Sb + 3MgS$	−872	Godočiková et al. (2007)
$As_2S_3 + 3Fe \rightarrow 2As + 3FeS$	−161	Baláž et al. (2005a)
$MoS_2 + 2Mg \rightarrow Mo + 2MgS$	−70	Danielian et al. (1991)
$3ZnS + 2Al \rightarrow 3Zn + Al_2S_3$	−107	Danielian et al. (1991)
$FeS_2 + Fe \rightarrow 2FeS$	−13	Baláž et al. (2004a)
$3FeS + 2Al \rightarrow 3Fe(Al) + Al_2S_3$	−271	Baláž et al. (2004a)
$2FeS + Si \rightarrow 2Fe(Si) + SiS_2$	+88	Baláž et al. (2004a)
$FeS + Mn \rightarrow Fe + MnS$	−117	Baláž et al. (2004a)
$3CoS + 2Al \rightarrow 3Co + Al_2S_3$	−405	Baláž et al. (2004a)
$HgS + Cu \rightarrow Hg + CuS$		Molčanov and Jusupov (1981)

4.3.7 Other Minerals

Thermodynamically, chrysocolla $CuSiO_3 \cdot 2H_2O$ could react with sodium sulfide to form nanocrystalline covellite CuS and water soluble sodium silicate according to the exchange reaction

$$CuSiO_3 \cdot 2H_2O + Na_2S \rightarrow CuS + Na_2SiO_3 + 2H_2O \tag{4.67}$$

It was shown that the solid state pretreatment using a vibration mill increases the conversion rate of chrysocolla [Banza and Gock 2003]. This procedure can be efficiently used for the recovery of copper in the form of nanocrystalline copper sulphide as an alternative to pre-heating or direct leaching.

Mineral malachite $CuCO_3 \cdot Cu(OH)_2$ has been also treated with the same sulphur precursor

$$CuCO_3 \cdot Cu(OH)_2 + 2Na_2S \rightarrow 2CuS + Na_2CO_3 + 2NaOH \tag{4.68}$$

and the overall transformation of malachite into the nanocrystalline covellite CuS was achieved.

Copper sulphate mineral chalcantite $CuSO_4{\cdot}5H_2O$ transformation have been studied by Indian authors using Fe, Mg, Sn, Mn, Co and Pb reducing elements to obtain nanocrystalline copper [Varghese et al. 2001; Varghese et al. 2004].

In ($CuSO_4{\cdot}5H_2O$+Fe) *system* the overall chemical reaction during milling can be written as follows

$$\begin{aligned} CuSO_4 \cdot 5H_2O + Fe &\rightarrow Cu + FeSO_4 \cdot 5H_2O \\ &\rightarrow Cu + FeSO_4 \cdot 5H_2O \end{aligned} \tag{4.69}$$

As milling proceeds (Fig. 4.64), the intensity of $CuSO_4{\cdot}5H_2O$ and Fe peaks gradually diminishes while that of $FeSO_4{\cdot}5H_2O$ and Cu peaks increases. On latter milling times $FeSO_4{\cdot}5H_2O$ is completely converted into $FeSO_4{\cdot}4H_2O$ [Varghese et al. 2001].

In ($CuSO_4{\cdot}5H_2O$+Mg) *system* $MgSO_4{\cdot}4H_2O$ and Cu_2O are formed as final products. An intermediate phase and hydrogen were observed before completion of mechanochemical reduction.

In $CuSO_4{\cdot}5H_2O$ + Sn *system* the reaction can be represented

$$\begin{aligned} CuSO_4 \cdot 5H_2O + Sn &\rightarrow Cu + \beta - brass + SnSO_4 + 5H_2O \\ &\rightarrow Cu + SnSO_4 + 5H_2O \end{aligned} \tag{4.70}$$

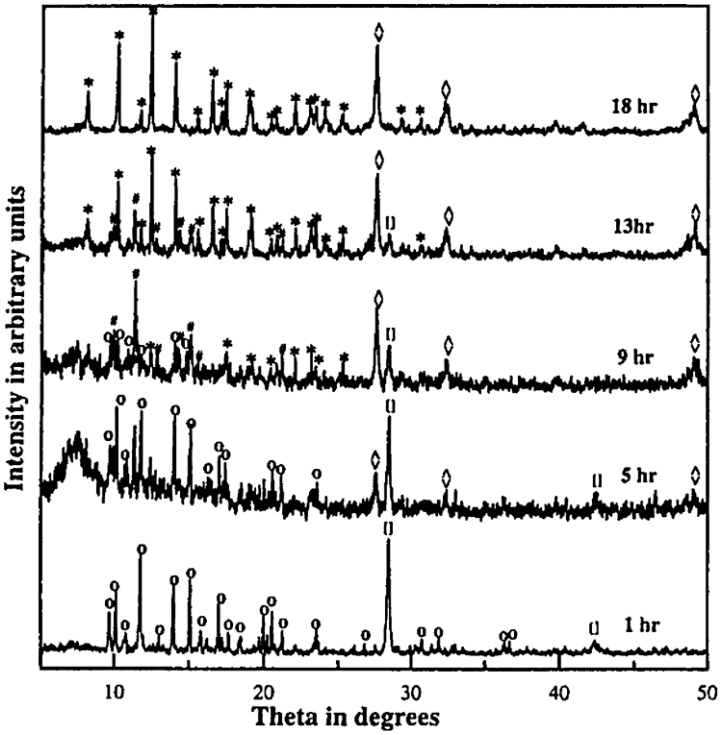

Fig. 4.64 X-ray diffraction patterns of mixture of starting $CuSO_4{\cdot}5H_2O$ with iron milled for different times: $CuSO_4{\cdot}5H_2O$, [ ] Fe, ◊ Cu, # $FeSO_4{\cdot}5H_2O$, ∗ $FeSO_4{\cdot}4H_2O$ [Varghese et al. 2001]

Table 4.10 Grain size, D for various substances in systems (metal sulphate+metal) [Varghese et al. 2001]

Reaction system	D (nm)
$CuSO_4 \cdot 5H_2O + Fe$	27 (Cu)
$CuSO_4 \cdot 5H_2O + Mg$	19 (Cu_2O)
$CuSO_4 \cdot 5H_2O + Sn$	54 (Sn)

There is no water of hydration associated with the product sulfate $SnSO_4$.

The grain size analysis of the products formed during reduction are given in Table 4.10.

In ($CuSO_4 \cdot 5H_2O$+Pb) *system* the reaction (4.71) is extremely rapid

$$CuSO_4 \cdot 5H_2O + Pb \rightarrow Cu + PbSO_4 + 5H_2O \tag{4.71}$$

and practically complete withing 20 min of planetary milling (Fig. 4.65). The reduction of bivalent copper by lead as reducing metal is extremely slow in solution

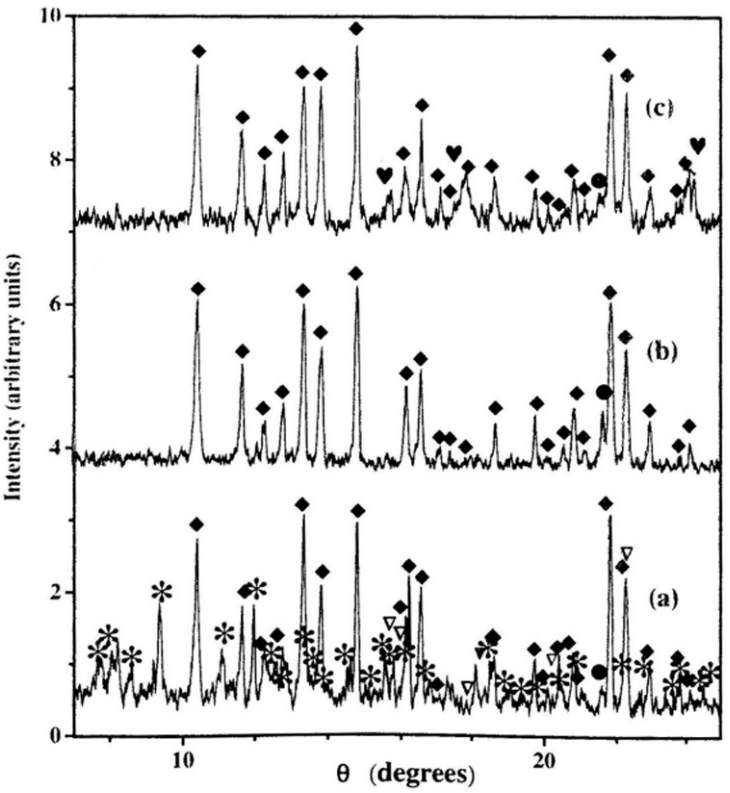

Fig. 4.65 X-ray diffraction patterns of mixture of starting $CuSO_4 \cdot 5H_2O$ with lead milled for different times: (**a**) 5 min; (**b**) 30 min; (**c**) 50 h: ∗ $CuSO_4 \cdot 5H_2O$, ▽ Pb, ●Cu, ♦ $PbSO_4$, ⊙ WC [Varghese et al. 2004]

due to the presence of electric double layer at the interface between lead metal and solution where the redox system has to occur. Since a similar electric double layer is absent in solid state, the resistance due to double layer does not play a part in the kinetics while milling ($CuSO_4 \cdot 5H_2O$+Pb) system. Thus, while the reaction (4.71) is slow in solution, it is much faster in solid [Varghese et al. 2004]. For the given process conditions, the kinetics and mechanism of the mechanochemical reduction can vary with the variation in the chemical nature of the reactants as well as products. A careful selection of systems becomes important in the process control [Varghese et al. 2001, 2004].

Bastnaesite $ReCO_3F$ (Re-rare earths) is one of the most important mineral resources containing rare earth elements especially La and Ce. A novel process for extracting rare earths contained in this mineral has been developed in Japan [Zhang and Saito 1998]. This process is composed of three steps combining milling, washing and leaching operations. Milling of bastnaesite and NaOH powders in the first step plays a significant role in achieving a high yield of rare earths elements in the leaching of the washed sample (Fig. 4.66). The leaching is governed by the reaction

$$LaCO_3F + 3NaOH \rightarrow La(OH)_3 + Na_2CO_3 + NaF \tag{4.72}$$

and extraction of the rare earth elements such as La, Ce, Pr, Nd, Sm included in bastnaesite was attempted with NaOH powder using planetary mill.

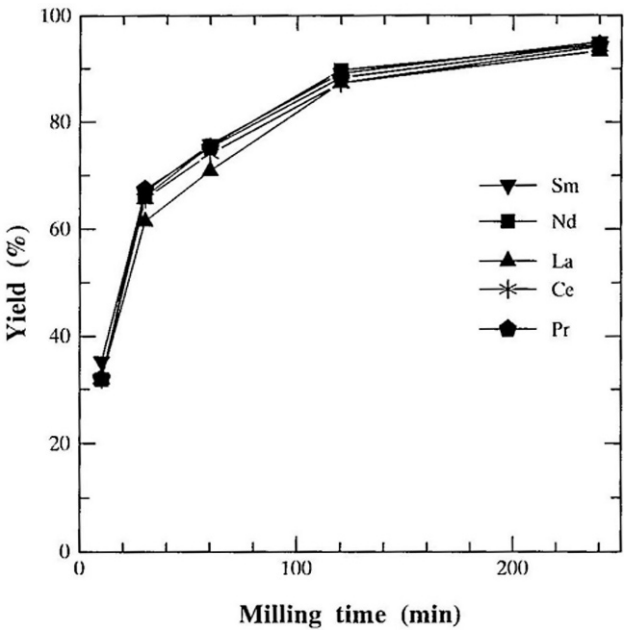

Fig. 4.66 Yield of the rare earth elements extracted from the washed samples by 10 N H_2SO_4 solution as a function of milling time [Zhang and Saito 1998]

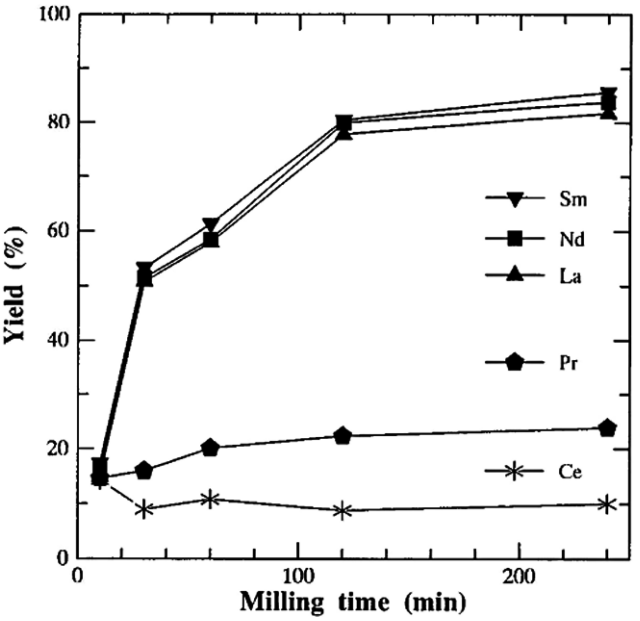

Fig. 4.67 Yield of the rare earth elements extracted from the washed samples by 0.05 N H_2SO_4 solution as a function of milling time [Zhang and Saito 1998]

The change in selectivity of the rare earth elements extraction can be achieved by the change of leaching conditions (Figs. 4.66 and 4.67).

References

Avvakumov, E.G., Djakova, V.E. and Strugova, L.I. (1974) Mechanical activation of solid-state reactions. 4. Solid state reduction of cassiterite. Izvestija SO AN SSSR, seria chimiceskich nauk 2, 26–29 (in Russian).

Avvakumov, E.G. and Strugova, L.I. (1974) Mechanical activation of solid-state reactions. 6. Application of diffusionsless kinetics for mechanochemical reactions in solid mixtures. Izvestija SO AN SSSR, seria chimiceskich nauk 2, 34–38 (in Russian).

Avvakumov, E.G., Matycin, L.I. and Staver, A.M. (1975) Solid state reduction of SnO_2 by compression and mechanical activation. Fizika gorenija i vzryva 6, 922–927 (in Russian).

Avvakumov, E.G. (1986) *Mechanical Methods of the Activation of Chemical Processes*. Nauka, Novosibirsk (in Russian).

Baláž, P., Post, E. and Bastl, Z. (1992) Thermoanalytical study of mechanically activated cinnabar. Thermochimica Acta 196, 371–377.

Baláž, P., Havlík, T., Bastl, Z. and Briancin, J. (1995) Mechanosynthesis of iron sulphides. Journal of Material Science Letters 14, 344–346.

Baláž, P. (2000) *Extractive Metallurgy of Activated Minerals*. Elsevier, Amsterdam.

Baláž, P. and Briančin, J. (2001) Direct reduction of mechanically activated galena and sphalerite with hydrogen. Journal of Thermal Analysis and Calorimetry 65, 769–776.

Baláž, P. and Godočíková, E. (2001) Thermal reduction of mechanically activated cinnabar (HgS) and stibnite (Sb_2S_3). Journal of Thermal Analysis and Calorimetry 65, 51–57.
Baláž, P., Boldižárová, E. and Bajger, Z. (2001c) Non-traditional way of magnetite recovery from metallurgical waste. Acta Metallurgica Slovaca 7, 97–100.
Baláž, P., Godočíková, E., Boldižárová, E., Luxová, M., Bastl, Z. and Jiang, J.Z. (2002a) Characterization of nanocrystalline products prepared by mechanochemical reduction of copper sulphide. Czechoslovak Journal of Physics, Supplement A 52, A65–A68.
Baláž, P., Takacs, L., Jiang, J.Z., Soika, V. and Luxová, M. (2002b) Mechanochemical reduction of copper sulphide. Materials Science Forum 386–388, 257–262.
Baláž, P., Takacs, L., Boldižárová, E. and Godočíková, E. (2003) Mechanochemical transformations and reactivity in copper sulphides. Journal of Physics and Chemistry of Solids 64, 1413–1417.
Baláž, P., Aláčová, A., Godočíková, E., Kováč, J., Škorvánek, I. and Jiang, J.Z. (2004a) Study of magnetic properties of nanopowders prepared by pyrite-troilite transformation via high energy milling. Czechoslovak Journal of Physics, Supplement D, 54, D197–D200.
Baláž, P., Godočíková, E., Aláčová, A., Škorvánek, I., Kováč, J. and Jiang, J.Z. (2004b) Magnetic properties of nanocrystalline pyrrhotite prepared by high-energy milling. Czechoslovak Journal of Physics, Supplement D 54, D121–D124.
Baláž, P., Takacs, L., Luxová, M., Godočíková, E. and Ficeriová, J. (2004c) Mechanochemical processing of sulphidic minerals. International Journal of Mineral Processing 74S, 365–371.
Baláž, P., Godočíková, E., Krilová, L., Lobotka, P. and Gock, E. (2004d) Preparation of nanocrystalline materials by high energy milling. Materials Science and Engineering A 386A, 442–446.
Baláž, P., Godočíková, E., Takacs, L. and Gock, E. (2005a) Mechanochemical preparation of metal/sulphide nanocomposite particles. International Journal of Materials and Product Technology 23, 26–41.
Baláž, P., Boldižárová, E. and Godočíková, E. (2005b) Preparation of nanocrystalline copper and copper silicon sulphide by mechanochemical route. Materials Science Forum 480–481, 453–456.
Baláž, P., Takacs, L., Godočíková, E., Škorvánek, I., Kovác, J. and Choi, W.S. (2007) Preparation of nanosized antimony by mechanochemical reduction of antimony sulphide Sb_2S_3. Journal of Alloys and Compounds 434–435, 773–775.
Banza, A.N. and Gock, E. (2003) Mechanochemical processing of chrysocolla with sodium sulphide. Minerals Engineering 16, 1349–1354.
Basset, D., Matteazzi, P. and Miani, F. (1994) Kinetic effects in mechanically activated solid-state reduction of hematite. Hyperfine Interactions 94, 2235–2238.
Beecroft, L.L. and Ober, C.K. (1997) Advanced nanocomposite materials for optical applications. Chemistry of Materials 9, 1302–1317.
Benjamin, J.S. (1970) Dispersion strengthened superalloys by mechanical alloying. Metallurgical Transactions 1, 2946–2951.
Boldyrev, V.V. (1993) Mechanochemistry and mechanical activation of solids. Solid State Ionics 63–65, 537–543.
Boldyrev, V.V. (1996a) Mechanochemistry and mechanical activation. Materials Science Forum 225–227, 511–520.
Boldyrev, V.V. (1996b) Reactivity of solids and new technologies. In: V.V. Boldyrev (Ed.) *Reactivity of Solids: Past, Present and Future.* Blackwell Science, Oxford, pp. 267–285.
Boldyrev, V.V. and Avvakumov, E.G. (1971) Mechanochemistry of inorganic solids. Uspechi chimiji 40, 1835–1856 (in Russian).
Boldyrev, V.V. (1979) Control of reactivity of solids. Annual Revne of Materials Science 9, 455–469.
Boldyrev, V.V. (1998) Mechanical activation and its application in technology. Materials Science Forum 269–272, 227–234.
Boldyrev, V.V. and Tkáčová, K. (2000) Mechanochemistry of solids: past, present and prospects. Journal of Materials Synthesis 8, 121–132.

Boldyrev, V.V. (2006) Mechanochemistry and mechanical activation of solids. Russian Chemical Reviews 75, 177–189.

Botta, P.M., Aglietti, E.F. and Porto Lopez, J.M. (2000) Thermal and phase evolution of mechanochemical reactions in the Al-Fe_3O_4 system. Thermochimica Acta 363, 143–147

Budnikov, P.P. and Ginstling, A.M. (1971) *Reactions in Solid Mixtures*. Strojizdat, Moscow (in Russian).

Burkin, A.R. (1966) *The Chemistry of Hydrometallurgical Processes.* Spou, London.

Butyagin, P.J. (1971) Kinetics and nature of mechanochemical reactions. Uspechi chimiji 40, 1935–1959.

Butyagin, P.J., Avvakumov, E.G. and Kolbanov, I.V. (1974) Žurnal fiziceskoj chimii 12, 3009.

Butyagin, P.J. (1984) Disordering of structure and mechanochemical reactions in solids. Uspechi chimiji 53, 1769–1789 (in Russian).

Butyagin, P.J. and Yuščenko, V.S. (1987) Kinetika i kataliz 27, 1035–1039.

Campbell, S.J., Kaczmarek, W.A. and Wang, G.M. (1995) Mechanochemical transformation of haematite to magnetite. Nanostructured Materials 6, 735–738.

Cao, G., Garcia, M.E., Alcala, M., Burgess, L.F. and Mallouk, T.E. (1992) Chiral molecular recognition in intercalated zirconium phosphate. Journal of American Chemical Society 114, 7574–7575.

Carter, R.E. (1991) Journal of Chemical Physics 34, 2010.

Cech, R.E. and Tiemann, T.S. (1969) The hydrogen reduction of copper, nickel, cobalt and iron sulfides and the formation of filamentary metals. Transactions of Metalurgical Society of AIME 245, 1727–1733.

Cech, R.E. (1974) Journal of Metals 26, 32–38.

Chen, Y., Marsh, M., Williams, J.S. and Ninham, B. (1996) Production of rutile from ilmenite by room temperature ball-milling-induced sulphurization reaction. Journal of Alloys and Compounds 245, 54–58.

Chunpeng, L., Zhonghua, L. and Zuze, Z. (1988) Reduction kinetics of stibnite with hydrogen and recovery of metallic antimony/lead by evaporation. In: F. Chongyne, L. Jianehun, L. Songren (Eds.) *Proceedings of the Ist International Conference on the Metalurgy and Materials Sciences of Tungsten, Titanium, Rare Earth and Antimony "W-Ti-Re-Sb 88"*, Vol. 1. Pergamon Press, Oxford, pp. 539–544.

Courtney, I.A. and Dahn, J.R. (1997) Electrochemical and in-situ X-ray diffraction studies of the reaction of lithium with tin oxide composites. Journal of Electrochemical Society 144, 2045–2052.

Čižikov, D.M. (1976) *Metallurgy of Non-ferrous Metals*. Nauka, Moscow (in Russian).

Danielian, N.G., Janazian, S.K. and Melnichenko, V.V. (1991) X-ray investigation of metal reduction by mechanical alloying and solid state reaction. Modern Physics Letters 5, 1355–1359.

Dutta, J. and Hofman, H., http:/www.mxsg3.epfl.ch/ltp/Cours/Nanomat/Nanomat/pdf

El-Eskandarany, M.S., El-Bahnasawy, H.N., Ahmed, H.A. and Eissa, N.A. (2001) Mechanical solid-state reduction of haematite with magnesium. Journal of Alloys and Compounds 314, 286–295.

Frost, B.R. (1991) Stability of oxide minerals in metamorphic rocks. Reviews in Mineralogy and Geochemistry 25, 469–488.

Gaffet, E. and Harmelin, M. (1990) Crystal-amorphous phase transition induced by ball-milling in silicon. Journal of Less-Common Metals 157, 201–222.

Gaffet, E., Bernard, F., Niepce, J.C., Charlot, F., Gras, C., LeCaër, G., Guichard, J.L., Delcroix, P., Mocellin, A. and Tillement, O. (1999) Some recent developments in mechanical activation and mechanosynthesis. Journal of Materials Chemistry 9, 305–314.

Gaffet, E. and Bernard, F. (2002) Mechanically activated powder metallurgy processing: A versatile way towards nanomaterials synthesis. Annales de Chimie Sciences des Materiaux 27, 47–59.

Gaffet, E. and LeCaër, G. (2004) Mechanical processing for nanomaterials. In: H.S. Nalwa (Ed.) *Encyclopedia of Nanoscience and Nanotechnology,* Vol. 5. American Scientific Publishers, pp. 91–129.

Gaines, R.V., Skinner, H.C.W., Ford, E.E., Mason, B., Rosenzweig, A., King, W.T. and Gowty, E. (1997) *Dana's New Mineralogy.* Willey, New York.

Gillan, E.G. and Kaner, R.B. (1996) Synthesis of refractory ceramics via rapid metal thesis between solid-state precursors. Chemistry of Materials 8, 333–343.

Godočíková, E., Bastl, Z., Spirovová, I. and Baláž, P. (2004a) A study of mechanochemical reduction of lead sulphide by elemental iron on the surface studied by XPS. Journal of Materials Science 39, 3025–3029.

Godočíková, E., Baláž, P., Boldižárová, E., Škorvánek, I., Kováč, J. and Choi, W.S. (2004b) Mechanochemical reduction of lead sulphide by elemental iron. Journal of Materials Science 39, 5353–5355.

Godočíková, E., Baláž, P., Takacs, L., Šepelák, V., Škorvánek, I. and Gock, E. (2007) Sb/FeS nanocomposite prepared by mechanochemical reduction. Kovové materiály 45, 99–104.

Godočíková, E., Takacs, L., Baláž, P., Kováč, J., Šatka, A. and Briančin, J. (2008) Mechanochemical reduction of antimony sulphide Sb_2S_3 with magnesium in a planetary mill. Reviews in Advanced Materials Science 18, 212–215.

Goya, G.F., Rechenberg, H.R. and Jiang, J.Z. (1998) Structural and magnetic properties of ball milled copper ferrite. Journal of Applied Physics 84, 1101–1108.

Habashi, F. (1969) *Extractive Metallurgy*, Vol. 1, General Principles. Gordon and Breach, New York.

Habashi, F. (1986) *Extractive Metallurgy*, Vol. 3, Pyrometallurgy. Gordon and Breach, New York.

Habashi, F. (1993) *A History of Metallurgy.* Métallurgie Extractive Québec.

Hedvall, J.A. (1938) *Reaktionsfähigkeit fester Stoffe.* Verlag Barth, Leipzig.

Henn, J.J. and Barclay, J.A. (1995) Journal of Applied Chemistry and Biotechnology 25, 561–568.

Jermakov, A.E., Barinov, V.A. and Jurcikov, E.E. (1982) Fizika Metallov i Metallovedenije 54, 90–96 (in Russian).

Jiang, J.Z., Larsen, R.K., Lin, R., Morup, S., Chorkendorff, I., Nielsen, K. and West, K. (1998) Mechanochemical synthesis of Fe-S materials. Journal of Solid State Chemistry 138, 114–125.

Jovanovic, S., Sinadinovic, D. and Durkovic, B. (1986a) Reduction of non-ferrous sulfides by hydrogen (I). Rud Geolog I Metal 37, 594–597 (in Serbian).

Jovanovic, S., Durkovic, B. and Sinadinovic, D. (1986b) Reduction of non-ferrous sulfides by hydrogen (II). Rud Geolog I Metal 37, 1247–1251 (in Serbian).

Kaczmarek, W.A. and Ninham, B.W. (1994) Preaparation of Fe_3O_4 and γ-Fe_2O_3 powders by magnetomechanical activation of hematite. IEEE Transactions on Magnetics 30, 732–733.

Karch, J., Birringer, R. and Gleiter, H. (1987) Ceramics ductile at low temperature. Nature 330, 556–558.

Kharitidi, G.P., Skopov, G.V., Chudjakov, I.F. and Veksler, S.F. (1981) Reduction of chalcopyrite by solid carbon in the presence of calcium oxide. Izvestija AN SSSR, Metalurgija 6, 21–27 (in Russian).

Kharitidi, G.P., Skopov, G.V., Lisina, N.N. and Ovchinnikova, L.A. (1983) Reduction and sublimation of lead sulfide in the lead-sulfide-calcium oxide-carbon system. Žurnal prikladnoj chimiji 56, 729–734 (in Russian).

Koch, C.C. (1991) Mechanical milling and alloying. Materials Sciences and Technology 15, 93–198.

Kosmac, T. and Courtney, T.H. (1992) Milling and mechanical alloying of inorganic nonmetallics. Journal of Materials Research 7, 1519–1525.

Lin, J.J., Nadiv, S. and Grodzian, D.J.M. (1975) Changes in the state of solids and mechanochemical reactions in prolonged comminution process. Minerals Science and Engineering 7, 313–336.

Ma, E., Pagan, J., Cranford, G. and Atzmon, M. (1993) Evidence of self-sustained $MoSi_2$ formation during high-energy ball milling of elemental powders. Journal of Materials Research 25, 1836–1844.

Mankhand, T.R., Singh, G. and Prasad, P.M. (1978) Transactions of Indian Institute of Metals 31, 194–199.

Marfunin, A.S. and Mkrtčjan, A.R. (1967) Mössbauer spectra of Fe^{57} in sulphide minerals. Geochimija 10, 1094–1103 (in Russian).
Matteazzi, P. and LeCaër, G. (1991) Reduction of haematite with carbon by room temperature ball milling. Materials Science and Engineering A 149, 135–142.
Matteazzi, P. and LeCaër, G. (1992a) Synthesis of nanocrystalline alumina-metal composites by room-temperature ball-milling of metal oxides and aluminium. Journal of American Ceramic Society 75, 2749–2755.
Matteazzi, P. and LeCaër, G. (1992b) Mechanically activated room temperature reduction of sulphides. Materials Science and Engineering A 156A, 229–237.
Matteazzi, P., Basset, D., Miani, F. and LeCäer, G. (1993) Mechanosynthesis of nanophase materials. Nanostructured Materials 2, 217–229.
McCormick, P.G. (1995) Application of mechanical alloying to chemical refining. Materials Transactions JIM 36, 161–169.
McCormick, P.G., Tsuzuki, T., Robinson, J.S. and Ding, J. (2001) Nanopowders synthesized by mechanochemical processing. Advanced Materials 13, 1008–1010.
Menzel, M., Šepelák, V. and Becker, K.D. (2001) Mechanochemical reduction of nickel ferrite. Solid State Ionics 141–142, 663–669.
Mills, K.C. (1974) *Thermodynamic Data for Inorganic Sufides, Selenides and Tellurides*. Butterworth, London.
Molčanov, V.I. and Jusupov, T.S. (1981) *Physical and Chemical Properties of Fine Ground Minerals.* Nedra, Moscow.
Morimoto, M., Koto, K. and Shimazaki, Y. (1969) Anilite, Cu_7S_4, a new mineral. American Mineralogist 54, 1256–1268.
Mrowec, S. (1988) On the defect structure and diffusion kinetics in transition metal sulfides and oxides. Reactivity of Solids 5, 241–268.
Mukopadhyay, D.K., Prisbrey, K.A., Suryanarayana, C. and Froyes, F.H. (1996) Ball-milling, a novel extraction process for production of W from WO_3 using magnesium as reductant. In: A. Bose, R.J. Dowding (Eds.) *Tungsten and Refractory Metals 3.* Metal Powder Industries Federation, New York, pp. 239–346.
Mulas, G., Monagheddu, M., Doppiu, S., Cocco, G., Maglia. F. and Anselmi Tamburini, U. (2001) Metal-metal oxides prepared by MSR and SHS techniques. Solid State Ionics 141–142, 649–656.
Nakatani, Y., Sakai, M., Nakatani, S. and Matsuoka, M. (1983) Mechanochemical effect of dry-grinding on the transformation phenomenon from γ-Fe_2O_3 to α-Fe_2O_3. Journal of Materials Science Letters 2, 129–131.
Nasu, T., Tokumitsu, K., Miazawa, K., Greer, A.L. and Suzuki, K. (1999) Solid state reduction of iron oxide by ball milling. Materials Science Forum 312–314, 185–190.
Nazar, L.F., Zhang, Z. and Zinkweg, D.J. (1992) Insertion of PPV in layered MoO_3. Journal of American Chemical Society 114, 6239–6240.
Niihara, K. (1991) New design concept of structural ceramic: ceramic nanocomposites. Journal of Ceramic Society of Japan 99, 974–982.
Onajev, I.V. and Spitčenko, V.S. (1988) *Reduction of Sulfides.* Nauka, Alma-Ata (in Russian).
O'Neill, H.S.C. and Navrotsky, A. (1983) Simple spinels: crystallographic parameters, cation radii, lattice energies, and cation distribution. American Mineralogist 68, 181–194.
O'Neill, H.S.C. and Navrotsky, A. (1984) Cation-distributions and thermodynamic properties of binary spinel solid solutions. American Mineralogist 69, 733–753.
Pardavi-Horvath, M. and Takacs, L. (1992) Iron-alumina composites prepared by ball milling. IEEE Transactions on Magnetics 28, 3186–3188.
Parson, A., Petrashov, V.T. and Sosnin, I.A. (2000) Anomalies in quantum and classical magnetoresistance of semi-metallic nanowires. Physica B: Condensed Matter 284–288, 1744–1745.
Patel, P., Roy, S., Kim, Il-Seok and Kumta, P.M. (2004) Synthesis and characterization of tin and antimony based composites derived by mechanochemical in situ reduction of oxides. Materials Science and Engineering B 111, 237–241.

Pavlyuchin, J.T., Medikov, J.J., Avvakumov, E.G. and Boldyrev, V.V. (1981) Defect formation by mechanical activation studied by Mössbauer spectroscopy. ISO AN ZSSSR, seria chimiceskich nauk 4, 11–16 (in Russian).

Pavlyuchin, I.T., Medikov, I.I. and Boldyrev, V.V. (1982) Cation re-distribution in spinel ferrites as a consequence of mechanical activation. Doklady akademii nauk SSSR 266, 1420–1422 (in Russian).

Pavlyuchin, J.T., Medikov, J.J. and Boldyrev, V.V. (1983) Magnetic and chemical properties of mechanically activated zinc and nickel ferrites. Materials Research Bulletin 18, 1317–1327.

Pavlyuchin, J.T., Medikov, J.J. and Boldyrev, V.V. (1984) On the consequences of mechanical activation of zinc and nickel ferrites. Journal of Solid State Chemistry 53, 155–160.

Pavlyuchin, J.T., Medikov, J.J and Boldyrev, V.V. (1988) Mechanical activation of close-packed inorganic crystals. Review of Solid State Sciences 2, 603–621.

Prasad, P.M. and Mankhand, T.R. (1983) Lime enhanced reduction of metal sulphides. In: H.Y. Sohn, D.B. George, A.D. Zunkel (Eds.) *Proceedings of International Sulphide Smelting Symposium.* The Metallurgical Society of AIME, San Francisco, pp. 371–392.

Saito, F., Zhang, Q. and Kano, J. (2004) Mechanochemical approach for preparing nanostructural materials. Journal of Materials Science 39 (2004) 5051.

Schaffer, G.B. and McCormick, P.G. (1989a) Reduction of metal oxides by mechanical alloying. Applied Physics Letters 55, 45–46.

Schaffer, G.B. and McCormick, P.G. (1989b) Combustion synthesis by mechanical alloying. Scripta Metallurgica 23, 835–838.

Schaffer, G.B. and McCormick, P.G. (1990) Displacement reactions during mechanical alloying. Metallurgical Transactions A 21A, 2789–2794.

Schaffer, G.B. and McCormick, P.G. (1991) Anomalous combustion effects during mechanical alloying. Metallurgical Transactions A 22A, 3019–3023.

Schaffer, G.B. and McCormick, P.G. (1992a) The direct synthesis of metals and alloys by mechanical alloying. Materials Science Forum 88–90, 779–786.

Schaffer, G.B. and McCormick, P.G. (1992b) Mechanical alloying. Materials Forum 16, 91–97.

Schrader, R. and Hoffman, B. (1973) Änderung der Reaktionsfähigkeit von Festkörpern durch vorhergehende mechanische Bearbeitung. In: V.V. Boldyrev, K. Meyer (Eds.) *Festkörperchemie*. Verlag Grundstoffindustrie, Leipzig, pp. 522–543.

Senna, M. and Kuno, H. (1973) Effect of preliminary pressing on isothermal transformation of maghemite to hematite. Journal of American Ceramic Society 56, 492–493.

Shi, Y. and Ding, J. (2001) Journal of Applied Physics 90, 4078.

Shuey, R.T. (1975) *Semiconducting Ore Minerals.* Elsevier, Amsterdam.

Sorescu, M. (1998) Phase transformations induced in magnetite by high energy milling. Journal of Materials Science Letters 17, 1059–1061.

Streleckij, A.N., Butyagin, P.J. and Leonov, A.V. (1996) Koloidnyj žurnal 58–62, 248–253 (in Russian).

Suryanarayana, C. (2001) Mechanical alloying and mixing. Progress in Materials Science 46, 1–184.

Szczygiel, Z., Lara, C., Escobedo, S. and Mendoza, O. (1998) The direct reduction of sulfide minerals for the recovery of precious metals. Journal of Metals 50, 55–59.

Šepelák, V., Steinicke, U., Uecker, D.C., Trettin, R., Wissmann, S. and Becker, K.D. (1997) High-temperature reactivity of mechanosynthesized zinc-ferrite. Solid State Ionics 101–103, 1343–1349.

Šepelák, V. and Becker, K.D. (2000) Mösbauer studies in the mechanochemistry of spinel ferrites. Journal of Materials Synthesis and Processing 8, 155–166.

Šepelák, V., Menzel, M., Becker, K.D. and Krumeich, F. (2002) Mechanochemical reduction of magnesium ferrite. Journal of Physical Chemistry B 106, 6672–6678.

Šepelák, V., Bergmann, I., Kipp, S. and Becker, K.D. (2005) Chemie mit der Hammer-Mechanochemie. Zeitschrift für Anorganische und Allgemeine Chemie 631, 993–1003.

Takacs, L. (1993) Metal-metal oxide systems for nanocomposite formation by reaction milling. Nanostructured Materials 2, 241–249.

Takacs, L. and Pardavi-Horvath, M. (1994) Magnetic properties of nanocomposites prepared by mechanical alloying. In: R.D. Shull, J.M. Sanchez (Eds.) *Nanophases and Nanocrystalline Structures.* TMS, Warendale, pp. 135–144.

Takacs, L. (1996a) Ball milling-induced combustion in powder mixtures containing titanium, zirconium or hafnium. Journal of Solid State Chemistry 125, 75–84.

Takacs, L. (1996b) Combustive mechanochemical reactions with titanium, zirconium and hafnium. Materials Science Forum 225–227, 553–558.

Takacs, L. (1996c) Nanocrystalline materials by mechanical alloying and their magnetic properties. In: C. Suryanarayana, J. Singh, F.H. Froes (Eds.) *Processing and Properties of Nanocrystalline Materials.* TMS, Warrendale, PA, pp. 453–464.

Takacs, L. (2002) Self-sustaining reactions induced by ball milling. Progress in Materials Science 47, 355–461.

Takacs, L., Torosyan, A.R. and Baláž, P. (2006) Ball milling induced reduction of MoS_2 with Al. Journal of Materials Science 7033–7039.

Tamman, G. (1932) *Lehrbuch der Metallkunde.* Verlag Barth, Leipzig.

Terry, B.S., Azubike, D.C. and Chrysanthou, A. (1994) Carbothermic reduction as a potential means for the direct reduction of Fe-WC and FeTaC, NbC metal-matrix composites. Journal of Materials Science 29, 4300–4305.

Thiessen, P., Heinicke, G. and Schober, E. (1970) Zur tribochemischen Umsetzung von Gold und CO_2 mit Hilfe radioaktiver Markierung. Zeitschrift für Anorganische und Allgemeine Chemie 377, 20–28.

Tkáčová, K. (1989) *Mechanical Activation of Minerals.* Elsevier, Amsterdam.

Torma, A.E. and Inal, O.T. (1979) Reduction of stibnite by hydrogen. Journal of Less-Common Metals 64, 107–114.

Torosyan, A.R., Tuck, J.R., Korsunskij, A.M. and Bagdasaryan, S.A. (2002) Metastable, mechanically alloyed and nanocrystalline materials. Materials Science Forum 386–388, 251–256.

Torosyan, A.R. and Takacs, L. (2004) Quantitative comparison of the efficiency of mechanochemical reactors. Journal of Materials Science 39, 5491–5498.

Treece, R.E., Gillan, E.G. and Kanner, R.B. (1995) Materials synthesis via solid-state metathesis reaction. Comments on Inorganic Chemistry 16, 313–337.

Tschakarov, C.G., Gospodinov, G.G. and Bontschev, Z. (1982) Über den Mechanismus der mechanochemischen Synthese. Journal of Solid State Chemistry 41, 244–252.

Urakajev, F.Ch., Takacs, L., Soika, V., Schevchenko, V.S. and Boldyrev, V.V. (2001) Mechanism of formation of "hot spots" in mechanochemical reactions of metal and sulfur. Russian Journal of Physical Chemistry 75, 1997–2001.

Urakajev, F.Ch., Ketegenov, T.A., Petrshin, E.J., Savintsev, Y.P., Tjumentseva, O.A., Chupakhin, A.P., Schevchenko, V.S., Jusupov, T.S. and Boldyrev, V.V. (2003) Complex investigation into the abrasion-reaction modification of quartz particle surface by amorphous iron compounds. Journal of Mining Science 39, 304–314.

Urakajev, F.Ch., Schevchenko, V.S. and Ketegenov, T.A. (2004) Synthesis of chalcogenide nanocomposites. Journal of Physical Chemistry 78, 551–554 (in Russian).

Varghese, V., Sharma, A. and Chattopadhyay, K. (2001) Reaction ball milling of systems involving ionic bonds. Materials Science and Engineering A304–306, 434–437.

Varghese, V., Chattopadhyay, K. and Narayanasamy, A. (2004) Factors influencing the kinetics of electrochemical reactions in milling. Journal of Materials Science 39, 5161–5167.

Vanjukov, A.V., Isakova, R.A. and Bystrov, V.P. (1978) *Thermal Decomposition of Metal Sulfides*. Nauka, Alma-Ata (in Russian).

Varnek, V.A., Strugova, L.I. and Avvakumov, E.G. (1974) Mechanical activation of solid-state reactions. 5. Study of solid-state reduction of SnO_2 Mössbauer spectroscopy. Izvestija SO AN SSSR, seria chimiceskich nauk 2, 26–29 (in Russian).

Vassilion, J.K., Ziebarth, R.P. and Disalvo, F. (1990) Chemistry of Materials 2, 738–746.

Vaughan, D.J. and Craig, J.R. (1978) *Minerals Chemistry of Metal Sulfides.* Cambridge University Press, Cambridge.

Vaughan, D.J. and Lennie, A.R. (1991) The iron sulphide minerals: their chemistry and role in nature. Scientific Progress Edinburgh 75, 371–388.
Weeber, A.W. and Bakker, H. (1998) Amorphization by ball milling. A review. Physica B: Condensed Matter 153, 93–135.
Weisser, O. and Landa, S. (1972) *Sulphide Catalysts. Their Properties and Applications*. Academia, Prague.
Welham, N.J. (1996) A parametric study of the mechanically activated carbothermic reduction of ilmenite. Minerals Engineering 9, 1189–1200.
Welham, N.J. (1997) Enhancement of the Becher process by ball milling. Proceedings of the Australasian Institute of Mining and Metallurgy 302, 61–61.
Welham, N.J. (1998a) Mechanical activation of the solid-state reaction between Al and TiO_2. Materials Science Engineering A 255A, 81–89.
Welham, N.J. (1998b) Mechanical activation of the formation of an alumina-titanium aluminide composite. Intermetallics 6, 363–368.
Welham, N.J. (1998c) Mechanochemical reduction of $FeTiO_3$ by Si. Journal of Alloys and Compounds 274, 303–307.
Welham, N.J. (1998d) Mechanochemical reaction between sulfur and ilmenite. Australian Journal of Chemistry 51, 947–953.
Welham, N.J. (1998e) Mechanochemical reaction between ilmenite (FeTiO3) and aluminium. Journal of Alloys and Compounds 270, 228–236.
Welham, N.J. (1998f) Mechanically induced reduction of ilmenite ($FeTiO_3$) and rutile (TiO_2) by magnesium. Journal of Alloys and Compounds 274, 260–265.
Welham, N.J. (1999) Room temperature reduction of scheelite ($CaWO_4$). Journal of Materials Research 14, 619–627.
Welham, N.J. (2000) Mechanical enhancement of the carbothermic formation of TiB_2. Metallurgical Transactions A 31A, 283–289.
Welham, N.J. (2002) Activation of the carbothermic reduction of manganese ore. International Journal of Mineral Processing 67, 187–198.
Williamson, G.K. and Hall, W.H. (1953) X-ray broadening from filled aluminium and volfram. Acta Metallurgica 1, 22–31.
Yang, H. and McCormick, P.G. (1993) Combustion reaction of zinc oxide with magnesium during milling. Journal of Solid State Chemistry 107, 258–263.
Yang, H. and McCormick, P.G. (1994) Mechanochemical reduction of V_2O_5. Journal of Solid State Chemistry 110, 136–141.
Ye, L.L., Liu, Z.G., Huang, J.Y. and Quan, M.X. (1995) Combustion reaction of powder mixtures of composition $Ni_{20}Ti_{50}C_{30}$ during mechanical alloying. Materials Letters 25, 117–121.
Zhang, Q. and Saito, F. (1998) Non-thermal process for extracting rare earths from bastnaesite by means of mechanochemical treatment. Hydrometallurgy 47, 231–241.
Zhang, Q., Wang, J., Saito, F., Okura, T. and Nakamura, I. (2001) Chemical Letters 160, 700.
Zhang, D.L. (2004) Processing of advanced materials using high-energy mechanical milling. Progress in Materials Science 49, 537–560.
Zviadadze, G.I., Turgenev, I.S., Kabisov, I.Ch. and Vasiljeva, O.J. (1985) Izvestija VUZ, Cvetnaja Metalurgija 1, 60–63 (in Russian).
Zviadadze, G.I., Turgenev, I.S., Kabisov, I.Ch. and Vasiljeva, O.J. (1986) Kinetics of lead sulfide reduction by hydrogen. Izvestija VUZ, Cvetnaja Metalurgija 2, 42–45 (in Russian).